INVESTIGATION OF AS-SPRAYED AND POST PROCESSED INCONEL625+30%Al_2O_3 COATINGS FOR WEAR AND CORROSION RESISTANCE

Thesis Submitted For the Award of the Degree of

DOCTOR OF PHILOSOPHY

in

Mechanical Engineering

By

Gaurav Prashar

41900405

Supervised By

Name of Supervisor: Dr. Hitesh Vasudev

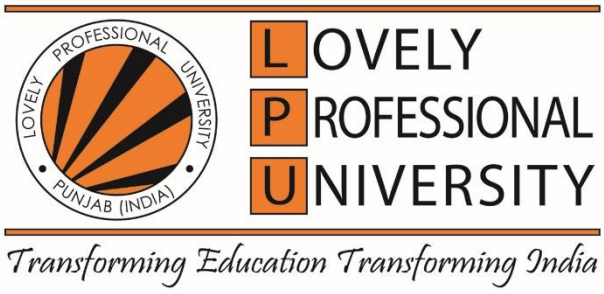

LOVELY PROFESSIONAL UNIVERSITY
PUNJAB
2022

DECLARATION

I, hereby declared that the presented work in the thesis entitled "INVESTIGATION OF AS-SPRAYED AND POST PROCESSED INCONEL-625+30%Al_2O_3 COATINGS FOR WEAR AND CORROSION RESISTANCE" in fulfilment of degree of **Doctor of Philosophy (Ph.D.)** is outcome of research work carried out by me under the supervision Dr. Hitesh Vasudev working as Associate Professor, in the School of Mechanical Engineering at Lovely Professional University, Punjab, India. In keeping with general practice of reporting scientific observations, due acknowledgements have been made whenever work described here has been based on findings of other investigator. This work has not been submitted in part or full to any other University or Institute for the award of any degree.

(Signature of Scholar)

Name of the scholar: Gaurav Prashar

Registration No.: 41900405

Department/school: School of Mechanical Engineering

Lovely Professional University, Punjab, India

CERTIFICATE

This is to certify that the work reported in the Ph.D. thesis entitled "INVESTIGATION OF AS-SPRAYED AND POST PROCESSED INCONEL-625+30%Al_2O_3 COATINGS FOR WEAR AND CORROSION RESISTANCE" submitted in fulfillment of the requirement for the reward of degree of **Doctor of Philosophy (Ph.D.)** in the School of Mechanical Engineering, is a research work carried out by Gaurav Prashar, Registration No.41900405, is bonafide record of his original work carried out under my supervision and that no part of thesis has been submitted for any other degree, diploma or equivalent course.

(Signature of Supervisor)

Name of supervisor: Dr. Hitesh Vasudev

Designation: Associate Professor

Department/school: Mechanical Engineeirng

University: Lovely Professional University, Punjab, India

ABSTRACT

High temperature degradation of component surfaces in power sectors, metallurgical furnaces, petrochemical installations, and aerospace industry is a cause of concern today. The shutting down of these sectors as a result of high temperature oxidation and erosion not only leads to huge financial burdens on the economy of any country but more importantly it will stop the service of power to the society. Failure of boiler tubes in power plants using coal as a fuel owing to high-temperature oxidation and erosion has emerge as an serious material issue in the designing and operation of coal-based power plants. The circumstances might vary greatly depending on the plant, but in recent years, temperatures have been raised across the globe in order to generate more energy, reducing the life of steel based boiler tubes. Replacement costs for broken tubes are likewise very significant. In an effort to prolong the life of these components, there has been a surge in interest in covering them with protective coatings. Because boiler steels are unable to achieve both high temperature strength and high temperature oxidation resistance requirements at the same time, protective coatings are applied to mitigate the latter.

Among various coating methods, plasma spray is low cost, simple, and flexible which can produce high flame temperatures (greater than 10,000 K) along with ultra-high cooling speed (10^{-5}–10^{-7} K/s). In this method, the coating is often developed in form of well flattened splats with good mechanical adhesion with the underlying substrate. Plasma sprayed coatings have been used in industrial or aerospace applications as a technique of enhancing the high temperature oxidation and erosion performance of parts operating under strenuous conditions. The performance of materials used in elevated temperature aggressive conditions is directly related to their ability to form thick and coherent protective oxide scales on the surfaces. During service, the thermal sprayed coatings are expected to develop slow growing protective oxides which should block the corrosive species to diffuse into the coating and sub-surface of the coated material.

Furthermore, due to high flame temperature and rapid cooling, unwanted residual stresses occurs due to formation of pores, un-melted particles and cracks in microstructure which in turn lowers the performance of the developed coating. Therefore existence of such zones in developed coating is harmful to the high temperature oxidation and erosion resistance. Hence, to improve the micro-hardness, and to minimize porosities and micro-cracks appropriate heat treatment (HT) or post-processing of plasma sprayed coatings is required.

To compensate for the decrease in oxidation resistance in metallic coatings blend of ductile phase with hard phase has been pinned down as a cost-effective approach. Coatings having more than one phase are recommended in literature by researchers to combat material degradation resulting from oxidation and other types of wear. The surface has to withstand high temperature oxidation and erosion at same time. Therefore, composite coatings are suitable to provide the synergic effect in such harsh conditions. Super alloys (Ni-based) and ceramic coatings have been extensively used to mitigate the harmful effects of oxidation and erosive wear at elevated temperatures. The oxidation resistance is delivered by Inconel-625 (IN625) matrix while the wear protection is mainly due to the reinforcement Al_2O_3. In the present research study, an attempt has been put in to develop bimodal IN625-Al_2O_3 composite coatings and to compare them with micrometric and nanometric coatings. The novelty in the present work is the replacement of the available Ni and Ni-Cr nimonics matrix with the IN625 matrix. Moreover, to compare the effect of the addition of 30wt% Al_2O_3 as reinforcement by varying the particle size in micrometric, nanometric, and bi-modal forms was also considered. In the current experimental study, the high-temperature erosion and oxidation performance of as-sprayed and heat treated plasma-sprayed coatings was studied. The micrometric, nano, and bimodal Al_2O_3 was reinforced with the IN625 matrix. The composite coatings were deposited on ASTM-SA210 GrA1 boiler steel. The substrate and coatings were evaluated at 900°C with a hot air-jet erosion tester at two angles. The oxidation tests were executed at a temperature of 900ºC under cyclic conditions to determine the high-temperature

oxidation resistance of developed IN625-30%Al_2O_3 (micro, nano, and bimodal) composite coatings.

The SEM-EDAX and XRD, micro-hardness and porosity analysis were used for the microstructure characterizations of as-sprayed, oxidized and eroded surfaces. The Plasma sprayed coatings were sprayed at M/S Metallizing Equipment Corporation Pvt. Ltd. (MECPL), Jodhpur, India. The cross-section of the developed coatings showed a typical coating thickness of 250-300 μm and coatings showed well bonding at the interface without any sign of diffusion of elements.

The porosity in general, has been found to be less than 2.5% for all the coatings. The heat treated IN625-BHT coated sample has shown least value of porosity (1%). The micro-hardness of the Plasma-sprayed coatings was found to be higher than the ASTM-SA210 GrA1. The maximum value of the hardness has been achieved by heat treated IN625-BHT coated sample of the order of 1299±25 $H_{V0.3}$ representing the outcome of the homogenous distribution of hard Al_2O_3 phase and a reduction in both the un-melted particles and porosity content induced by HT.

The XRD diffraction pattern of the as coated samples prepared by Plasma spraying technique indicated the retained identity of the coating powder used and also showed the formation of low intensity peaks of NiO observed in XRD analysis. A nearly uniform lamellar structure consisting of typical splat-like morphology was observed in the FE-SEM analysis.

The cyclic oxidation test on prepared specimens in air was conducted at 900°C, under cyclic conditions for total of 50 cycles. One cycle consisted of 1 h heating followed by 20 min cooling in ambient temperature. SEM/EDS and XRD analysis has been used for the study of oxidised samples from the surface as well as along the cross-section.

The uncoated ASTM-SA210 GrA1 showed intense spalling and thick oxide scale formation during oxidation studies in the aggressive cyclic environment at 900°C for 50 cycles. Presence of Fe and O in the oxide scale of bare substrate is responsible for the growth of weak oxides like FeO, Fe_2O_3, Fe_3O_4 endorsed by XRD analysis of oxidised uncoated substrate.

All the Plasma sprayed IN625-Al_2O_3 coatings were found beneficial in increasing the resistance to cyclic oxidation in air. On the basis of the oxidation resistance provided by the coatings at 900°C for 50 cycles, the plasma sprayed heat treated IN625-BHT was the best amongst all the coated samples.

The Plasma Sprayed IN625-BHT oxidized coating was best among all composite coatings and it reduces the weight gain of ASTM-SA210 GrA1 boiler steel by 96.5% which could be related to the existence of dense and coherent protective phases like, Al_2O_3 Cr_2O_3, TiO_2 and spinels $NiCr_2O_4$ and $CrNbO_4$. In addition to the surface oxides, it has been established that the HT plays an important role in providing oxidation resistance. Better oxidation resistance of IN625-BHT coating may be associated to the rapid development of oxides of Cr and Al at the splat boundaries of the coating and within open pores owing to penetration of the oxidizing species via spalt boundaries or open pores during HT of the coated samples in oxidizing conditions. The coating becomes dense after the oxides form at splat boundaries and locations of porosity; as a result, corroding species diffusion to the internal portions of the coatings is hindered, and oxide growth is constrained mostly to the specimen's surface and as a result steady state rate of oxidation is achieved.

The weight gain data was collected after each cycle of oxidation test and parabolic rate constants for deposited coatings were calculated. The minimum value of K_P was found in case of IN625-BHT coating in order of 0.7 and therefore responsible for highest oxidation resistance amongst all deposited coatings. For uncoated GCI, the value of K_P was found to be 619.35.

The erosion testing was carried out on a hot air-jet erosion test rig apparatus *(Model: TR-471-800, Manufacturer: Ducom instruments-India)* with ASTM standard G76-02 available with GNE, Ludhiana, India. The erosion behaviour of uncoated and coated samples has also been evaluated at 900°C at 30° and 90° impact angles. The erosive wear rate (*g/g*) (ratio of wear loss of mass in *g* to the mass of the supplied erodent in *g)* was calculated for both the substrate and coated specimens. Scanning electron

microscopy (SEM) technique has been used to analyse the eroded samples at higher and lower magnifications.

All composite coatings with or without HT exhibited the brittle erosion mode irrespective of the impact angle. The splat removal, cracks, and fracture are the major erosion mechanism responsible for material removal in coated IN625-ALC, IN625-ALN, and IN625-ALB samples. SEM surface morphology of IN625-CHT, IN625-NHT and IN625-BHT coating samples appeared to be solely cracking, splat removal and chipping brittle mechanism. The better performance of IN625-BHT coating amongst all the coatings is related with the positive interactions among micron and nanostructured Al_2O_3 particles. The developed cracks were arrested and deflected in the bimodal structure of the IN625-BHT coating and therefore providing maximum erosion resistance.

Amongst all the coatings under investigation, the IN625-BHT coating has given the best performance on ASTM-SA210 GrA1 exposed cyclic oxidation in air at 900°C for 50 cycles and solid particle at 900°C.

ACKNOWLEDGEMENT

First and Foremost, I am very much heartily thankful to my dissertation Supervisor, **Dr. Hitesh Vasudev**, Associate Professor in School of Mechanical Engineering, Lovely Professional University, for his invaluable guidance and support during the present research work.

I wish to express my heartily thanks to **Dr. Amit Bansal**, Assistant Professor in Mechanical Engineering Department, IKGPTU Kapurthala for giving valuable inputs during every phase of my Ph.D. work.

I would like to acknowledge **Dr. Jasmaninder Singh Grewal**, Professor and head, Production Engineering Department, Guru Nanak Dev Engineering College Ludhiana, for providing me all the infrastructural facilities to carry out this work in the department.

I also express my sincere thanks to **Dr. Satish Tailor,** General Manager, at Metallizing Equipment Company Pvt LtdJodhpur,for providing guidance and support in coating process facilities.

I wish to thank **Mr. Amrinder Mehta**, in-charge of XRD, CIF cell, LPU, **Mr. Shiv Kumar**, in-charge of FE-SEM, Institute Instrumentation Centre, IIT Roorkee and **Mr. Puran Singh**, Technical Assistant in Research and Manufacturing Lab, Guru Nanak Dev Engineering College Ludhiana for providing technical assistance.

I express my profound regards to my parents for their blessings and for being the main source of inspiration to succeed in my endeavours. I would like to express particular thanks to my family, my mother for her advises, care and love. I would like to thank my wife, **Mrs. Vandana Sharma** for her advises, care and continuous motivation she provided me throughout my research work. I feel proud to my brother **Mr. Saurav Prashar and his wife Mrs. Ekta Sharma**, for their extensive love and supporting me in my entire life.

I would like to thank everyone who supported me for completing this work successfully and I express my apology that I could not mention everyone individually. Above all, I would like to express my sincere gratitude from the core of my heart to **ALMIGHTY** for giving courage, strength and patience to carry out my research out.

(GAURAV PRASHAR)

Contents

List of Tables

List of Figures

List of Appendices

Chapter 1

INTRODUCTION

At high temperatures, degradation of component surfaces in engineering systems is imposing a huge cost burden. To reduce these enormous economic burdens and to enhance the efficiency of high-performance plants, susceptible to oxidation and erosion, their premature failures must be avoided or delayed. Therefore, high-temperature material degradation owing to wear is a major challenge in high-temperature areas.

1.1 SURFACE DEGRADATION

Engineering components used in different industrial applications have to operate under high heat loading conditions and has to deal with the problem of high-temperature corrosion and erosion especially in power plants that use coal as a fuel. This is particularly true for wear resistant components and corrosion resistant components because in aggressive environments, surface of the component has to play a vital role (Liu *et al.,* 2017). Therefore, material behavior is solely dependent upon the material surface, contact area of surface and the conditions or environment under which the material operates. The boiler tube faces regular failures, for which erosion and corrosion are the main diagnostic causes.

Coal used for power generation in India has a significant volume of ash around 50%, including up-to 15% abrasive particles like hard quartz which raises the erosion intensity of coal (Kumar and Sapra, 2016). As the flue gases pass through tubes of the boiler, erosion of tube surface starts at various sections, primarily at tube side walls reducing its thickness and finally premature collapse of tube occur with time. The interaction time among erodent and directed material in solid particle erosion is momentary (Roy, 2006), which separates it from other associated processes like sliding and abrasive wear, machining and grinding. Localized long term over-heating and

erosion are responsible for premature collapse of tubes when boiler temperature exceeds 700°C and phase changes takes place (Husain and Habib, 2005). The hot corrosion commonly known as high temperature oxidation, which initiates when the salt contaminants formed during the combustion of fuel starts to deposit on the tubes in the form of molten ash and dissolves the protecting oxide layer, resulting in the degradation of the material (Kamal et al., 2010a; Stringer, 1996). Hence the main reason for the catastrophic failure of the components fitted in a power plant is the simultaneous attack of erosion and oxidation(Matthews *et al.,* 2009; Wang, 1996). As a whole, due to oxidation and erosion power plant will fail to meet his functional requirement and consequently in this event power plant will remain shut down for a prolonged period resulting in the huge economic loss and more importantly stoppage of service to the society. Hence, oxidation and solid particle erosion have become major issues of concern for many industries (Zhou and Bahadur, 1995; Yang *et al.*, 2012).

The carbon steel water wall tubes which were commonly used tube material across northern region of India have a high rate of failure owing to elevated temperature erosion and corrosion resulting in reduction of tube thickness and premature failure. Above 400°C, there is rapid decline in the yield strength of tubes made up of carbon steel (Mohamed and Wilson, 2015). If the temperature of the tube metal is steadily raised above this temperature, it can deform plastically and then rupture takes place. The efficiency of these serviceable components not only depends upon the bulk properties of the material but also on surface characteristics and properties. This is particularly true for those components which are prone to wear and corrosion, as the surface of these components plays a significant role in aggressive environments. Coatings having more than one phase are recommended in the literature by researchers to combat material degradation resulting from oxidation and other types of wear. For erosion-corrosion cyclic studies in the actual boiler environment (Bala et al., 2017) compared the uncoated and the Ni based coated specimens in the middle zone of the low temperature super-heater of the Stage-II Boiler of Guru Gobind Singh Super Thermal Power Plant, Punjab (India). It was observed that the coated specimens gave better performance than the

uncoated steel. Therefore, composite coatings developed by thermal spraying are suitable to provide the synergic effect in such harsh conditions.

1.2 OXIDATION

Degradations due to high-temperature oxidation, is the main failure modes of components in the hot sections of gas turbines, boilers industrial waste incinerators, metallurgical furnaces, and petrochemical installations. Failure of boiler tubes in coal-fired boilers due to high-temperature oxidation and erosion caused by the impact of fly ashes has become a key material issue in the design and operation of thermal power plants. It is recognized as one of the main causes of downtime.

Oxidation is defined as a reaction occurring between the metal surface and oxygen (O_2) to form a metal oxide (He *et al.,* 2001; Birks *et al.,* 2006; Rapp, 1984; Reid, 1971).The sequence of events occurring during high-temperature metal oxidation is presented in **Fig.1.1**

Initially, oxygen gas contacts the metal surface and gets decomposed. Thereafter, adsorption of O_2 atoms onto the surface of the metal takes place. After adsorption of oxygen, once the thermodynamic criteria are met, Metal oxide (MO) start forming on the metal surface in the form of islands and they tend to grow in the lateral direction to cover up the whole metal surface (Deb *et al.,* 1996; Shukla *et al.,* 2012). As the oxygen is still adsorbed on the surface then depending upon the diffusion ability of oxygen atom, oxygen diffusion process is initiated and oxygen starts to dissolve into the metal surface. Once the entire metal surface is covered up by the oxide layer, then this oxide layer tries to grow in the perpendicular direction, as indicated by arrows in diagram (c) and the oxide layer thickness starts to increase. The growth process of the metal oxide is decided by the diffusion of metal ions (M^{+2}), oxygen ions (O^{2-}) as well as the conduction of electrons, “e” through this oxide layer. The O_2 can come out in form of oxygen ion and can react with metal ion then oxidation occurs on anodic surface or metal ion will also diffuse out and helps

in the oxide scale growth on the surface of cathode (Stringer, 1987; Nicholls, 2000; Meier, 1989).

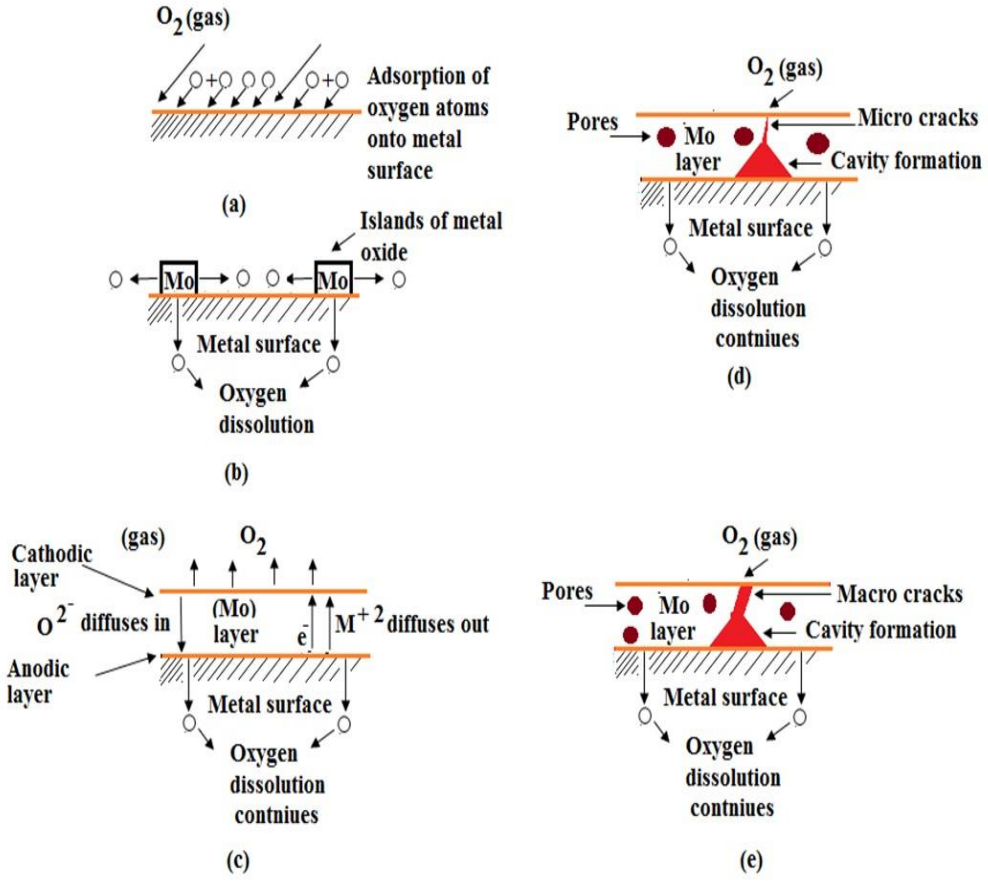

Fig.1.1 The sequence of events during the elevated temperature metal oxidation: (a) Oxygen gas (O_2) adsorption, (b) dissolution of O_2, (c) formation of thin oxide film, (d) growth of oxide layer, (e) emergence of a thick oxide layer.

General reactions taking place are:

$M^{+2} + O^{2-} = MO$ to form M^{+2} two electrons can be taken out from metal atom i.e., M^{-2e} and can form M^{+2} and these two electrons can go to oxygen and oxygen can take these two electrons to form O^{2-}.

$M^{-2e} = M^{+2}$ is anodic reaction whereas $M^{+2e} = O^{2-}$ is a cathode reaction. This process can happen on the surface when two electrons are excess in metal and these

two electrons can transmit through the oxide layer and then adsorbed oxygen can take care of these two electrons; thus, reduction process takes place at cathode interface. The gas-oxide interface is acting as the cathode and the oxide-metal interface is acting as the anode. It should be noted that the oxide layer will be acting as a conductor by transmitting electrons from one surface to another and also it acts as an electrolyte because ions movement is also taking place. Due to the continuous growth of oxide scale and diffusion of oxygen defects starts occurring in form of the cavities, pores, and small sized cracks (Kumar *et al.,* 2013; Sadeghi *et al.,* 2019; Oksa *et al.,* 2014). With the continuous dissolution of oxygen the formation of macro-cracks and pore occurs which ultimately degrade the performance of structural components. Hence protective coatings are being used on structural alloys in energy conversion and utilization systems to protect surface from oxidation.

1.2.1 KINETICS OF OXIDATION AT HIGH TEMPERATURES (OXIDATION RATES)

During the high temperature oxidation of metals, different growth models have been observed. The oxidation kinetics as exhibited by the weight gain curves in **Fig.1.2.** can follow three common empirical rate laws. All these laws are idealized, and in actual practice, they describe only part of the oxidation process.

1.2.1.1 LINEAR LAW

This law applies in the situations where the oxidation of metals proceeds at constant rates. Typically, the rate of oxidation is determined by reactions at phase boundaries; however, there are other processes that can also illustrate linear kinetics. Oxide scale growth by linear rate law is most common in the initial stages of oxidation before the oxide scale becomes thick enough to effectively separate the various reactants. Even if there is no protective oxide, linear oxidation can occur but the transportation of ions and electrons will occur at a faster rate regardless the oxide thickness, and the rate of

oxidation will remain linear. It occurs in metals with crack and porous oxide film. Mathematically, the linear rate law is described as

$X = k_{lin}t;$

where x is the oxide thickness,

k_{lin} is the linear rate constant,

and t is the subjection time (Birks *et al.*, 2006).

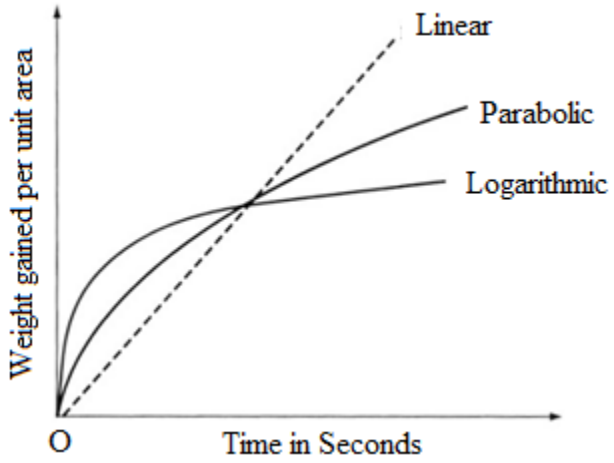

Fig.1.2 Weight gain curves for three common empirical rate laws.

1.2.1.2 PARABOLIC RATE LAW

Most metals and alloys used at elevated temperature usually follow parabolic rate law. The oxidation rate depends upon the transportation of ions and electrons through oxide scale. Consequently, the weight gain curve levels decrease as the thickness of oxide scale increases. It occurs in metals having thick coherent oxides. The mathematical expression for growth model was given by

$x^2 = k_p t + C,$

where kp is the parabolic rate constant and C is the constant of integration.

1.2.1.3 COMBINED RATE LAWS

The oxidation process can follow various rate laws during the different oxidation stages, when abrupt changes occur in the oxidation behavior as exhibited in **Fig.1.2.** This may take place when protective growing oxide layer suddenly loses its protectiveness, then an occurrence called as breakaway oxidation is noticed. Reasons for such a behavior may be due to changes in chemical composition of the oxide scale and/or mechanical failure of the oxide scale. **Fig.1.3,** depicts the oxidation according to this law, with breakaway oxidation after t^b (time for breakaway).

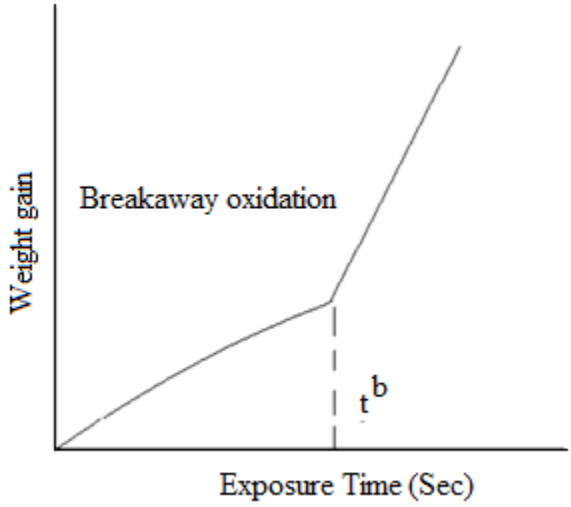

Fig.1.3 Breakaway oxidation after time t^b.

1.2.2 REQUIREMENT FOR THE MAKE-UP OF PROTECTIVE OXIDES

1. The thermal coefficient of oxide and metal will be similar. If they are not similar, stress generation occurs in oxide which ultimately leads to cracks and exposes the metal surface to oxygen gas.
2. No evaporation of oxide should be there for example, V_2O_5 evaporates and will not provide any protection to the underlying metal.

3. Plastic deformation ability of oxide should be good as if the oxide is brittle, it will break under stress at high temperatures.
4. The low diffusion coefficient of the metal ions or oxygen ions species will be better through oxide layers.
5. Oxide layer should develop at a lower rate.

1.3 HIGH TEMPERATURE EROSION

When solid particles strike the surface of the target material at low or high temperatures with some velocity and remove the material in the form of debris, it is known as the erosion of material (Hoop and Allen, 1999). In India power plants are the vital and traditional source for electricity generation and power comes mainly from coal. One of the major divisions in coal-fired power plant is boiler and the main structural components of the boiler are walls of the boiler, super-heater tubes, air heaters and economizer. These structural components are exposed to the fly ash erosion both at the room temperature and high temperature. Parameters that mostly influence the material surface and erosion process are temperature and impact angle. In order to know the effectiveness of the above-mentioned parameters there is no universal model. Experimental studies of the said parameters on the erosion process are one of the influential methods to examine the mechanism of the erosion.

1.3.1 SOLID PARTICLE EROSION MECHANISM

Different engineering components used in industries are degraded because of elevated temperature erosive wear. Various systems exposed to elevated temperature erosion are highlighted in **Table 1.1**. At elevated temperatures, removal of the material is controlled by the combined effects of (E-O) erosion and oxidation. In-depth analysis of the eroded surfaces has been conducted by using SEM, TEM and OM techniques. Elevated temperature erosion-oxidation mechanism for a pure Ni surface can be divided into four types as shown in **Fig.1.4**.

Table 1.1 Various systems exposed to elevated temperature erosive wear (Roy, 2006).

Systems	**Structural components**
Combustion systems	Re-heater, Super-heater, Heat exchanger, Economizer tube banks, Bed coils etc.
Coal gasification systems	Turbines, Hopper valves
Gas turbines	Blades of the turbine
Coal liquefaction systems	Steam valves to throttle the steam flow

In first case no oxide scale forms, when temperature is low, and erodent has high velocity and feed rate. Still if oxides scale forms it is thin and it deform in the similar manner as the surface of the target. This mode is called metal erosion as shown in **Fig.1.4(a).** In this regime material removal takes place by two modes; (a) cutting, and (b) ploughing. In second case, during extreme high temperatures, low velocity and feed rate, thick oxide scale develops during erosion, as shown in **Fig.1.4(b).** The erosion behavior in this regime is termed as brittle erosion response and it depends on velocity but is independent of feed rate. This mechanism is known as oxide erosion and material removal during this type occurs mainly due to development of radial cracks. When temperature, velocity, and feed rates are intermediate then oxide scale with intermediate thickness forms. But, the depth of deformed zone forms can extend beyond the oxide scale and the cracking of oxide scale occurs under the impact of eroding particles and it gets further pushed down. In the process material gets pulled out through the medium of cracks in this oxide scale. With the passage of time, this process is repeated and composite layer consisting of bulk material and small broken pieces of the oxide scale forms. Erosion occurs through this

layer and detailed mechanism is presented in **Fig.1.4(c)** is known as oxidation affected erosion and erosion mechanism in this region can change from the ductile to brittle. Erosive wear rate in oxidation affected erosion is a function of temperature, velocity and feed rate of the particles. Oxidation controlled erosion is the final erosion mechanism and is exhibited in **Fig.1.4(d).** During this regime brittle and non-adherent oxide scale develops under relatively elevated temperatures, low feed rates and velocities that got removed easily after attaining critical thickness (Roy, 2006).

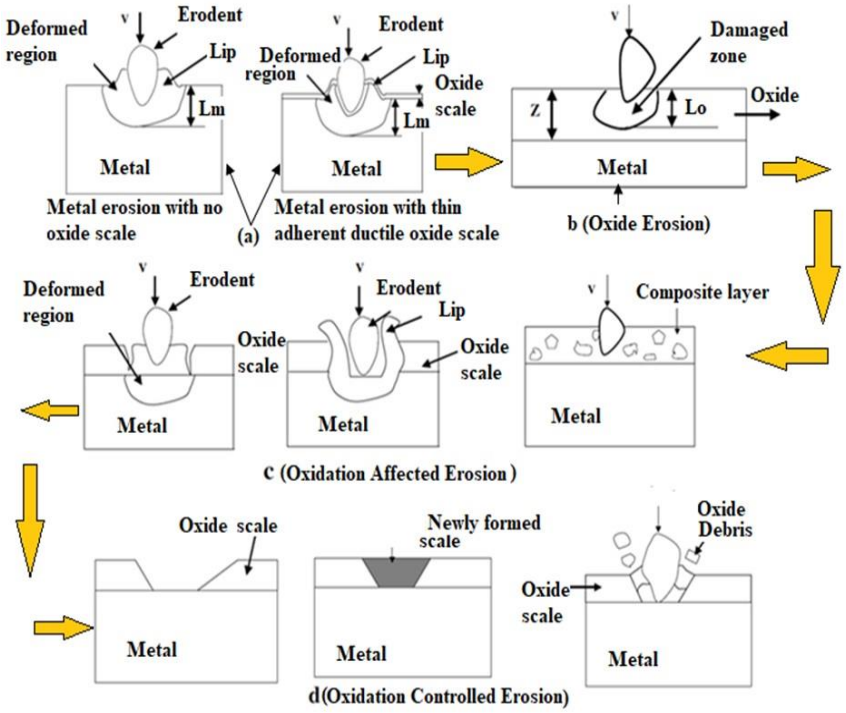

Fig.1.4 Schematic representations of different erosion mechanisms at elevated temperature (Roy, 2006).

1.3.2 EFFECTS OF EROSION

Erosion alone can eat up a country GDP. Rust, corrosion, wear and tear, accidental damages, and other reasons cost India thousands of crores of rupees every year. Damage of the boiler super-heater and water wall tubes due to erosive wear is exhibited in **Fig.1.5**. Thickness of the tube reduces so much that it will no longer sustain the hoop stresses and will burst leading to the catastrophic failure of

the tube. Maintenance expenses associated with this damage scan rise to 54% of the total production cost. In another study, CFB (circulating fluidized bed) furnace has to be shut down completely due to the erosion caused by coal powder and limestone grits (Wang *et al.*, 2013).

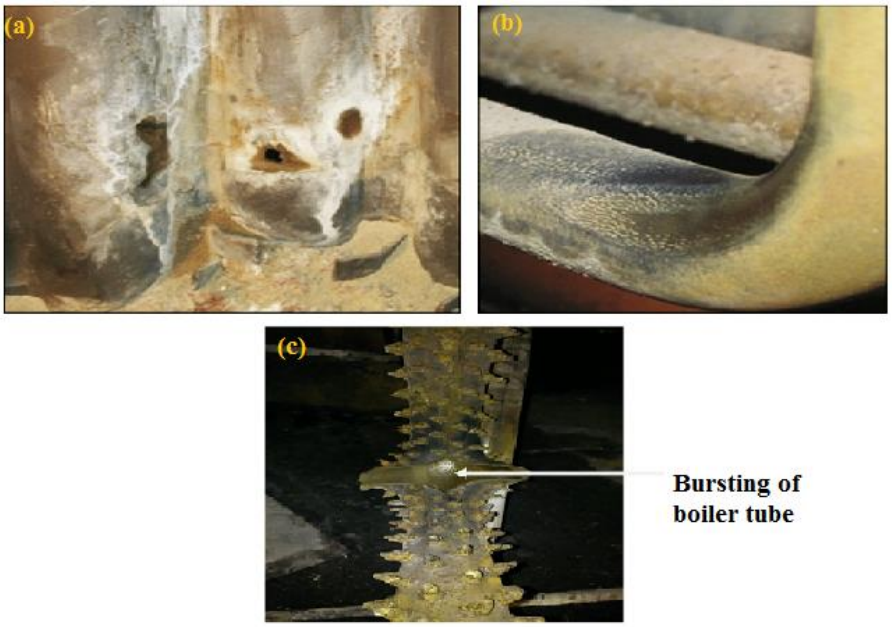

Fig.1.5 Failures of boiler tube due to erosion in fluidized boilers: (a) Damage due to erosion of wall, (b) Damage super-heater tube, and (c) Bursting of boiler tube.

1.4 OXIDATION AND EROSION PREVENTION METHODS

The case study conducted by (Prakash *et al.*,2001) for coal based power plant reported that a total of 89 failures had occurred during one year and it was found that 50 failures had resulted only from the erosion and corrosion related problems. Hence, solid particle erosion and corrosion have become major issues of concern industries, especially, in areas where operating temperatures are above 600°C. Therefore, it becomes essential to predict oxidation and erosion rates in power plants so that appropriate measures can be taken to prevent the degradation of the structural components (Hidalgo *et al.*, 2001). Modification of the environment, improving the material properties, or by depositing a coating onto the surface of the substrate is the

available choices. The first approach straightaway lowers the boiler efficiency if the temperature range is reduced (Deuerling*et al.,* 2009; Jiménez and Ballester, 2005). In the second approach, material properties (corrosion and erosion resistance) can be enhanced by addition of elements like Aluminum, Chromium, and Yittrium but excess concentrations badly affect the mechanical properties and also raises cost (Rana *et al.,* 2012; Ohkubo*et al.,* 1994). Therefore, the corrosion-erosion related problems can be easily, economically, and effectively combat with the help of surface treatment techniques. In the recent years, TS coatings have increased to overcome the issues related to corrosion and erosion of the mechanical components (Fantozzi *et al.,* 2017; Boulos et al., 2021; Sidhu *et al.,* 2006a).

1.5 THERMAL SPRAY (TS) COATING TECHNOLOGY

Thermal spray coatings are widely adapted hard facing methods, which is practicable for depositing the corrosion and wear resistant materials on the surfaces of structural parts. Different TS methods are available but selection depends on some parameters like equipment availability and its cost, properties and quality of the coating etc. During the process stream of high temperature particles is directed towards the surface of the substrate with specific velocity and upon impacting the substrate surface these particles flattened in form of disc like shape known as splats as shown in **Fig.1.6**.

It has been observed that metallic coatings on tubes minimize the degradation and erosion in selected situations. To overcome this issue material that may has the combination of better mechanical and tribological properties need to be designed urgently. The issue of surface degradation owing to chemical or wear action cannot be completely eliminated, but it can be reduced by employing surface modification methods like laser cladding (Pereira *et al.,* 2015), thermal spraying, weld overlays (Zahrani and Alfantazi, 2014), heat treatments, chemical vapour deposition (CVD), and physical vapour deposition (PVD) etc. Because of its adaptability in depositing coatings of many types of materials, thermal spraying has been widely employed for surface modification

among all of the procedures outlined above. These coatings extend the life of components by minimizing the effect of wear and corrosion that occurs on surface (Pawlowski, 2008; Davis, 2004).The classification of thermal spraying is shown in **Fig.1.7.**

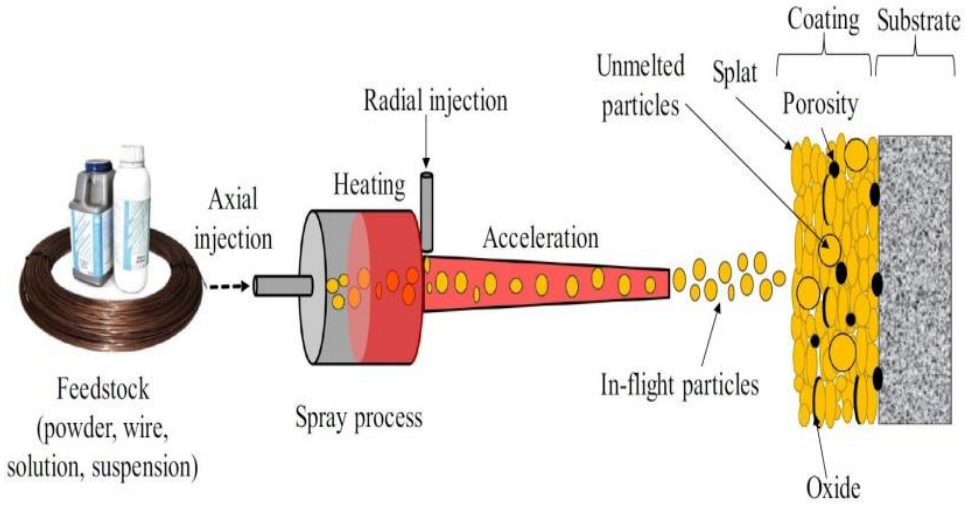

Fig.1.6 Diagrammatical representation of the thermal spraying (Sadeghi *et al.,* 2019).

The different variants of thermal spraying techniques are available such as high-velocity oxy-fuel, atmospheric plasma spraying (APS), arc spraying, detonation gun spraying (Vasudev *et al.,* 2018) and cold gas spraying. However, the final microstructure of the deposited coating depends upon the type of method selected for the deposition of feedstock material. Therefore, the selection of coating material and technique plays a significant role to meet the particular need for protective coating (Gao *et al.,* 2002). Plasma spraying has the advantage over other processes that it can spray very high melting point materials such as refractory metals like tungsten and ceramics like Alumina. Plasma sprayed coatings are generally much denser, stronger and cleaner than the other thermal spray processes with the exception of HVOF and detonation processes. Plasma spray coatings probably account for the widest range of thermal spray coatings and applications and makes this process the most versatile.

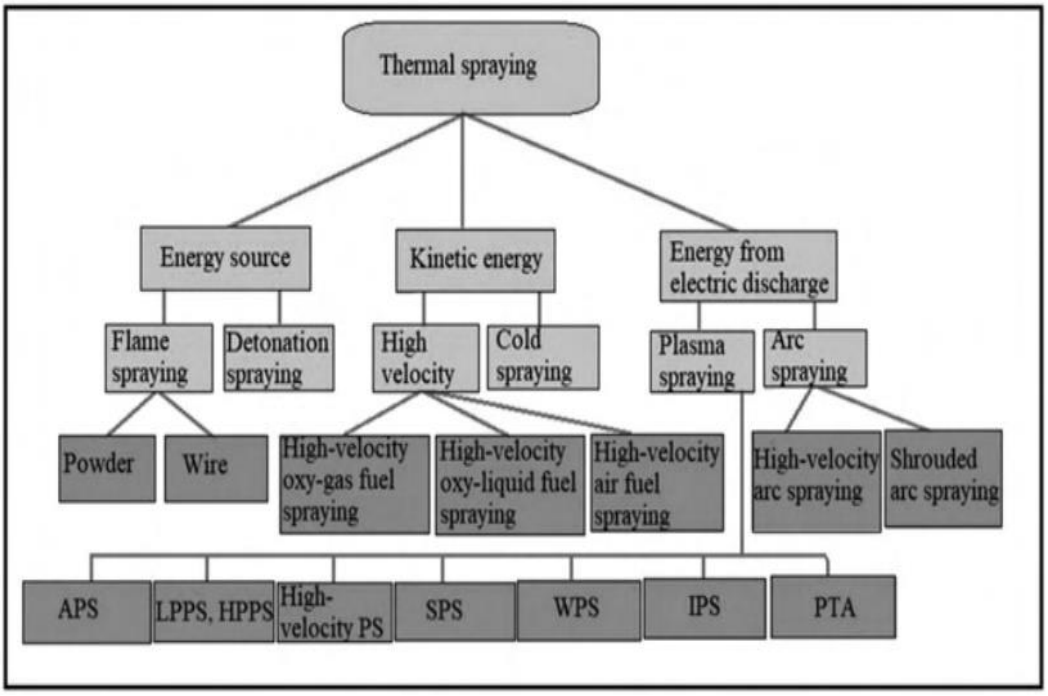

Fig.1.7 Classification of the thermal spraying methods (Sadeghi *et al.,* 2019).

1.6 PLASMA SPRAY (PS)

Two major types of PS methods used for spraying are (a) atmospheric and (b) vacuum assisted PS. In both methods high temperature plasma is achieved by flowing an inert gas among a high energy DC electric arc. Often high purity gases like Ar, N, H, or blend of them are used for plasma generation. The maximum temperatures lie around 19,000 °C, while at the site of feedstock powder injection, located at some distance from the exit point of spraying nozzle, the temperatures varies from 6,100-15,000°C (Davis, 2004). Spray rates vary subjected to the feedstock material employed, gun type used for spraying, powder injection system adopted, gas or gas mixture choosen, etc. The power outputs range for commonly used plasma spray guns are from 20 kW to 250 kW and various configurations of spray guns were available according to varying spraying requirements (Tucker, 2013; Pawlowski, 2008).Feed stock material is fed into this hot stream of plasma and due to high temperature in the stream material gets melted. To achieve supersonic velocities convergent-divergent nozzle is preferred so that particles

entertained in the plasma stream attain high velocities and strikes the substrate surface with impact. Flexible nature of plasma spray allows depositing any kind of feed stock such as slurry, liquid, powder and suspensions. Plasma spraying provides good resistance against erosive and sliding wear and is also used in the deposition of hydroxyapatite coatings in field of dental and orthopaedics implants (Awasthi *et al.,* 2020; Roy *et al.,* 2011). It also produces thermally resistant or conductive surfaces and can be used commonly for the salvage and restoration of the worn surfaces. Schematic of PS is shown in **Fig.1.8.**

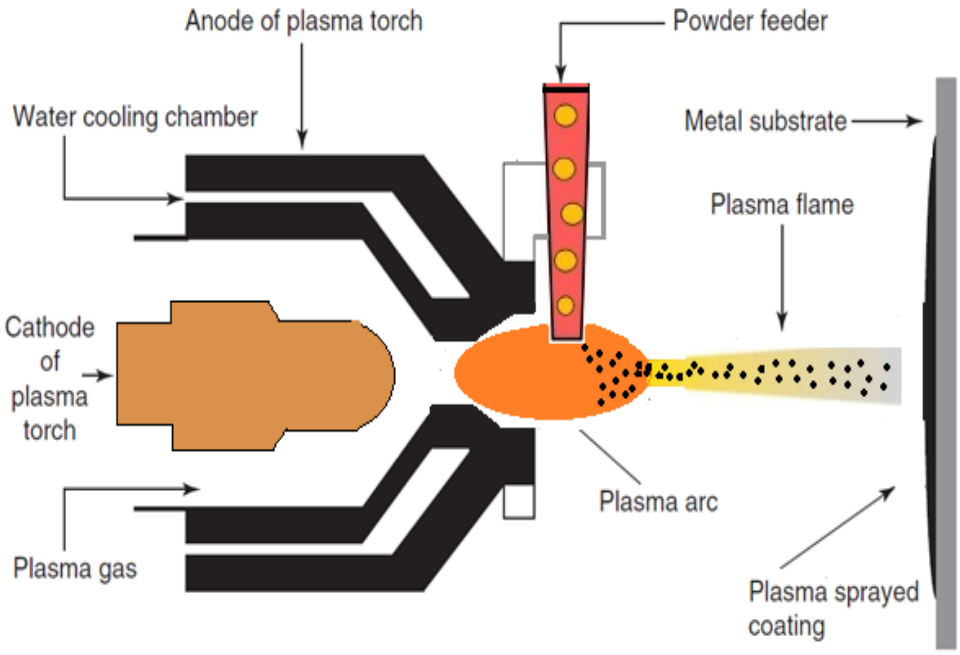

Fig.1.8 Schematic representation of PS set-up.

Plasma sprayed comes under category of high temperature range amongst the thermal spraying techniques (Kumar *et al.,* 2012). Investigations available in literature also indicates that during plasma spraying phase transformations occur and the final deposited coating have set of properties which was different than the powder properties. These properties are generally owing to development of metastable phases. If additional HT is done to the as-sprayed coatings then crystallization of amorphous phase takes

place, thus giving crucial new set of properties to the developed coatings. Furthermore, due to high flame temperature and rapid cooling, unwanted residual stresses occurs due to formation of pores, un-melted particles and cracks in microstructure which in turn lowers the fracture toughness and micro-hardness of the developed coating. Therefore existence of such zones in developed coating is harmful to the deposited coating resistance. Hence, to improve the micro-hardness, toughness, adhesion among splats and to minimize porosities and micro-cracks appropriate HT or post-processing of plasma sprayed coatings is required. (Bergant and Grum, 2009; Bergant *et al.*, 2014) reported that HT at 930°C enhances the adhesion strength between the deposited coating and substrate. (Wen *et al.*, 2015) performed vacuum re-melting method to enhance the wear resistance of plasma-sprayed NiCrMoY coating. (Liu*et al.*, 2017) developed NiCrBSi coatings by plasma spraying method and studied the effects of HT on structure and mechanical properties. The results affirmed that after HT the microstructure becomes homogeneous and micro-hardness of NiCrBSi coatings clearly improved. Similar findings were also reported by (Li *et al.*, 2019) on plasma sprayed Ni-based coatings. Authors reported that HT results in homogeneous microstructure of the coatings leading to improved corrosion-wear performance of heat treated coatings.

1.7 SUPERALLOYS

Super alloys have been used for wide range of applications like jet engines, gas turbines, steam generators and nuclear industries where high temperature strength, wear and corrosion resistance is required and are developed to be used at elevated temperatures of 1200ºC (Pereira and Lerch, 2001). An significant or notable characteristic of a Ni based super alloy is that it can be used in load bearing applications at temperatures in excess of 80% of their incipient melting temperatures, a fraction higher for any other class of alloy. Hence super alloys are can be classified into three major types; (a) Ni base, (b) Co base, (c) Fe base. Advanced emerging materials like Ni-based superalloys can be a candidate choice for these strenuous conditions due to its exceptional properties. Because of its superior creep strength and thermal shock qualities, IN625 a Ni-based superalloy

may be selected when service temperatures may exceed 900°C. Due to its composition, (Galedari *et al.*, 2019) suggested that super alloy Inconel-625 (IN625) be evaluated for erosion-corrosion resistance. IN625 is Ni based having FCC structure with Cr, Mo, Nb and Fe as major constituents. Solid solution strengthening mechanism provided by Mo and Nb enhances its resistance to oxidation, corrosion and improved its fatigue properties over a broader temperature range.

1.7.1 ROLE OF ELEMENTS IN SUPER ALLOYS

Super alloys have large number of alloying elements in order to provide necessary strength, toughness and durability at high temperatures. **Table 1.2** shows the role of various elements in Ni, Iron or cobalt based super alloys:

Table 1.2 Role of elements in Ni based super alloys.

Effect	**Iron base**	**Cobalt base**	**Nickel base**
Solid-solution strengtheners	Cr, Mo	Nb, Cr, Mo, Ni, W, Ta	Co, Cr, Fe, Mo, W, Ta
FCC matrix stabilizers	C, W, Ni	Ni	……..
Carbide form			
MC type	Ti	Ti, Ta, Nb	Ti, Ta, Nb, W, Mo
M7C3 type	…..	Cr	Cr
M23C6 type	Cr	Cr	Cr, Mo, W
M6C type	Mo	Mo, W	Mo, W
Carbonitrides			
M(CN) type	C,N	C,N	C,N
Forms γ′ Ni3 (Al, Ti)	Al, Ni, Ti	…..	Al, Ti
Retards formation of hexagonal Ŋ (Ni3 Ti)	Al, Zr	…..	……
Raise solvus temperature of γ′	……	…..	Co

Hardening precipitates or intermetallics	Al, Ti, Nb	Al, Mo, Ti(a), W, Ta	Al, Ti, Nb
Forms γ″ (Ni3 Nb)	……	……	Nb
Oxidation resistance	Cr	Al, Cr	Al, Cr
Improves hot corrosion resistance	La, Y	La,Y, Th	La, Th
Sulfidation resistance	Cr	Cr	Cr
Increases rupture ductility	B	B, Zr	B(b), Zr
Causes grain boundary segregation	……	……	B, C, Zr

1.7. 2 NEED OF SUPER ALLOYS

In order to get the efficiency of power plant above 45% its steam temperature and pressure needs to be increased above 600ºC and 25Mpa. This increased in efficiency can also reduced CO_2 emission levels less than 722 g/Kwh. T o achieve this material needed for the fabrication of structural components (reheaters, superheaters, and bed coils) must possess high creep strength followed by resistance to corrosion. Martensitic alloys have poor creep strength performance above 600ºC(Tan, 2012). Hence materials that have more creep strength will serve as a substitute in place of martensitic and ferritic materials. Ni based super alloys is the candidate material due to its excellent mechanical properties like creep, high strength and fatigue resistance for 900ºC technology.(Delaunay *et al*., 2000) studied the high temperature oxidation behavior of super alloy (Inconel-718) and proposed that alloy-718 provide resistance to oxidation at 900ºC due to the formation of minor alloying elements like Al_2O_3, TiO_2 and the formation of quasi continuous scale of inter-metallic phase Ni_3Nb at oxide alloy interface will be a good contribution to resistance against oxidation.

(Kamal *et al*., 2010b) in another investigation studied the oxidation and hot corrosion behavior of three super alloy superfer 800H, superni-718 and superni-75 under

Na_2SO_4 and 60%V_2O_5 corrosive environment at 900ºC in cyclic conditions. Among three superni-75 was the best in terms of oxidation and corrosion resistance. Super alloys exhibits better resistance to oxidation than hot corrosion. NiO, Cr_2O_3 and Fe_2O_3 formations were responsible for oxidation and hot corrosion resistance. (Dorcheh *et al*., 2016) in their experimentation studied the corrosion resistance of two ferritic steels, two austenitic steels and one super alloy Inconel-625 in eutectic composition at 600ºC up-to 5000hrs. Authors reported that super alloy Inconel-625 was best among all due to the formation of thick NiO layer and low kinetics. (Vasudev *et al*., 2019) compared the hot corrosion behavior of Inconel-718 deposited by HVOF process with bare cast iron for 50 cycles followed by 20 minutes cooling. From the characterization techniques it was found that Inconel-718 performed better at 900 ºC against hot corrosion due to the formation of stable oxides or phases like $NiCr_2O_4$, Cr_2O_3, Al_2O_3 and TiO_2 in coating. Further it was also proposed that coating protect the substrate effectively.

1.7.3 EFFECT OF CHEMICAL COMPOSITION

1.7.3.1 EFFECT OF Cr Content

(Gagilano *et al*., 2009) conducted tests to examine the effect of Cr content on 19 alloys both in laboratory and field. Authors concluded that resistance to corrosion depends upon Cr content. More the % of Cr better will be the material resistance to corrosion. Alloys that have Cr content greater than 22% displays better performance against corrosion during laboratory tests. On the other hand in field tests alloys that have Cr content 25% exhibits satisfactory performance. In another investigation (Hussian *et al*., 2013a) exposed Ni base coatings to a temperature 650ºC in simulated conditions and concluded that Ni-Cr coating was the best performer and has 46%Cr content in it. Based on another study related to hot corrosion on steels and super alloys it was concluded that weight loss decreases with increase in Cr content. However this condition of Cr content doesn't fit for Ni based austenitic alloys when environment is SO_2/SO_3 rich. It was concluded that despite of similar Cr content in 617 and 263 grades, both performed differently (Stein-Brzozowska *et al.,* 2013).

1.7.3.2 EFFECT OF COBALT (Co)

As compared to Ni, cobalt exhibits less hot corrosion resistance. (Zhao *et al*., 2005) investigated the hot corrosion behavior of super alloy 740 and proposed that if the level of Co is decreased in 740 then it will provide better resistance to corrosion. (Lu*et al*., 2018) examine the effect of cobalt content on oxidation and corrosion in coal fired power plants at 750ºC. Cobalt content was varied between 6-20% wt in three Ni-Fe based super alloys. Authors concluded that high sample with high percentage of Co shows good resistance to oxidation by forming a layer of Cr_2O_3 but on the other hand it does not stop the inward diffusion of sulphur. Therefore there is not much improvement in the corrosion resistance with high percentage of Co.

1.7.3.3 EFFECT OF TEMPERATURE

In future industries like gas turbine engines, steam turbines and coal gasification will reach new heights in terms of operating temperatures and efficiencies. These advancements in technologies bring challenges for engineers to develop corrosion resistant materials for these systems to minimize corrosive wear, which are the main factors responsible behind downtimes at elevated temperatures. But temperatures strongly affects the sulfidation tendency during hot corrosion of Ni based super alloys (Aung and Liu, 2014). Sulfides leads to the formation of low melting eutectic. Fe, Co and Ni base super alloys can also form low melting sulfides. Ni results in Ni_3S_2 and have a melting point of 635ºC, Co leads to Co_4S_3 with melting point of 880 ºC and iron forms FeS having melting point of 985ºC. Therefore Ni based super alloys are more prone to degradation in type-II hot corrosion in sulfur containing environments as they have lowest melting point among all super alloys.

However at high temperatures or type-I hot corrosion they perform better due to decrease in sulfidation rate (Aung and Liu, 2014). Authors have studied the effect on corrosion rate of Inconel-740 between temperature ranges 700-800ºC. They concluded that up-to 700ºC corrosion rate is within the limits, but as the temperature is increased to 750 ºC there is remarkable increase in the corrosion rate due to internal sulfidation and

titanium sulfide formation. Moreover when temperature was increased up-to 800ºC corrosion rate drops due to decrease in sulfidation and titanium sulfide formation.

1.7.3.4 EFFECT OF MOLYBDENUM (Mo)

Mo oxide can react with Na_2SO_4 and results in the formation of an acidic flux that ultimately leads to failure of the components. In literature authors have reported the effect of molybdenum in accelerating the hot corrosion of super alloys (Misra, 1986; Peters *et al.*, 1976). So super alloys which have high levels of Mo in their chemical composition should be avoided.

Although the IN625 alloys has good corrosion resistant properties, but owing to its poor wear resistance and low hardness, IN625 fails to meet the modern industries requirements. With the development of power plants for increased efficiency, parts must be built of stronger materials to extend the service life of structural components used in power plants. As a result, composite coatings containing IN625 and thermally stable reinforcing particles are a viable option for providing erosive wear protection in demanding conditions (Dooley, R. and Wiertel, 2009). The structural properties like hardness and toughness will further tuned effectively with development of composite coatings. Among ceramics, Al_2O_3 coating is a preferred candidate used to combat erosion and corrosion in high temperature applications, owning to their chemical inertness, high hardness and high melting point (Vasudev et al., 2020a; Vasudev et al., 2020b; Vasudev et al., 2021a). These coatings retain up to 90% of their strength even at 1100°C.

(Vasudev et al., 2020a; Vasudev et al., 2020b; Vasudev et al., 2021a), reinforced hard ceramic phase of Al_2O_3 (conventional and nano) with Ni based super alloy. The addition of hard ceramic phase not only improves the micro-hardness but also increases the oxidation and erosion resistance. (Wang and Lee, 2000) compared the erosion behavior and thermal shock resistance of three different composite coatings: a) NiAl-40Al_2O_3, b) Cr_3C_2-NiCr and c) Cr_3C_2/TiC-NiCrMo coatings. Authors found that the composite coating reinforced with Ni shows higher erosion resistance and maximum thermal shock resistance. Hence, Nickel-based composite coatings are the potential candidates, which

offer oxidation and erosive wear resistance at high temperature operating conditions in comparison with other metallic or ceramic based coatings (Edris *et al.*, 1997). Nickel can be used with elements such as Cr, Al, Mo, Mn, Nb, Ta and Si to increase the mechanical properties (hardness and toughness) and hot corrosion and erosion resistance of coatings as shown in **Fig.1.9**.

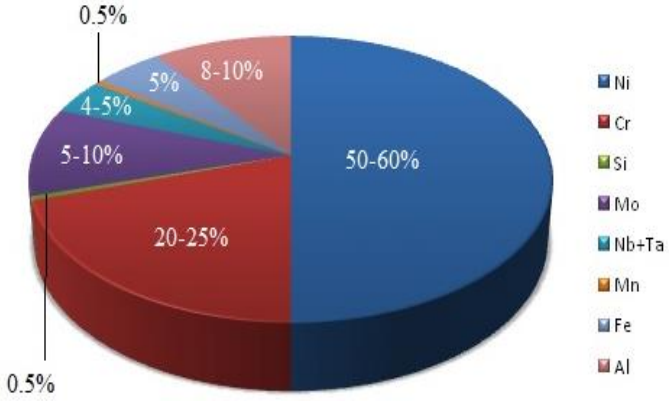

Fig.1.9 Probable elemental selection in Ni-based alloys.

1.8 ROLE OF NANO COATINGS

The demand for renewable energy sources for power generation has attracted the attention of the research community in the last decade owing to the depletion of fossil fuels and environmental issues. Extensive experimental investigations have been conducted to extract maximum energy from natural resources in the dams and power plants. The coating technologies play a significant role in protecting the components used in power plants. The thermal spraying technique is considered as an effective and economical hard-facing method for applying coatings consisting of multilayer stacks on the surface of structural components. However, the latest material development in the form of nano-size scale enhances the material properties like hardness, toughness, and resistance to sliding wear. This is mainly due to reduction in inherent defects and dislocation of grain boundaries. Hence, the deposition of nano-structured material leads to an engineered surface with outstanding coating efficiency. The main advantage of nano coatings is their capability to promote selective oxidation.

The novelty in the present work is the replacement of available Ni, Ni-Cr matrix with IN625 and to compare the effect of addition of 30wt% Al_2O_3 as reinforcement by varying the particle size in micrometric, nano and bi-modal form. The rationale for choosing a reinforcement content of 30wt% in this experimental work is due to the fact that if hard phase reinforcement exceeds a specific limit, it would alter the mechanical and tribological characteristics of the deposited coatings, as brittleness, and porosity of the composite coating increases which is detrimental for the coatings. In current experimental study, high-temperature erosion and oxidation performance of micrometric, nano and bimodal Al_2O_3reinforced with IN625 composite coating was evaluated. The composite coatings with various sizes of reinforcement particle were deposited using plasma spray technique. Commercially available ASTM SA210 GrA1 was selected as base material due to its wide use in the boiler tubes across northern region of India. Elevated temperature erosion and oxidation tests for bare substrate, micrometric, nano and bimodal composite coatings (both as-sprayed and heat treated) were conducted at 900°C with a hot air-jet erosion tester and silica tube furnace. The SEM/EDAX and XRD analysis were used for the microstructure characterizations of the samples. The outcome of the present research work may be helpful in enhancing the elevated temperature erosive wear and oxidation resistance in boiler steels.

Chapter 2

LITERATURE REVIEW

This chapter provides a complete assessment of the literature, with a focus on engineering materials' performance in elevated-temperature applications. The influence of the surrounding environment on component surface was investigated. The Plasma spraying method has been investigated and described in terms of high-temperature studies incorporating cyclic oxidation and air jet erosion. This focuses on the review of the latest developments that have taken place in the field of oxidation and erosion resistance coatings for elevated temperature by using different thermal spraying techniques with Nickel based powders, Nickel plus various reinforcements and also post heat treatments of the developed coatings. A lot of research is going on in the field of developments of wear and erosion resistance coatings for elevated temperatures. Following a careful assessment of the literature, the problem is formulated and the objectives were set.

2.1. SURFACE DEGRADATION OF BOILER TUBES

The most frequently occurring failure mechanisms in boiler tubes are of two types: (a) external damage of the surface, which includes oxidation, fatigue, corrosion, creep, erosion, degradation of the surface because of overheating (Lobley and Al-Otaibi, 2008; Malik *et al.,* 2005), (b) internal damage which includes microstructural damage. Failure of the boiler tubes occurs from time to time. Long-term overheating and fly-ash erosion (also termed as dry erosion) phenomenon's are associated with the degradation of boiler tubes. These major factors are responsible for the damage of boiler tubes used in the production of energy (Yu *et al.,* 2002). The maintenance expenses (damaged tubes) can rise to 54% of the total production cost (Suckling and Allen, 1997). Costs associated with erosion alone can rise to around US$150 million/year, as a whole solid particle erosion dramatically reduces the service life and performance of such

components. Therefore, to enhance the efficiency and reliability of the boilers, detailed investigations must be done on the failed boiler tubes. Identifying and rectifying the leading cause of tube failures is vital to help to minimize the chances of future problems. A comprehensive assessment is the most effective method of determining the root cause of a failure. A tube failure is usually a symptom of other problems. A schematic outline indicating the actual failure region of a failure associated with boiler water tubes working at elevated temperatures inside an industry at Hoshiarpur, Punjab. India is shown in **Fig.2.1.** Damage has occurred on the impact side of the tube. Ultimate failure results from the rupture due to increasing strain as tube material erodes. It was concluded that failure of bed coils occurred due to thinning of bed coil (Fig.2.1b) with time, caused by the abrasive nature of bed material ash which strikes the boiler bed coils with high velocity. As a result, thinning of bed coils occurs from the outer diameter of the tube.

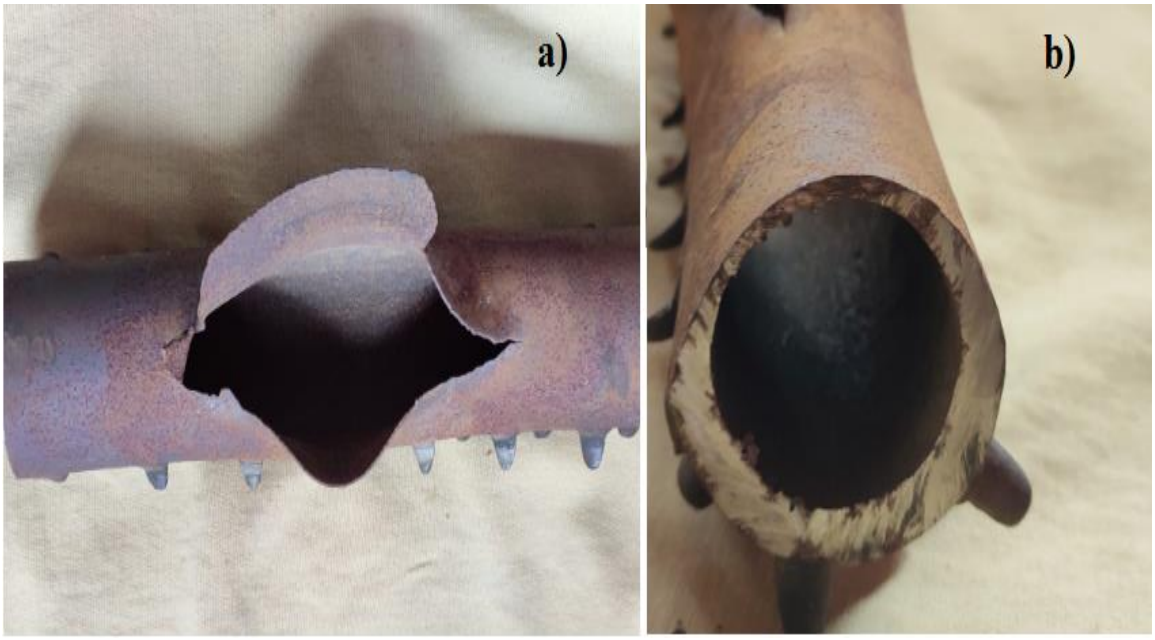

Fig.2.1 (a) Bursting of boiler bed coil tube, (b) thinning of wall tube due to erosion.

Nickel-based coatings are the potential candidates, which offer oxidation and erosive wear resistance at high-temperature operating conditions.

2.2. STUDIES RELATED TO NI-BASED ALLOYS AND COMPOSITE COATINGS DEPOSITED BY VARIOUS THERMAL SPRAY PROCESSES.

Sidhu and Prakash, 2005a, investigated the oxidation behavior of plasma sprayed Ni_3Al coating. Authors concluded that the oxygen penetrates the base metal and Ni_3Al plasma sprayed coatings fail to protect the substrate from oxidation due to loosely adherence porous scale comprising of NiO.

Sidhu *et al.*,2006b, developed Ni-Cr coatings on materials T-11, T-22 and GrA-1 by using HVOF technique. Hot corrosion behavior of all the coated materials was studied at temperature of 900ºC in a molten salt environment. From the characterization techniques it was reported that coatings successfully reduced the hot corrosion of T-11, T-22 and GrA-1in the order 94.13, 95.26 and 96.97% respectively. Major reason was the formation of oxides like NiO, $NiCr_2O_4$ and Cr_2O_3.

Singh *et al.,* 2007a, investigated cyclic oxidation performance of the Ni_3Al coatings at 900°C in the molten salt environment ($60\%V_2O_5$ and $40\%Na_2SO_4$) and air, on some nickel-based alloys. It was observed that the coatings, decreases the hot corrosion rates due to presence of protective oxide scales composed Al_2O_3, NiO and $NiAl_2O_4$.

Singh *et al.,* 2007b, Ni–20Cr alloy powder was deposited on three Ni-base superalloys; Superni 75, Superni 600 and Superni 601 by shrouded plasma spray process. Oxidation kinetics was established for the uncoated as well as the coated superalloys in air at 900 °C under cyclic conditions for 50 cycles by thermogravimetric technique. Each cycle consisted of 1 h heating followed by 20 min of cooling in air. The coating was found to be successful in maintaining its integrity with the superalloy substrates in all the cases.

Singh *et al.*, 2007c, conducted studies to ascertain the role of plasma sprayed Ni–20Cr–10Al–1Y (NiCrAlY) and Ni–20Cr metallic coatings to combat hot corrosion of a Ni based superalloy Superni 75. Both the coatings were found to be useful in protecting the base superalloy against oxidation. Moreover the coatings, in

general were successful in maintaining their continuous surface contact with the substrate superalloy during the whole tenure of cyclic exposure.

Yang *et al.,* 2008, found that erosion rate of mild steel substrate increases with increase in temperature (800˚C) both for oblique & normal impact angles. However, erosion rate decreases at elevated temperatures due to good resistance of HVOF sprayed Cr_3C_2-NiCr coatings.

Kaur and Prakash, 2009,Cr_3C_2-NiCr coating was deposited on SAE-347H boiler steel by HVOF spray method. Thereafter, high-temperature corrosion behavior of the bare SAE-347H and coated boiler steel was in quested at 700°C for total of 50 cycles. Under the specified conditions, the HVOF-spray Cr_3C_2-NiCr coating was successful in maintaining its adhesion.

Bala and Prakash, 2010,The hot corrosion demeanor of Ni-20Cr and Ni-50Cr coatings deposited onto the SA-516 (grade-70) and SA213-T22 boiler steels by using the Cold spray (CS) process was investigated. The performance of un-coated boiler steels and developed coatings was examined in simulated boiler atmosphere (Na_2SO_4-$60V_2O_5$) as well as in air under the cyclic conditions at 900°C for 50 cycles. The hot corrosion rate was calculated after each cycle by measuring the weight change of the specimens. Results exhibited that severe spalling of an oxide scale can be observed in un-coated boiler steels due to the formation of un-protective Fe_2O_3 scales. Oxides of Ni/Cr and their spinels decreased the hot corrosion rate in coated boiler steels.

Kaushal *et al.,* 2011, compared the hot corrosion performance of HVOF and Detonation techniques. Ni-20Cr coatings were deposited onto T-22 steel for experimentation studies. Authors reported that the HVOF sprayed coatings provides better resistance against hot corrosion at high temperatures whereas detonation gun sprayed coating exhibits spalling of oxide scale when exposed to molten salt environments.

Bala and Prakash, 2011,also compared HVOF and CS techniques with similar coating composition (Ni-20Cr) but in actual environments. It was found that HVOF outperform the cold spray in actual conditions.

Chatha *et al.*,2013, In their high temperature experimentation at 900ºC examined the Erosion-Corrosion performance for a duration of 1500hrs of Ni-20Cr alloy coating in the super-heater zone. From the results it was concluded that Ni-20 Cr coated steel outperforms the bare substrate due to presence of Cr_2O_3 in scale.

Kaur*et al*.,2012, The authors developed Cr_3C_2-25NiCr coating by using HVOF to evaluate the performance of the developed and bare steel in: a) air, b) molten salt and, c) in real boiler environments. Authors reported that after exposure there was no spallation of scale observed in coating and also it remains intact under all tested conditions.

Mishra *et al.,* 2013,The plasma-spraying process is widely used to deposit MCrAlY thick coatings or bond coats on the surfaces of industrial components to protect the degradation of surfaces from oxidation, corrosion, and erosion. NiCrAlY coatings were deposited on Superfer 800-H, superni-75, 600 and 718 by PS technique. From characterization techniques, it was concluded that due to the oxides of NiO, Cr_2O_3, Al_2O_3 and SiO_2, the Ni-20Cr coating on Superfer800-H showed maximum erosion resistance.

Hussain *et al.,* 2013b,studied four different Ni and Fe based compositions of alloys that were deposited by using the PS process and thereafter exposed in actual power plant conditions for 1000 h at 650°C under a coal ash deposit The Ni-Cr coating performed better than his counterparts (order being NiCr>FeCrAl>Alloy625>NiCrAlY).

Li *et al.,* 2014, investigated high temperature wear and oxidation behavior performance of CS nickel-alumina composite coating. When a Ni-Al_2O_3 feedstock powder was employed, a higher weight fraction of Al_2O_3 can be retained in as-sprayed coating by CS and composite coating exhibited a remarkable wear performance.

Singh *et al.,* 2015, 75Cr_3C_2–25(Ni–20Cr) coatings was developed onto the superni-75 superalloy substrate. The developed coatings were tested in actual medical waste incinerator plant and Na_2SO_4–10%NaCl environments at 900 °C. Microstructure obtained in cold spray coating was dense, hard, having fewer porosity levels which were significant to restrict the corrosive species to enter the substrate.

Kumar *etal.,* 2015, deposited nano Ni-20Cr (powder size 42 nm and 57 nm)coatings using CS process onto T-22 and SA-516boiler steels. Main purpose of the study is to examine the high temperature erosion-corrosion demeanor of nano-structured coatings. It was reported that after 1500 hr of exposure in actual conditions of thermal power plant, Ropar India only marginal loss in thickness was observed. This may be attributed o the fact that with decrease in powder size micro-hardness of the coating increases as compared to conventional powders and also due to the presence of protective oxides such as NiO and Cr_2O_3.

Mishra and Prakash, 2015, Ni-20Cr coatings were deposited by PS technique. and tested in actual boiler conditions. From characterization techniques it was concluded that due to the oxides of NiO, Cr_2O_3 Al_2O_3 and SiO_2, the Ni-20Crcoating on superfer 800-H showed the maximum erosion resistance.

Praveen *et al.,* 2015, deposited NiCrSiB/Al_2O_3 composite coating on SS-304 using APS technique. The coatings were put under tests at 450˚C to study erosion behavior at 30˚ and 90˚ impact angles and it was found that resistance to erosion increases in coated specimens as compared to bare samples. Greater resistance to erosion was shown at 30˚ impact angle due to pinning and shielding effect of alumina particles. Coatings show 2.5 times more erosion resistant than substrate. Micro-cutting and ploughing was the main erosion mechanisms.

Singh *et al.,* 2016, Cr_3C_2-25(Ni-20Cr) and Ni-20Crcoatings deposited onto T-91 boiler steel by HVOF process. Hot corrosion studies were carried out for duration of 50 cycles at a temperature of 900ºC in molten salt environment. Cr_3C_2-25(Ni-20Cr) performs better than its counterpart. Un-coated substrate exhibited higher weight gain because of un-protective Fe_2O_3 scale.

Chatha *et al.,* 2016, 75Cr_3C_2-25NiCr coating was developed onto T-91 boiler steel by HVOF technique. High temperature performance of both coated and un-coated was tested for 1500hr at temperature of 900ºC. Total of 15 cycles was used; each cycle consists of 100hr followed by 1hr of cooling. HVOF sprayed 75Cr_3C_2-25NiCr coating

shows good resistance against erosion-corrosion and has not shown internal oxidation attack which confirms that oxide scale of 75Cr_3C_2-25NiCr coating was found to be intact.

Mishra *et al.*, 2017, Ni_3Al powder were plasma sprayed on Ni and Fe base superalloys and evaluated at a temperature of 540°C in a super-heater zone of coal thermal power plant under cyclic conditions. After exposure to the actual conditions it was observed that Ni_3Al coating partially oxidize and coating remains intact even after 1000hrs of exposure and will act as a barrier against erosion-corrosion.

Singh *et al.*, 2017,The comparative cyclic high temperature oxidation behavior of NiCrAlY coating with uncoated substrate has been investigated experimentally. The cyclic oxidation studies were carried out at 900°C for 50 cycles. Each cycle consists of 1 hour heating in silicon carbide tube furnace followed by 20 minutes cooling in air. The NiCrAlY coating showed better resistance to high temperature oxidation due to the formation of Al_2O_3, Cr_2O_3, and NiO protective oxides which lead to a reduced rate of corrosion.

Zhang *et al.*,2017, Erosion behavior ofCr_3C_2-NiCr coating at three different temperature ranges 400, 500 and 600˚C were examined. The results showed that the coating may be more suitable for use in relative high-temperature conditions. The volume erosion rates of composite coating decrease with the increase in the erosion temperature. This may be related to the occurrence of plastic deformation and oxidation protection at high temperature.

Premkumar *et al.,* 2018, Studied the behavior of nano composite coatings. HVOF sprayed nano composite and conventional 27%Cr_3C_2-23%Ni-50%Cr coatings were deposited onto SA 210 Gr C. Erosion experiments were performed at temperature 450˚C and impact angles 30, 60 & 90˚. It was concluded that erosion resistance of nano composite was better than conventional & uncoated substrate due to presence of Cr_2O_3 layer that acts as a protective barrier against incoming erodent particles. Less porosity of nano composite was also found to be the reason for low erosion rates. At oblique angles erosion rate was higher for all materials showing ductile behavior. Moreover both nano

composite & conventional coatings provide 7.5 times & 3.5 times better erosion resistances at bleak (30˚) impact angle in comparison to uncoated substrate.

Prasanna, 2018**,** Examined high temperature corrosion resistance of Cr_3C_2-25% NiCr coated on alloy X22CrMoV12-1 at 600ºC. Formation of un-protective phases of Fe_2O_3 and MoO_3 leads to high corrosion rate of un-coated substrate. On the other hand formation of Ni_2O and $NiCr_2O_4$enhance the corrosion resistance of coated substrate in both molten salt and air environment.

Swaminathan*et al.,* 2019, studied microstructure and oxidation demeanor of nano-structured Ni-20Cr coating deposited on SA-516 grade 70 steel by using CS technique. Oxidation experiments were conducted at 900°C up to 50 hr in air. Coatings were examined by various characterization techniques (TEM, SEM, EDX, SAED, and FIB) before and after oxidation experiments. Authors observed that no cracking and spalling of scale takes place in coating after exposure. High-temperature oxidation resistance was provided by thin layer of chromium oxide along with nano-sized chromium oxide present within the nano-structured matrix. Furthermore, nano-sized Cr_2O_3 precipitates surround the nickel metallic grains and will serve as grain pinning objects. It was concluded that nano-structured Ni-20Cr coating exhibit enhanced oxidation resistance at 900°C.

Vasudev *et al.,* 2019,studied high temperature oxidation and erosion performance of both the coated and bare cast iron sample. The authors reported alloy-718 has a better oxidation and erosion resistance than cast iron substrate. Enhanced erosion resistance is associated with high micro-hardness and formation of protective and stable oxides like (Al_2O_3 and Cr_2O_3) on the exposed surface.

Praveen and Arjunan, 2019, deposited two weight compositions 1.4wt% and 0.17wt % of nano Al_2O_3 with NiCrSiB by HVOF technique. Authors reported that with addition of 1.4wt% nano Al_2O_3 micro hardness increases from 576 to 748Hv which in turn improves the erosion resistance.

Reddy *et al.,* 2019, Examined the high temperature corrosion behavior of HVOF sprayed Ni_3Ti and Ni_3Ti+(Cr_3C_2+20NiCr) coatings. Corrosion conditions were accelerated by applying 40%V_2O_5 and 60%Na_2SO_4 on to the specimen surfaces. Each

specimen was exposed to 50 cycles at temperature of 650ºC. Corrosion rate was reported in terms of weight gain/unit area. It was reported that coated specimens shows less weight gain as compared to bare substrates. The main reason for better performance of the coatings was due to the formation of protective oxides as reported during XRD analysis. Severe spalling of oxide scale was reported during analysis [74].

Vasudev *et al.,* 2020c, in another investigation examined the effect of microwave post processing technique on micro-structure and mechanical properties of alloy-718 coating that is deposited by HVOF technique. Authors reported that there was significant improvement in microstructure as porosity and micro-cracks were healed after post processing. SEM micrographs of as sprayed coating exhibits presence of un-melted particles and pores but after post processing healing of pores takes place due to flow of material during microwave processing. Furthermore micro-hardness, fracture toughness and surface roughness also improved.

Daram and Banjongprasert, 2020, also studied influence of post treatments onto the microstructure and corrosion performance of NiCrMoAlY alloy coating. Authors concluded that there is a reduction of pores after heat treatment that results in improving the corrosion resistance.

Singh *et al.,*2020, Two powder coating compositions, namely, Ni22Cr10Al1Y alloy powder and Ni22Cr10Al1Y (80wt%; microsized)–silicon carbide (SiC) (20wt%; nano (N)) powder, were deposited on a T-22 boiler tube steel. The hot corrosion behavior of bare and coated steels was tested at 900°C for 50 cycles. The Ni22Cr10Al1Y–20wt%SiC (N) composite coating was more effective than the Ni–22Cr–10Al–1Y coating against corrosion in the high-temperature fluxing process.

Vasudev *et al.,*2020a,IN718-Al_2O_3composite coatings were deposited on grey cast iron substrate using HVOF spray method. The effect of varying hard phase Al_2O_3 contents(10, 20, and 30 wt. %) on the microstructure, and oxidation resistance of IN718 coating were studied. Improved oxidation of composite coatings can be associated with the formation of protective and stable phases such as Al_2O_3, $NiCr_2O_4$ and Cr_2O_3.

Dhzurinskiy *et al.,* 2021, deposit plasma sprayed Cr_3C_2-NiCr based coatings on SS-304 L substrate and investigated its erosion performance. The coating developed features a dense microstructure with few flaws such as micro-cracks and pores, as well as high hardness and toughness. Enhanced erosion resistance will be attributed with high value of fracture toughness and hardness in developed coatings.

Sun *et al.,* 2021, investigated the erosion behavior and mechanical properties of atomspheric plasma sprayed NiAl-20 wt% Bi_2O_3 coatings with varying the Cr_2O_3 contents. The findings revealed that Cr_2O_3 greatly improved the coatings' mechanical strength without compromising their plasticity. In addition to this Cr_2O_3also improves the wear behavior of the coatings due to high hardness and plastic deformation resistance.

Ansari*et al.,* 2022,uses a plasma spray process to deposit Al_2O_3–TiO_2 coatings on three substrates. With thicknesses ranging from 200 to 250 µm, the deposited coating was found to be dense and homogeneous.The presence of protective phases (Al_2O_3, TiO_2, and $Al_2Ti_7O_{15}$) in the oxidized scale resulted in the deposited coating's strong resistance to the harsh oxidising environment.

2.3. RESEARACH GAPS

From available literature it is observed that very few attempts have been made to investigate the thermal spray coatings of super alloys combined with ceramics as reinforcement such as Al_2O_3, WC and SiC etc. Since, the composite coatings composed of superalloys as a matrix with reinforcements like Al_2O_3 in micrometric, and nanometric sized, and bi-modal forms of coatings deposition by using PS technique are still in research and development stage and hence have been selected for present research work.

Moreover, it is clear from literature that work is done only on conventional and nano-structured coatings by using Nimonic coatings like Ni-50Cr and Ni-20Cr. So in this work micrometric and nanometric sized and bi-modal forms of coatings are introduced in the form of the composite coatings of superalloys as a matrix with reinforcements like Al_2O_3 against high temperature erosion and oxidation.

There is need to study the mechanical and micro-structural characteristics of super alloys combined with ceramics in the form of composite coatings. Super alloys have high creep strength, good oxidation resistance, but due to ductile nature its hardness may be low and same can be improved by adding ceramics. Selection of substrate material for the present study has been made after the investigation of the literature survey and the past work done and future work that can be conducted and are feasible in the present life situations and may help the society. ASTM-SA210 GR A1 boiler steel has been selected as a substrate. Furthermore, the PS thermal spray technique has been selected for the present work as it offers the smoothest, hardest; well bonded coatings with the homogeneous microstructure. Further, the microstructure of coatings before and after the wear and corrosion test would be checked by using characterization techniques like FE-SEM/EDS analysis to ensure the effectiveness of coatings in terms of porosity, density, presence of semi-melted particles, cracks and to understand the failure mechanism of wear and corrosion.

2.4 PROBLEM FORMULATION

The basic reason behind the selection of this material was its extensive use in the manufacturing of boiler tubes. This material is widely used in the power plant by JCT Industries Limited. Chohal, Hoshiarpur. It was found during the plant visit that the boiler tubes fail due to two major reasons at elevated temperatures up to 900ºC (a) corrosion leading to dissolving of the protecting oxide layer resulting in the degradation of material, and (b) due to erosion of bed coil tubes because of the abrasive nature of ash particles. It has also been found in literature that a material which is subjected to any kind of aggressive environment will erode away from the surface with the passage of time and to enhance the surface properties of the material there is need to provide some protection on the interface of two bodies which are in contact. This research will focus on the prevention of surface by depositing nickel base super alloy in combination with ceramic phase (Inconel-625+30%Al_2O_3) which would help the material against such failures.

ASTM-SA210 GrA1 has been used as a substrate material due to its wide use in the manufacturing of boiler tubes.

2.5 RESEARCH OBJECTIVES:

The present work has been planned in order to fulfill following objectives:

1. To develop Inconel-625+30%Al_2O_3 composite coatings (micrometric and nanometric sized, and bi-modal/multi-modal) on metal based material (such as commercially available stainless ASTM-SA210 GrA1 boiler steel) through Plasma spray coating.
2. To examine the as-sprayed and post treated Inconel-625+30%Al_2O_3 composite coatings for comparison in terms of mechanical and micro-structural characteristics.
3. To characterize the as-sprayed and post heat-treated coatings through Mechanical, Metallurgical and Functional techniques that involves high temperature oxidation and erosion at 900°C**.**

Chapter 3

EXPERIMENTAL EQUIPMENTS AND METHODOLOGY

The method of coating deposition, as well as the process parameters of the apparatus employed to deposit the coating, are described in this chapter. The instruments/tools utilised to characterize uncoated and coated samples at different stages of the research effort have been detailed. The methodologies for cyclic oxidation and erosion testing studies at high temperatures were also discussed. The SEM/EDAX and XRD analysis were used for the microstructure characterizations of the samplesto characterize the products formed on the surface during studies and to understand the mechanism of wear.

3.1.METHODOLOGY

The proposed research work is aimed at the deposition of Inconel625+30%Al_2O_3 composite coatings by using Plasma spraying process and studying oxidation and erosion performance of these coatings on ASTM-SA210 GrA1, which is commonly used material of boiler bed coils. This work comprises of following phases:

- Inconel-625 powder with an average particle size of 40-50µm and Al_2O_3 powder in micron scale and nano scale with an average particle size of 40-50µm and 200nm were chosen as a coating material.
- ASTM-SA210 GrA1 boiler steel has been selected as substrate materials for the study (cutting of substrate according to various sizes according to the tests by using Wire-cut Electro-Discharge Machining process). For oxidation- 20mmx15mmx5mm, for erosion- 25mmx25mmx5mm at 90° impact angle and 25mmx20mmx5mm at 30° impact angle
- Deposition of coatings: The Plasma spray process has been chosen for the deposition of coatings on substrate material.
- Characterization of coatings using microscopic examination by using SEM-EDS and XRD analysis.

- Oxidation and wear test of coated and uncoated and samples in simulated boiler environment at high temperature 900°C by using the tube furnace and air-jet erosion tester.
- SEM-EDS and XRD analysis to characterize the products formed on the surface during oxidation studies and to understand the mechanism of wear.
- Comparison of all the coatings in order to find the best suited coating for high temperature oxidation and erosion resistance.

STEP-BY-STEP PROCEDURE

Following steps will be followed to accomplish the research objectives:

- **STEP 1:** Purchase of base material, cutting of material as per required size for deposition of coatings from Bharat Aerospace Limited, Mumbai [Substrate].
- **STEP 2:** Deposition of coatings using Plasma spray process by optimizing the parameters at MECPL, Jodhpur [coating services].
- **STEP 3:** Microstructural characterization of coatings with SEM-EDS and XRD analysis.
- **STEP 4:** High temperature oxidation test at 900°Cfor substrate and Plasma sprayed coatings.
- **STEP 5:** High temperature erosion test at 900°Cfor substrate and Plasma sprayed coatings.
- **STEP 6:** Characterization of oxidised and eroded samples with SEM-EDS and XRD analysis.

3.2 SUBSTRATE SELECTION

ASTM-SA210 GR A1 has been used as a substrate material due to its wide use in the manufacturing of boiler tubes. The composition of ASTM-SA210 GrA1 substrate is presented in **Table 4.1** in chapter 4. The chemical composition of ASTM-SA210 GrA1 was evaluated as per American society for testing of materials (ASTM) E 1086–08 standard using the optical emission spectroscopy technique (Make: Shimadzu, Model: PDA-7000).

3.3 COATINGS DEVELOPMENT

3.3.1 SUBSTRATE MATERIAL PREPARATION

The steel specimens were cut with electric-discharge machining (EDM) to the size of 25x25x 5mm^3 and 25x20x5mm^3 for erosion testing at 90° and 30°, respectively and for oxidation testing it was 20x15x5mm^3 shown in **Fig.3.1**. The setup employed for cutting of samples is shown in **Fig.3.2**. The cut samples were grit blasted using shot blasting machine with coarse Al_2O_3 powder (grit mesh size-16) before application of plasma spray coating (inset **Fig.3.3**). Surface roughness (R_a) value of 6µm was maintained for the substrate to ensure the better mechanical anchorage of coating powders with surface of substrate.

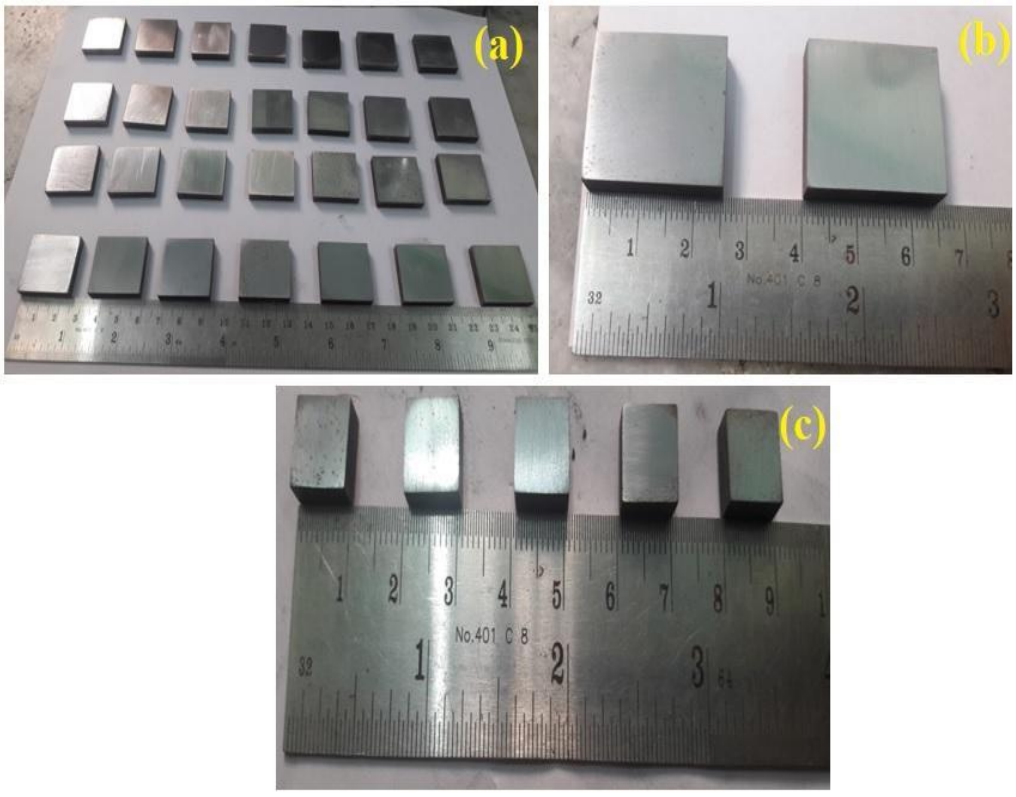

Fig.3.1(a) Specimens prior to coatings, (b) specimens for air-jet erosion test, and (c) specimens for cyclic oxidation test.

Fig.3.2 EDM M/C used for cutting of samples

Fig.3.3(a) Front view and (b) side view of shot blasting machine and, (c) medium of blasting (Virgin alumina)

3.3.2 COATING POWDER

Three distinct powder combinations containing IN625 and alumina were deposited on ASTM-SA210 GrA1 substrate utilising the Plasma S technique. The 30 wt% of Al_2O_3 was mixed with IN625 in the first combination. Then 30 wt% of nano-Al_2O_3 was blended with IN625 in the second combination. The third combination was prepared by mixing 15 wt% micrometric and 15 wt% nano-Al_2O_3 to form a bi-modal powder. The rationale for choosing a reinforcement content of 30 wt% in this experimental work was that if the hard phase reinforcement exceeds a specific limit, it would alter the mechanical and tribological characteristics of the deposited coatings. The characteristics such as brittleness, and porosity of the composite coating increase are detrimental to the coatings (Vasudev *et al.,* 2022; Grewal *et al.,* 2013; Vasudev *et al.,* 2021a; Kumar *et al .,* 2017). In chapter 4 of this study, the morphology and particle size of the powders, as well as their compositions, are discussed.

3.3.3 DEPOSITION OF COATINGS

The plasma spraying of composite feedstock powders was executed by an *F-4 PLASMA SPRAY* gun (*Make: M/s MEC, Jodhpur, Rajasthan, India*). The plasma spray process parameters employed for the development of composite coatings are presented in **Table 3.1**. The process parameters were selected as per the standard range suggested by the coating manufacture for IN625, Al_2O_3, and Ni-based composite coatings. The process parameters were selected after performing several trial runs before finalizing the final values. The coatings were visually inspected by experienced operators during the trial runs. The problems such as coating peel-off and de-lamination were also observed during the coating process. Therefore, the parameters were finalized accordingly, where coatings were shown well bonding to the surface of a substrate with no signs of distorted edges and peeling off for the final composite coatings. The expected thickness of the coating to be coated is determined by the average particle size of the feedstock powder and the number of passes. As a result, coating deposition with 40µm average particle size powder requires around 7 passes for a 280µm coating thickness.

Table 3.1 Illustrating process parameters employed for deposition of Plasma sprayed composite coatings.

Parameters selected for spraying/units	Values for composite coatings
Argon gas flow rate- slpm	40
Spray angle- degree	90
Powder feed rate (pfr)- g min^{-1}	30
Hydrogen gas flow rate- slpm	2
Nozzle size- mm	6
Spraying distance of substrate from gun- mm	101.6

3.4 COATINGS CHARACTERIZATION

3.4.1 SPECIMEN PREPARATION

For the cross-sectional characterization of the coatings, the coated specimens were sectioned, utilizing a slow-speed precision diamond cutter (Ducom Instruments, Bangalore). To get mirror polish finish, samples were then polished using a different grade of emery papers. Further, fine polishing of samples was achieved using 1 µm diamond paste. Appendix has more information about the diamond saw (**Fig.A-6**).

3.4.2 MEASUREMENT OF COATING THICKNESS

During the coating deposition process, the thickness was measured with a thickness gauge designed for thin films (Version: Minitest 2000; Manufacturer: Elektro-Physik Koln Company, Germany) with a precision of ±1µm. The thickness measurements were further confirmed by mounting and sectioning the deposited coatings according to the process outlined in section 3.3.1. The SEM/EDAX (*Produce: Carl-Zeiss, Type: Gemini ultra plus*) techniques was used for obtaining the cross-sectional back scattered electron (BSE) images. Appendix contains a detailed description of the

SEM apparatus (**Fig. A-3**). The average thickness of the deposited coating was calculated and observed using BSE images and same is presented in chapter 4 of the current study.

3.4.3 MEASUREMENT OF COATING POROSITY

The porosity content in coatings was determined using image analyzer software and BSE pictures as per ASTM-247 standard. The average values of ten readings of porosity were considered. Prior to measuring porosity, the sprayed samples were polished. For microstructure study, the coating's as-sprayed surface was polished down to 1200 grit emery size. Porosity was measured using a Dewinter inverted optical microscope (Version: LT-2B, Manufacturer: Chennai metco Pvt. Ltd, Chennai, India) and image analyzer software (Dewinter Material Plus, Model 4.3). Appendix describes the Dewinter inverted optical microscope in detail (**Fig. A-2**). The porosity is important property for the oxidation resistance of coatings. As more porosity in coatings will allow the harmful corrosive species to penetrate deep inside the coating and this in turn will initiate the formation of harmful oxides. These oxides delaminate the coating from the top of substrate thus initiating the failure of the coatings.

3.4.4 MEASUREMENT OF MICRO-HARDNESS

The Vickers micro-hardness tester was used to conduct the micro-hardness measurements (*Type: VH1MD, Produce: Chennai Metco, Chennai, India*). The hardness indents were made on the cross-section of coatings with a load of 300 g and a dwell time of 15s. Finally, for composite coatings, the average values of ten readings of micro-hardness were recorded. Appendix describes the micro-hardness tester in detail (**Fig. A-4**).

3.4.5 XRD ANALYSIS

By using the X-ray technique with Cu-K radiation, the patterns of feedstock powders and the various phases produced in the as-sprayed composite structures were investigated (*Bruker D8, Germany; at Lovely Professional University, Phagwara, India*). The different peaks generated were recorded with a scanning rate of 2°/min and 2θ range of 10° to 100°. Appendix describes the micro-hardness tester in detail (**Fig. A-1**).

3.4.6 FIELD EMISSION-SCANNING ELECTRON MICROSCOPY (FE-SEM) AND ENERGY DISPERSIVE SPECTROSCOPY (EDS) ANALYSIS

3.4.6.1 SURFACE MORPHOLOGY /CROSS-SECTIONAL ANALYSIS/EDS ANALYSIS

The SEM/EDAX (*Produce: Carl-Zeiss, Type: Gemini ultra plus*) techniques were used to analyze the surface morphologies of IN625 and Al_2O_3 feedstock powders (both micrometric and nano) and as-sprayed IN625-ALC, IN625-ALN, and IN625-ALB composite coatings. EDS mapping was used to determine the elemental distribution in the composite matrix. The coated specimens were gold coated to create elemental maps for the examination of different elements present on the surface and throughout the coating's cross-section. The surface morphology of as-sprayed coatings was investigated in order to identify melted splats, partially melted, un-melted particles, and pores created on the surface. For the cross-section analysis of the coatings before and after testing, samples were prepared according to the procedure outlined in section 3.3.1. Along with the point and line scans, SEM micrographs at various magnifications were taken. In Chapter 4 of the current research study, SEM/EDS examination of the as-coated and uncoated specimens was reported.

3.5 HIGH TEMPERATURE CYCLIC OXIDATION STUDIES

For oxidation studies, prepared samples were tested in simulated boiler conditions at a temperature of 900°C using a tube furnace (**Fig.3.4**). The test samples were coated from all the faces to maintain the identical condition and to minimize reading error. The simulated studies comprised of a total of 50 cycles; with every individual cycle of 1hr of exposure to temperature 900°C followed by air cooling at room temperature for 20min. These cyclic oxidation settings were chosen because they closely approximate actual industrial environment circumstances in which shutdowns are common. Cyclic studies provide more severe testing settings, which may be identical to the real-world industrial environment of repeated breakdowns and shutdowns (Verma and Kaushal, 2021; Kaushal *et al.,* 2010; Kaushal *et al.,* 2012; Kaushal *et al.,* 2014).

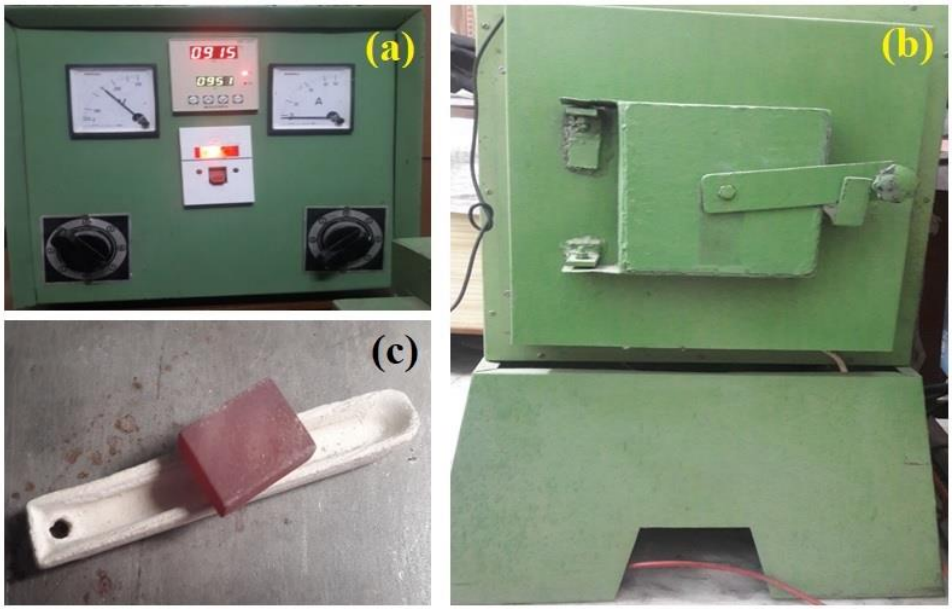

Fig.3.4(a) Controller of tube furnace (b) Tube furnace and, (c) Oxidised sample in alumina boat.

After the completion of every cycle, the weight change readings were taken using an electronic weight balance *(Model: ML-220)* with a sensitivity 0.01mg to approximate oxidation kinetics. For each cycle, three samples were examined and their average readings were noted down for analysis. The surface morphology of all samples was observed visually to record color changes followed by scale spalling during cyclic oxidation studies. The specimens after oxidation run were analyzed using XRD, SEM, and EDAX for surface analysis

3.6 EROSION TESTING

The erosion testing was carried out on a hot air-jet erosion test rig apparatus (*Model: TR-471-800, Manufacturer: Ducom instruments-India*) with ASTM standard G76–02 available with GNE, Ludhiana, India. The alumina particles with an average size of 60μm were utilized as erodent material. For the erosion tests, the alumina particles had a blocky and angular appearance and were fed at a rate of 6 g/min with a velocity of 60 m/s. At 900ºC, erosion testing was performed at 30˚ and 90˚ impact angles,

respectively. The schematic set-up of the High temperature air jet erosion test rig is presented in **Fig.3.5**. The coated and uncoated samples were tested for 10 min duration. Thereafter, the samples were taken out and cleaned with acetone, and then finally mass loss was calculated with weight measurement of the eroded samples. The erosive wear rate (g/g) is calculated as the ratio of erosive wear mass loss to the erodent particle mass. The erosive wear testing was conducted five times to ensure the test repeatability and then the average value was calculated. The mechanism of material removal was predicted by studying the eroded surfaces through the SEM images. The erosion testing set-up was not able to perform testing above 1000°C for ultra-high temperature range. But the boiler related issue involves a temperature of 900°C. Two angles i.e 30° and 90° were selected based on literature survey. In boiler tubes fly-ash strikes the surface of tubes at these two angles.

Fig.3.5(a) High temperature air jet erosion test rig set-up used for Experimentation.

3.7 FURNACE HEAT TREATMENT (HT)

To strengthen the quality of PS sprayed coatings, post-treatment of the coatings are necessary. Post-processing can be achieve during different approaches like HT, Microwave heating, electron-beam, laser beam, etc. Compared to other different post-treatment processes, furnace HT method is available easy and is a cost-effective approach. But improper HT parameter selection like range of HT temperature and its duration may yields negative results (Sadeghimeresht *et al., 2016).* The higher HT temperatures and long time durations leads to poor coating's performance as brittle fracture takes place due to thermal mismatch (Guilemany *et al.,* 2002).

Therefore, resistance to solid particle erosion solely depends upon the heat treated coatings microstructure. Generally, for ductile Ni-based materials, a standard HT technique as recommended by (Price *et al.,* 1992), called direct aging is recommended. The HT temperature lies in the range of 538°C to 900°C, and the duration of HT ranges between 0.5 hours to 22 hours, most suggested between 4 to 16 hours. Furnace employed for HT (*Model-RHF 1400; Make- Carbolite Gero*) in present experimental work is shown in **Fig.3.6.** Macrograph of coated samples before and after HT is shown in **Fig.3.6b.** The procedure followed for HT is shown in **Fig.3.7.** Initially samples were heat treated at 720ºC for 6 hrs, then temperature is reduced to 620 ºC and samples were heated at this temperature for 6hrs. After this samples were allowed to cool in furnace.

3.8 ANALYSIS OF CORROSION PRODUCTS

3.8.1 THERMO-GRAVIMETRIC STUDIES

The value of the parabolic rate constant (Kp) for all samples was evaluated using a standard linear least-square algorithm in the equation form $(x)^2 = Kp\ t$, where, 'x' shows the weight gain/surface area (mg/cm^2) and 't' show the number of oxidation cycles representing exposure time. Weight change data of the composite coatings in (mg/cm^2) versus 50 cycles are plotted. The surface morphology of all samples was observed visually to record color changes during oxidation testing.

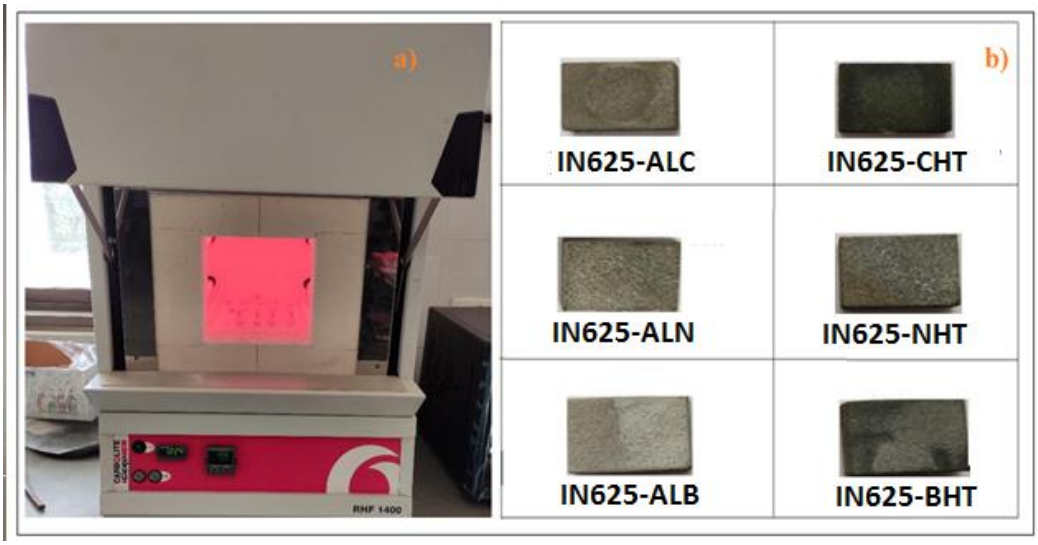

Fig.3.6 a) Furnace used in HT of the composite coatings, and b) Macrographs of composite coatings before and after HT.

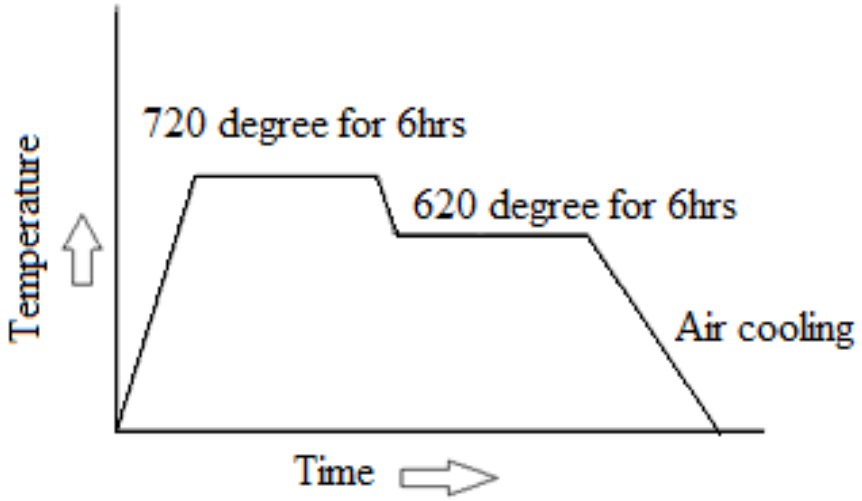

Fig.3.7 Procedure followed for HT of composite coatings.

3.8.2 XRD ANALYSIS

The main phases present in the oxidized(assprayed and heat treated coatings) were investigated using XRD (Make: Bruker, Model: D8-Advance) with Cu-Kα radiation source produced at 40 kV and 40 mA. The scanning angle range was varied from 10° to 100°, by a step width of 2°/min.

3.8.3 SEM ANALYSIS

The oxidized surface of ASTM-SA210 GrA1 and plasma sprayed coated samples (both as-sprayed and heat treated) were analyzed using SEM/EDAX micrographs from the cross-sectioned surfaces at different magnifications after 50 cycles of oxidation.

3.9 ANALYSIS OF EROSION TESTING

3.9.1 VISUAL OBSERVATIONS

In all the samples, the erosion starts at the center first, and then proceeds towards the edges of the samples. At a 90° impact angle the material is eroded forming a circular depression both for uncoated and coated samples; while at a 30° impact angle, material is eroded creating an elliptical shape depression. The macrographs of eroded samples clearly revealed three zones; a central area from where most of the eroded material has been produced, a second zone of faint color where somewhat lesser erosion can be seen and a third outside region where a negligible amount of erosion is observed. This can be clearly seen from the macrographs of the eroded samples.

3.9.2 SEM ANALYSIS

The erosive wear mechanism of the worn-out surface of ASTM-SA210 GrA1 and plasma sprayed coated samples (both as-sprayed and heat treated) were analyzed using SEM micrographs from the surface at different magnifications. Similar investigations were done on oxidized samples also

Chapter 4

As-Sprayed Composite Coatings Characterization

The current chapter focuses on the characterization of as-sprayed and heat treated composite coatings deposited by PS process. The coatings' surface and cross-section SEM/EDS analyses, as well as elemental mappings, are presented. The micro-hardness and porosity values of the coating combinations are reported. The reported findings are addressed in light of the existing literature.

4.1 ASTM-SA210 GRA1 SUBSTRATE

4.1.1 CHEMICAL COMPOSITION OF SUBSTRATE

ASTM-SA210 GrA1 has been used as a substrate material. The composition of ASTM-SA210 GrA1 substrate is presented in **Table 4.1.** The chemical composition of ASTM-SA210 GrA1 was evaluated as per American society for testing of materials (ASTM) E 1086–08 standard using the optical emission spectroscopy technique (Make: Shimadzu, Model: PDA-7000).

Table 4.1 Chemical composition of substrate (wt%).

Elements	Actual composition
C	0.27
Si	0.1
Mn	0.93
S	0.058
P	0.048
Fe	Bal.

4.2 COATING MATERIALS (FEEDSTOCK)

The IN625 was chosen because of its outstanding creep strength and thermal shock capabilities at high temperatures. The Al_2O_3 was selected owing to its thermal stability at high temperatures, less cost, and high hardness. The IN625 powder was supplied by *MECPL, Jodhpur, India*. The nano-Al_2O_3 was purchased from *Hangwu Group, Hong Kong, China*, and micrometric Al_2O_3 was procured from *HC Starc, Germany*. Three combinations of powders were used to deposit the coatings. **Table 4.2**presents the designation system used for the various coatings. Here HT means heat treated coatings. The 30 wt% of Al_2O_3 was mixed with IN625 in the first combination. Then 30 wt% of nano-Al_2O_3 was blended with IN625 in the second combination. The third combination was prepared by mixing 15 wt% micrometric and 15 wt% nano-Al_2O_3 to form a bi-modal powder.

Table 4.2 Nomenclature and the composition of the different composite coatings developed using plasma spraying.

Nomenclature	Matrix	Al_2O_3 size	Micro Al_2O_3 content %	Nano Al_2O_3 content %
IN625-ALC,	IN625	Micro	30	-
IN625-ALN and	IN625	Nano	-	30
IN625-ALB	IN625	Micro + nano	15	15
IN625-CHT,	IN625	Micro	30	-
IN625-NHT and	IN625	Nano	-	30
IN625-BHT	IN625	Micro + nano	15	15

The morphological characteristics of coating powders IN625 and Al_2O_3 (both micrometric and nano) are presented in **Fig.4.1**. The micrometric-Al_2O_3 powder showed a flaky and angular appearance with the average size of Al_2O_3 particles approximately 50

μm (**Fig.4.1b**). The less degree of sphericity of micrometric-Al_2O_3 powders would almost likely be detrimental to their flowability, which lowers the coating performance. The EDS corresponding to location 2 in **Fig.4.1(e)** shows the dominance of Al and O in Al_2O_3 powders. On the other hand, the agglomerated alumina powders had a substantially higher degree of sphericity. It can be compared with the traditional fused and crushed micrometric-Al_2O_3 powders with an average size of 200 nm (**Fig.4.1c**). Furthermore, the fine nanostructures in the agglomerated nano-Al_2O_3 powder particles were highly retained. IN625 exhibits a spherical form (**Fig.4.1a**) with an average size of about 40 μm. For IN625 powder, EDS reports have validated the presence of Cr, Ni, and Mo as major elements corresponding to spot 1 (**Fig.4.1d**).

The morphological details of the processing and blending of powders are presented in **Fig.4.1(f).** Point 1 represents the IN625-ALC powder in **Fig.4.1(f).** The nano-Al_2O_3 was obtained in an un-agglomerated form from the supplier. To assure the flowability of the powder during the coating process, the powder was agglomerated by employing a manual agglomeration practice (Point 2 in **Fig.4.1f**). A small fraction of nano-sized Al_2O_3 powder particles (25 g) were placed in a glass mortar in this approach. Appendix contains a detailed description of the agglomerated apparatus (**Fig. A-5**).This powder was steadily mixed with a glass pestle, and the slurry of 10% polyvinyl alcohol and distilled water was added to it drop by drop. A visual inspection and assuring flowability of the treated nano-Al_2O_3 particles inside the glass mortar proved their agglomeration. A broad range of powdered agglomerates with sizes ranging from 15 μm to 150 μm was obtained during the granulation process. This size range of powder particles was incompatible with the plasma spraying method. As a consequence, mechanical sieving was used to achieve powder particles in the 25–65 μm size range, as desired for plasma spraying.

To eliminate the moisture in the powder, the agglomerated particles were dried in an oven at 140ºC for 6 h. Finally, feedstock powders were blended for 5 h at 400 rpm in a V-type mixer(mechanical mixing) to achieve a homogenous combination. The

morphological details of IN625-ALN and IN625-ALB blended powders are presented in Point 3 and Point 4 in **Fig.4.1(f)**

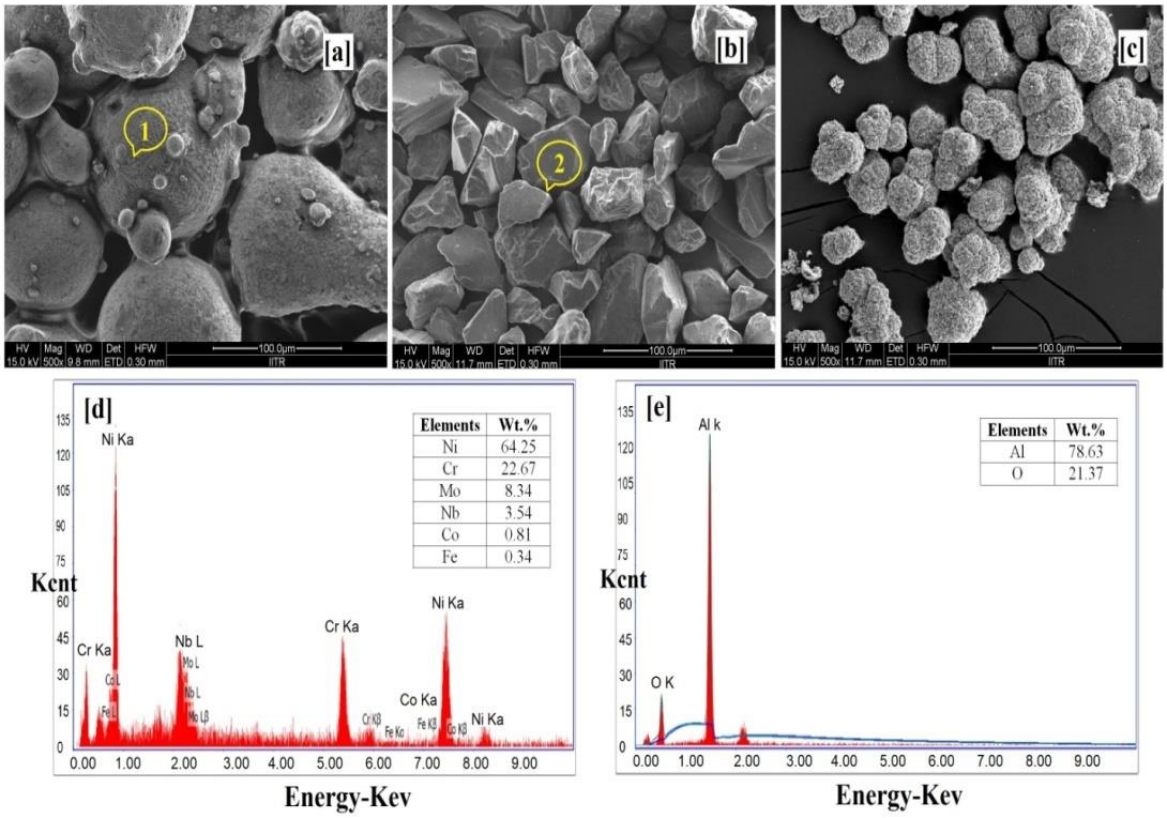

Fig.4.1(a) SEM micrograph of IN625 powder, (b) SEM micrograph of micrometric-Al_2O_3, (c) SEM micrograph of micrometric nano-Al_2O_3, (d) EDS corresponding to point 1 for IN625 powder, (e) EDS corresponding to point 2 for micrometric Al_2O_3 powder and, (f) details related to the processing of different powders,. ***contd. on next page***

XRD peaks of coating powders IN625 and Al_2O_3 (both micrometric and nano) are presented in **Fig.4.2.** IN625 XRD pattern indicated γ-phase (111) (**Fig.4.2a**), where γ represents a solid solution composed of Ni-Cr with FCC structure (*JCPDS refer. no. 00-001-1243*). The XRD patterns for micrometric and nano-Al_2O_3 coating powder corresponding to α-Al_2O_3 as a major phase are shown in **Fig.4.2(b) &(c)**, respectively. The composition of feedstock powders and ASTM SA210 GrA1 substrate is presented in **Table 4.3.**

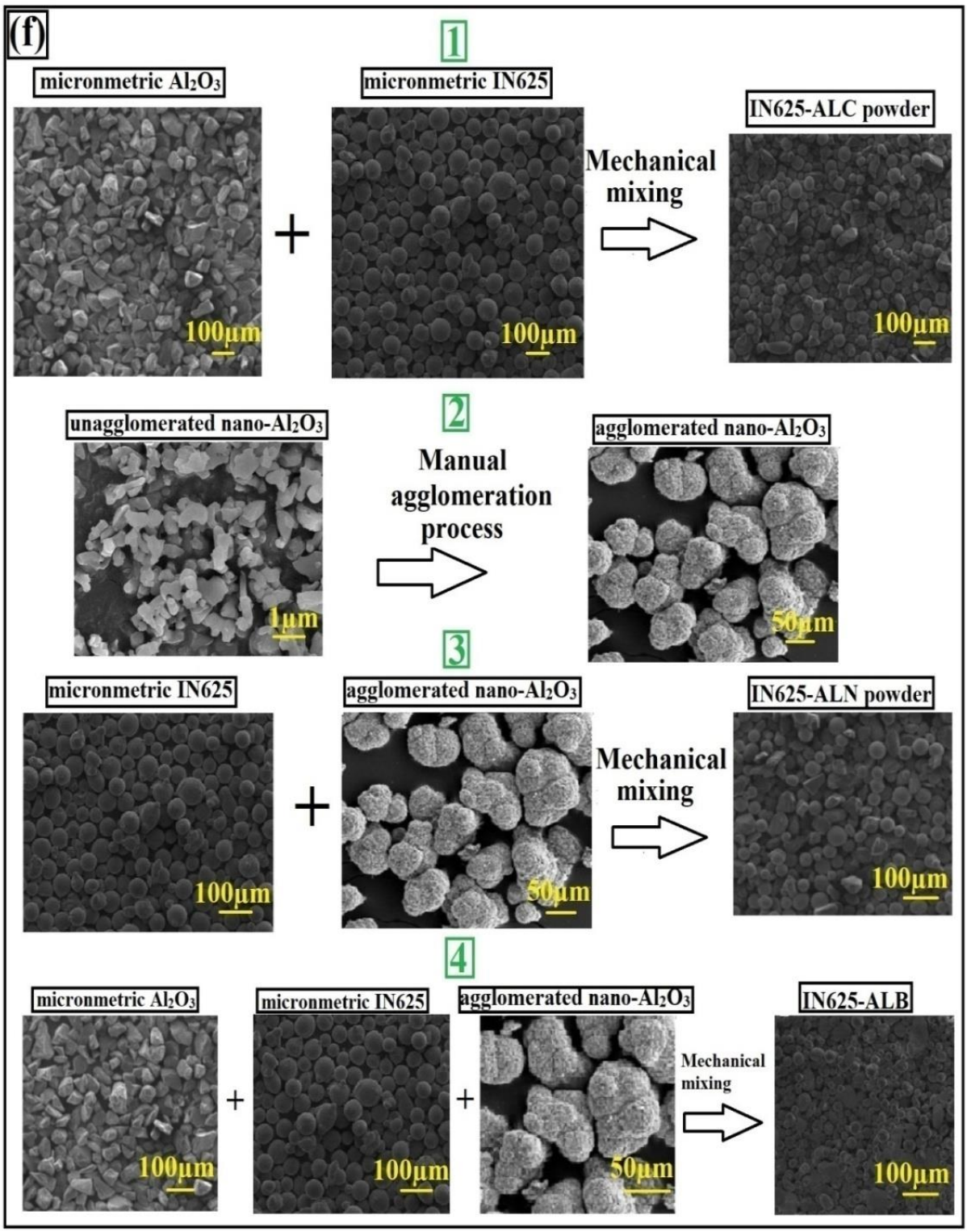
(f)
1
micronmetric Al_2O_3
micronmetric IN625
IN625-ALC powder
Mechanical mixing
100µm
100µm
100µm
2
unagglomerated nano-Al_2O_3
Manual agglomeration process
agglomerated nano-Al_2O_3
1µm
50µm
3
micronmetric IN625
agglomerated nano-Al_2O_3
IN625-ALN powder
Mechanical mixing
100µm
50µm
100µm
4
micronmetric Al_2O_3
micronmetric IN625
agglomerated nano-Al_2O_3
IN625-ALB
Mechanical mixing
100µm
100µm
50µm
100µm

Fig 4.1 contd.

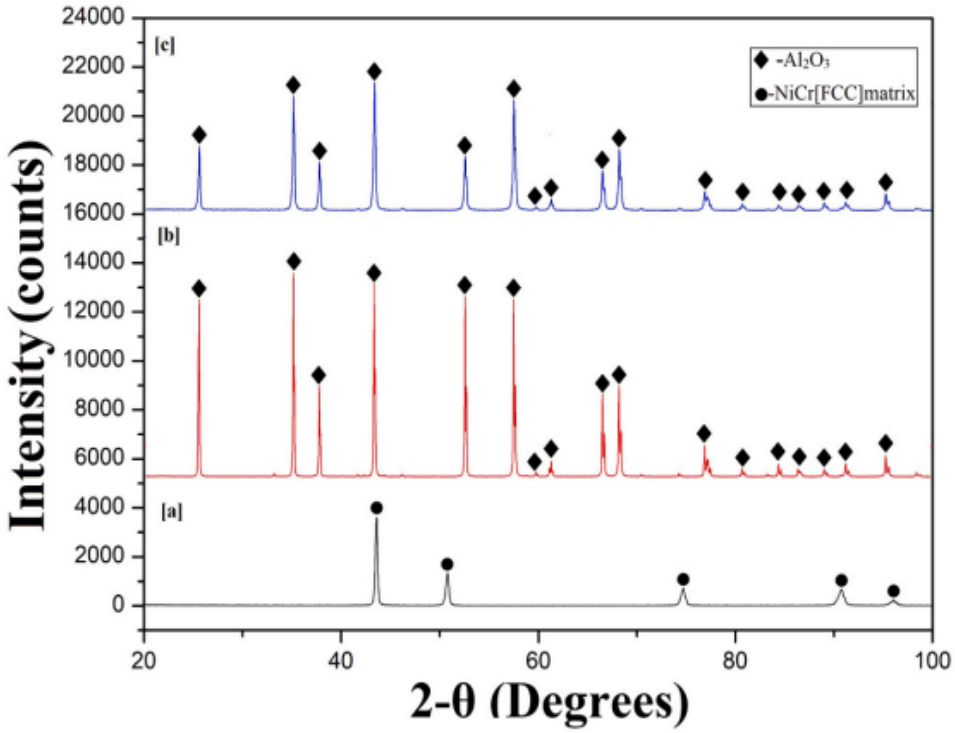

Fig.4.2(a) XRD of IN625, (b) micrometric-Al_2O_3 and, (c) nano-Al_2O_3 powders.

Table 4.3 Nominal composition of materials used (wt%).

Materials	**C**	**Si**	**Mn**	**S**	**P**	**Mo**	**Cr**	**Ni**	**Nb**	**Al**	**O**	**Fe**	**Others**
Substrate	0.27	0.1	0.93	0.058	0.048	-	-	-	-	-	-	Bal.	-
IN625	0.01	-	-	-	-	8.89	21.98	63.25	3.65	-	-	0.34	Bal.
Al_2O_3	-	-	-	-	-	-	-	-	-	78.63	21.37		-

Macrograph of coated samples before and after HT is shown in **Fig.4.3**. The as-sprayed IN625-ALC (inset **Fig.4.3a**), IN625-ALN (inset **Fig.4.3c**), and IN625-ALB

(inset **Fig.4.3e**) is lighter in color in comparison to heat treated IN625-CHT (inset **Fig.4.3b**), IN625-NHT (inset **Fig.4.3d**), and IN625-BHT (inset **Fig.4.3f**) composite coatings. All of the deposited coatings had no visible cracks on their surfaces and appeared to be smooth.

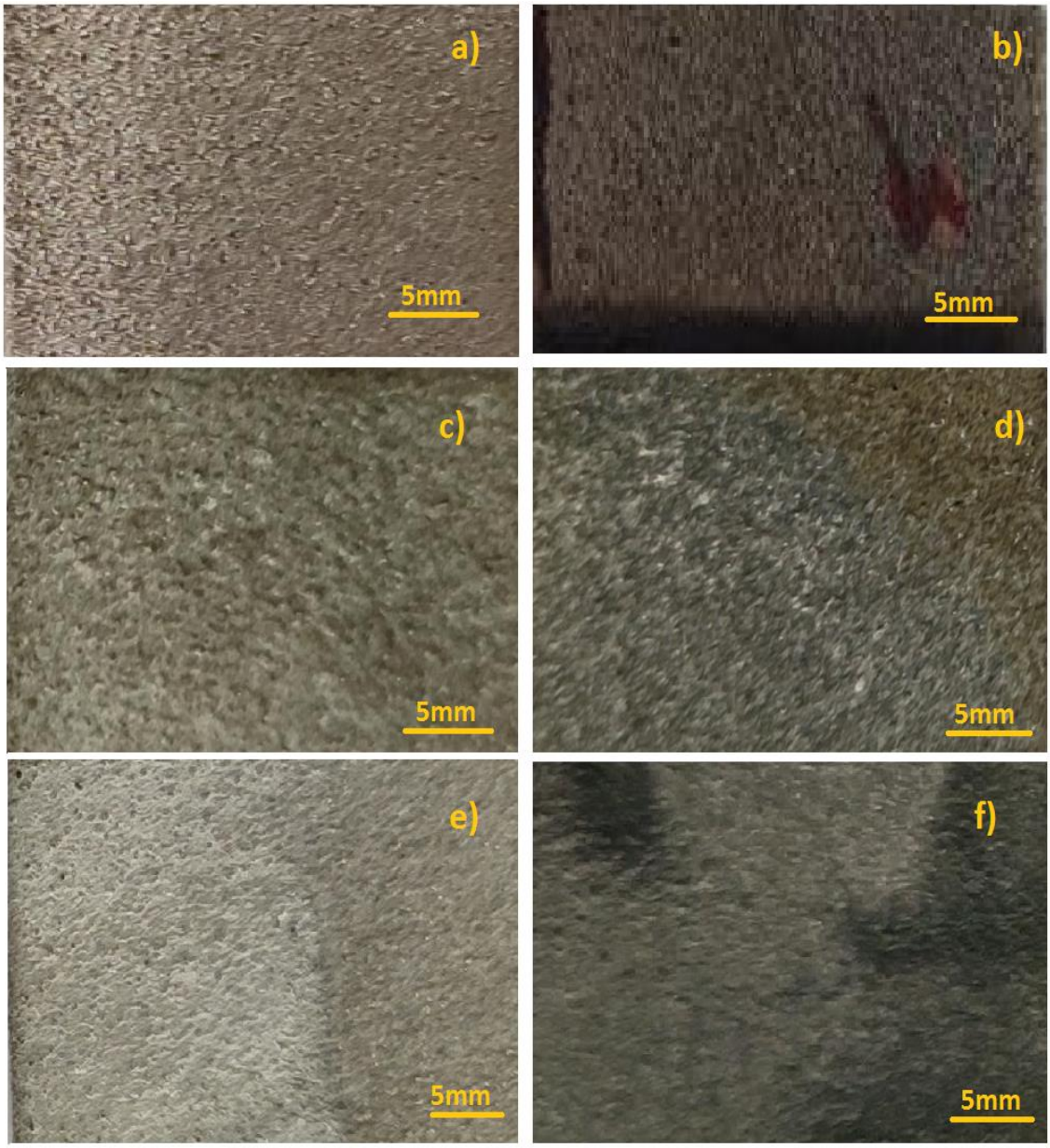

Fig.4.3 Macrograph of coated samples before and after HT: a) IN625-ALC, b) IN625-CHT, c) IN625-ALN, d) IN625-NHT, e) IN625-ALB, and f) IN625-BHT.

4.3 AS-SPRAYED COATINGS SEM ANALYSIS

4.3.1 ANALYSIS OF SURFACE MORPHOLOGY

SEM micrographs of plasma-sprayed IN625-ALC, IN625-ALN, and IN625-ALB composite coatings, respectively is exhibited in **Fig.4.4**. The composite coating IN625-ALC exhibits splats, partial melted and un-melted particles along with the presence of pores, some cracks, and voids as shown in **Fig.4.4(a)**. The pores and voids are likely to appear in plasma spray coatings. The pore formation is primarily due to the differences in the cooling velocity of feedstock particles and gas expelled from the molten droplets during the solidification process (Yin *et al.,* 2007; Praveen *et al.,* 2015). For a given condition of plasma jet (axial and radial temperature gradient drop), the big size particles were insufficiently heated and could lead to big differences in particle cooling velocity. The partially melted particles were also noticed in the magnified SEM images (inset **Fig.4.4b**), which may be developed owing to insufficient temperature. Further, un-melted particles remained on the surface of the coating and rebounded out to develop irregular stack morphology. Lastly, owing to the thermal stresses few cracks were also seen in the coating microstructure (**Fig.4.4b**). These cracks might have been developed as a result of high-energy hits from incoming splats or as a result of the cooling process.

The dispersion of nano-alumina particles in the IN625-ALN composite coatings was found to be nearly uniform. The fewer cracks and pores caused by the technical characteristics of plasma spraying can be observed in **Fig.4.4(c)**&**4.4(d)**, respectively. The Al_2O_3 splats were noticed as white regions with the dark greyish IN625 matrix.

The IN625-ALB composite coatings have represented a duplex structure. The structure was comprised of completely melted splat lamellae (IN625) and un-melted or partial melted areas of nano-Al_2O_3 particles within the splats (**Fig.4.4f**). The un-melted state of nano-alumina particles could be primarily related to two factors. The first one is the use of agglomerated Al_2O_3 nano-powder for IN625-ALN and IN625-ALB composite coatings in comparison to crushed and fused solid Al_2O_3 particles for IN625-ALC. The second factor is the less residence time for Al_2O_3 particles inside the plasma jet. There is

a limited time for Al_2O_3 agglomerated powders to melt completely in comparison to micrometric Al_2O_3 powders. In comparison with micrometric sized powder, nano-scale powder exhibits less thermal conductivity. The behavior of melting may be distinct, depending upon their trajectory and size in a hot plasma jet (Vasudev *et al.,* 2021a; Vasudev *et al.,* 2021b).

Moreover, nano-sized Al_2O_3 powder is reconstituted in the granular form that enters into the different regions of the plasma plume during plasma spray. The powder particles have not remained in the center of the plasma plume owing to their low weight and thereby resulted in the partial melting of a nano-powder. Whereas powder passing within the central zone of the plasma plume gets completely melted, leading to a bimodal structure comprised of partially and fully melted particles. Finally, the coating properties rely strongly on the splats morphology deposited on the surface of a substrate by plasma spray. The surface and splats were free from splashing in IN625-ALN and IN625-ALB composite coatings (**Fig.4.4d & f**).

The heat treated microstructure of coatings IN625-CHT, IN625-NHT, and IN625-BHT on the other hand indicates reduction in number of micro-pores and cracks as shown in **Fig.4.5**. The pores are the most common pathways for the corrosive species to enter into the substrate. (Sidhu and Prakash, 2005b)found diffusion and oxidation of Fe from the substrates to the upper layer of scale along with the oxidation of the substrate steels, which has been attributed to the porosity and ultimately it will decline the bonding strength of coating. Some infiltration of harmful corrosive species is reported even in case of HVOF sprayed coatings (Uusitalo *et al.,* 2004). HT of thermal spray coatings improve the corrosion resistance of deposited thermal spray coatings by transforming the microstructure form lamellar to bulk-like (Sundararajan*et al.,* 2009; Bolelli*et al.,* 2008a).

The microstructure of composites IN625-CHT, IN625-NHT, and IN625-BHT appears to be dense and homogenous as shown in **Fig.4.5a, b, & c** respectively. This may be related with the fact that during HT exposure at 720ºC for 6hr, the diffusion process occurs in the composite coatings and moreover due to precipitation strengthening heat treated coatings exhibits dense microstructure and good mechanical properties. These HT

results are in agreement with the previous available studies in literature on Nickel based coatings (Gil *et al.*, 2002; Bansal and Zafar, 2017; Bansal *et al., 2017*). EDS analysis for the heat treated composite coatings reveals the strong dominance of Cr, Ni, Al and O (inset **Fig.4.5**). High presence of O element along with elements Cr and Ni in the composition affirms the possible development of oxides of Al, Cr and Ni.

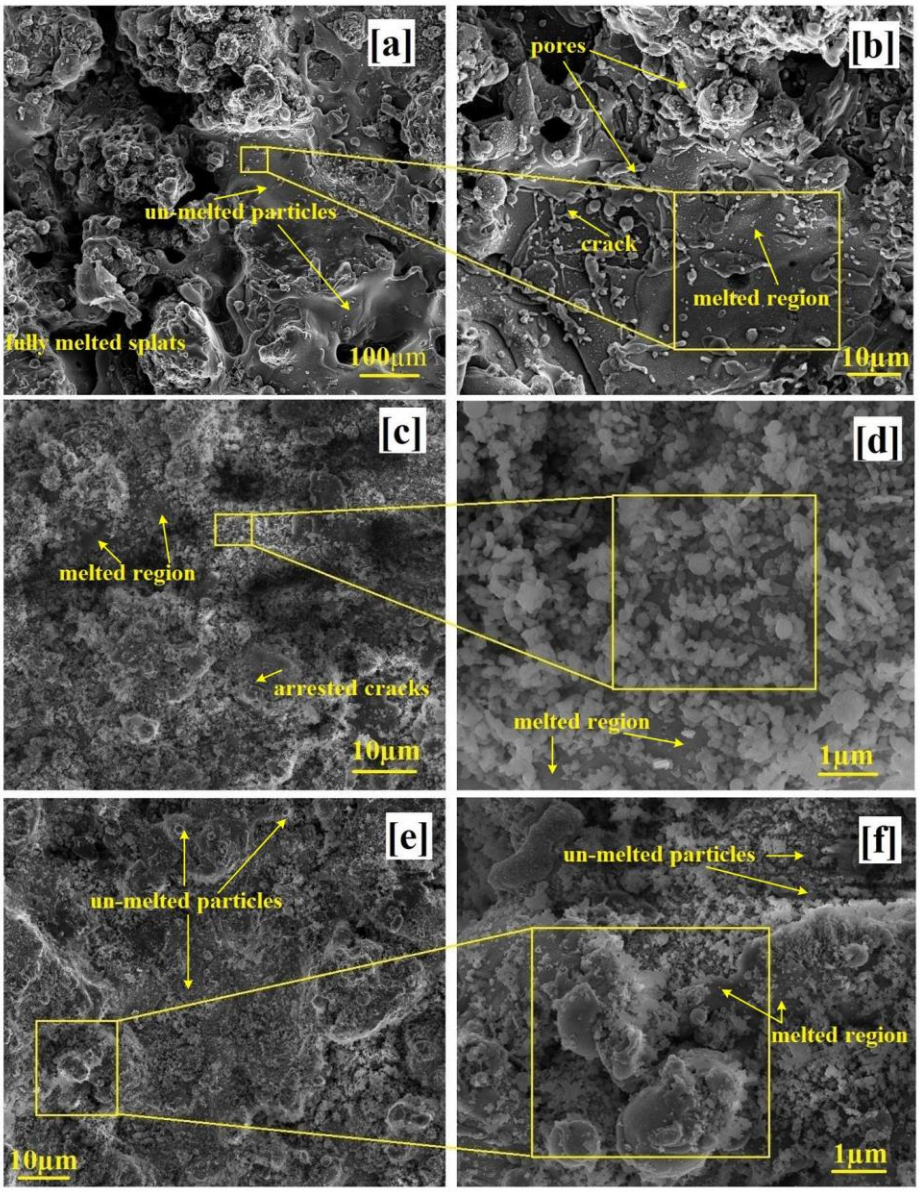

Fig.4.4 SEM images of as-sprayed (a & b) IN625-ALC coating, (c & d) IN625-ALN coating, (e & f) IN625-ALB coating.

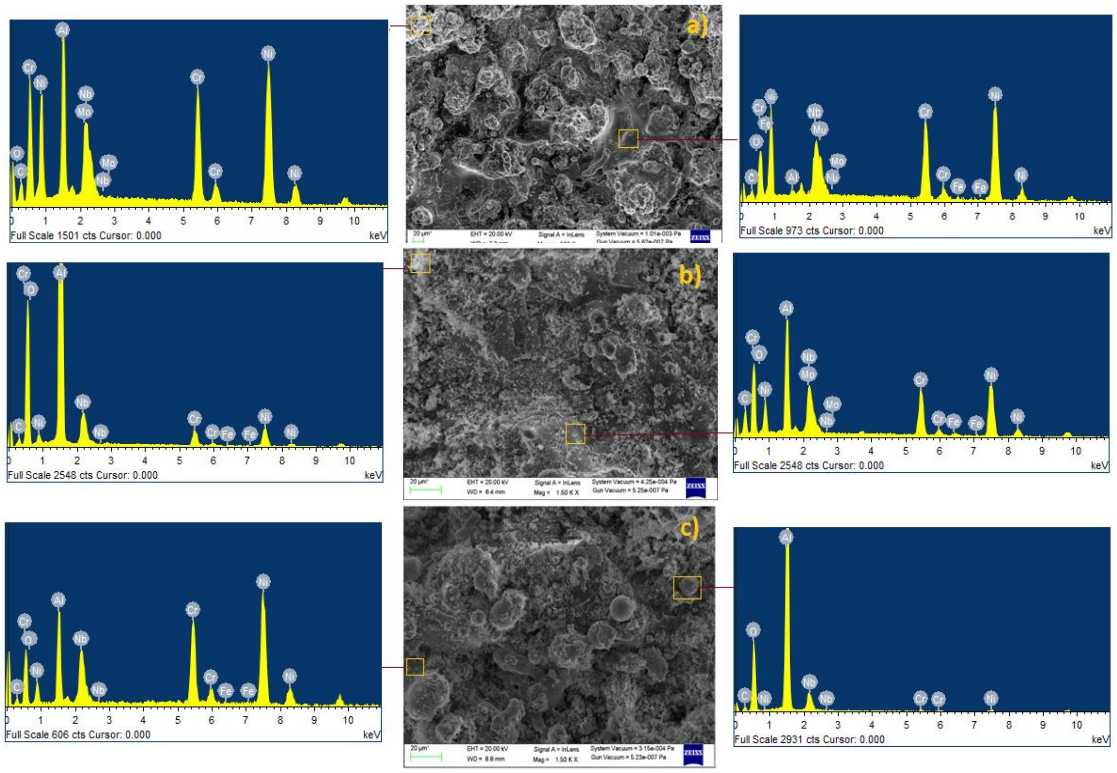

Fig.4.5 SEM/EDS images of heat treated: a) IN625-CHT coating, b) IN625-NHT coating, and (c) IN625-BHT coating.

4.4 X-RAY DIFFRACTION (XRD) ANALYSIS

The XRD results of plasma spray deposited IN625-ALC, IN625-ALN, and IN625-ALB composite coatings are presented in **Fig.4.6.** XRD analysis indicates peaks of Ni-Cr (FCC phase) in the IN625-ALC, IN625-ALN, and IN625-ALB composite coatings. A few low-intensity peaks of Cr_2O_3 were also observed in all deposited coatings. The XRD pattern of alumina *(JCPDS reference no.00-001-1243)* demonstrates the presence of the α-Al_2O_3 phase in the feedstock powder. It indicates that Al_2O_3 has maintained its identity even during the deposition of coatings. The Al_2O_3 in all coatings is corundum α-phase and this may be due to the following mentioned reasons. Firstly, the lower spraying velocity was achieved during plasma spray allowed for higher corundum content in the deposited coatings. This finding can be explained by the fact that the

feedstock powder is fused in the hot flame of plasma during the deposition, resulting in the formation of γ-alumina. But γ-Al_2O_3 can be converted back to corundum α-phase as the granules in the deposited coatings cool more slowly owing to lesser spraying velocities. Secondly, due to shorter residence times at higher temperatures, part of the initial corundum α-phase has not converted to γ-alumina and was retained in the final deposited coatings, thereby maintaining the primary powder nanostructure. Finally, in the SEM micrographs (**Fig.4.4d&f**), Al_2O_3 particles can also be seen in the un-melted form in the deposited coating. A portion of the low-weight agglomerated Al_2O_3 feedstock cannot reach the center of the spray flame. In this situation, a portion of the feedstock could not melt properly, resulting in the formation of the α-Al_2O_3 phase within the deposited coatings.

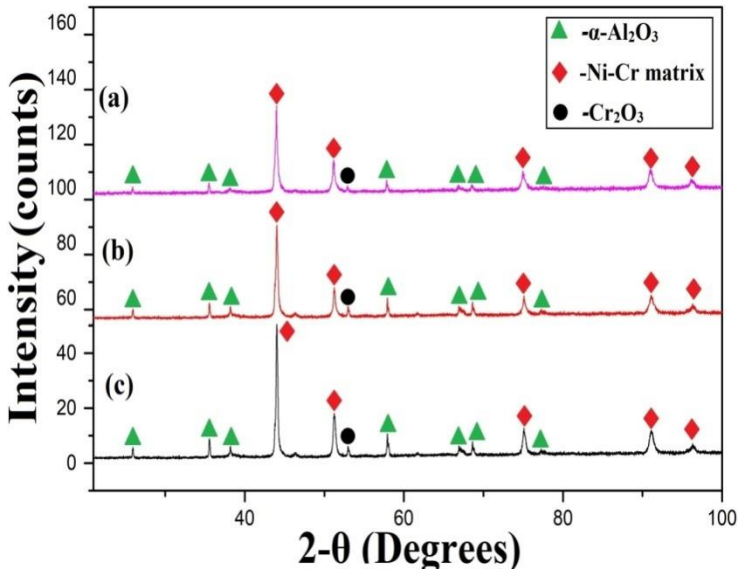

Fig.4.6 XRD patterns of the developed composite coatings: a) IN625-ALC, b) IN625-ALN and c) IN625-ALB.

The metal matrix dissolution affirm the peak broadening along with peak intensity reduction at 2θ of about 44º can be found for the as-sprayed composite coatings in contrast with the starting feedstock powders XRD pattern. This difference highlights the development of amorphous matrix in as-sprayed composites.

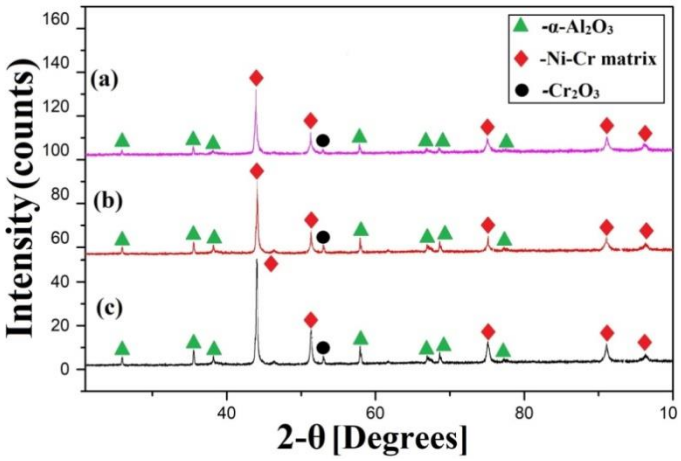

Fig.4.7 XRD patterns of the developed composite coatings after heat treatment: a) IN625-ALC, b) IN625-ALN and c) IN625-ALB.

Post HT is usually needed for achieving a dense coating along with high adhesion and cohesion strengths. The broad peak formed during plasma spraying became sharper after HT (inset **Fig.4.7**), reporting the amorphous phase transformation to crystalline.

The phenomenon of transformation of amorphous phase into crystalline has been suggested by (Gross *et al.*, 1998). These effects are consistent with the findings reported by (Morks, 2008) in literature.

4.5 CROSS-SECTIONAL ANALYSIS

The cross-sectional SEM micrographs of plasma-sprayed IN625-ALC, IN625-ALN, and IN625-ALB composite coatings are shown in **Figs.4.8-4.10**. As exhibited, all the plasma spray composite coatings were stacked tightly on the substrate with a coating thickness of around 250-300 μm. The magnified image of all the composite coatings (**Fig. 4.8b, 4.9b & 4.10b**) shows a tightly packed lamellar structure and indicates that molten particles were compacted more effectively. The distribution patterns of micrometric-Al_2O_3 and nano-Al_2O_3 show considerable differences. The flattened splats can be seen in the IN625-Al composite coating with micrometric reinforcement as shown in **Fig 4.8b.** The organic binder (PVA) used for agglomeration of nano-Al_2O_3 powders was burned during the deposition process in a plasma torch. The agglomerate nano-Al_2O_3 powder

was dissociated, resulting in the creation of fine granules and splats in the IN625 matrix (**Fig.4.9b**). Some of the nano-Al_2O_3 particles were not melted sufficiently and retained in the IN625-ALN coating. In the IN625-ALB composite coating, the Al_2O_3 and flattened splats can be observed, with axes essentially parallel to the plane of the substrate. The same has better interfacial consistency with the IN625 matrix, pointing out that the added reinforcements are molten (**Fig.4.10b**). The presence of a dark phase in all composite coatings indicates the Al_2O_3 hard phase, which was further confirmed by the EDS mapping of all three composite coatings as shown in **Fig.4.8-4.10**. Other researchers have documented the presence of Al_2O_3 in the microstructure in the form of a dark phase (Grewal *et al.,* 2013; Kumar *et al.,* 2017). The presence of alumina at these locations was confirmed with X-ray maps. A-line scan has revealed huge random changes in Al and oxygen percentages. It is also worth noting that these locations are evenly dispersed over the majority of the cross-section. The EDS analysis of plasma spray coatings reveals a high concentration of Cr and Ni throughout the thickness of the coatings. The lack of Fe along the coating thickness implies that no diffusion took place from the substrate to the coating. The elemental wt.% of various elements present in the coating region corresponding to the (**Fig. 4.8a, 4.9b, and 4.10a**) coatings has been represented in **Fig.4.11. Fig.4.11 (a-c)** shows the dominant presence of elements present corresponding to the elements present in the powders. IN625-ALC and IN625-ALN showed a similar wt.% in the coating region as presented in **Fig. 4.11(a) and 4.11(b),** respectively. The concentration of Al and O is somewhat higher than the other two coatings and is attributed to the high intensity of α-Al_2O_3 in IN625-ALB coating as presented in **Fig.4.11(c).** The wt.% of all elements corresponding to the coating region are shown in **Fig. 4.11(d).**

The elemental distribution is also projected on the line scan region in **Fig.4.12.** The black phase correlates to hard Al_2O_3 particles in the coatings as depicted in **Fig. 4.12(b).** There is Al and O enrichment and reduction of Ni, Fe, and Cr across this black phase in the area of the line scan.

The black phase correlates to hard Al_2O_3 particles in the coatings. The black phase has also been shown as alumina in previous studies on Ni-Al_2O_3 composites sprayed by distinct thermal spraying procedures (Grewal *et al.*, 2013; Kumar *et al.*, 2017). The percentage area of the black phase was calculated by image analysis software in IN625-ALC, IN625-ALN, and IN625-ALB coatings and was found to be 29 %, 29.60 %, and 29.95 %, respectively.

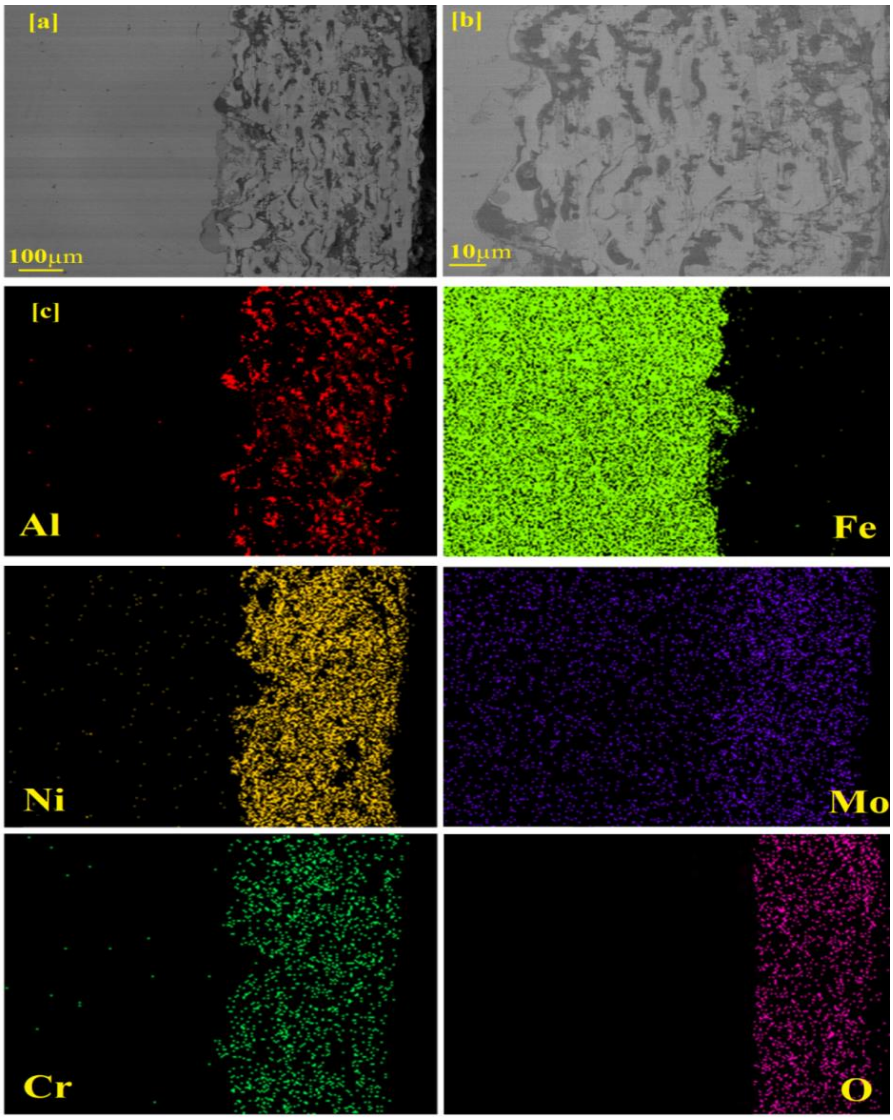

Fig.4.8 (a) Cross-sectional micrograph of IN625-ALC, (b) SEM micrograph at high magnification and, (c) x-ray maps corresponding to the SEM micrograph (Fig.4.8a).

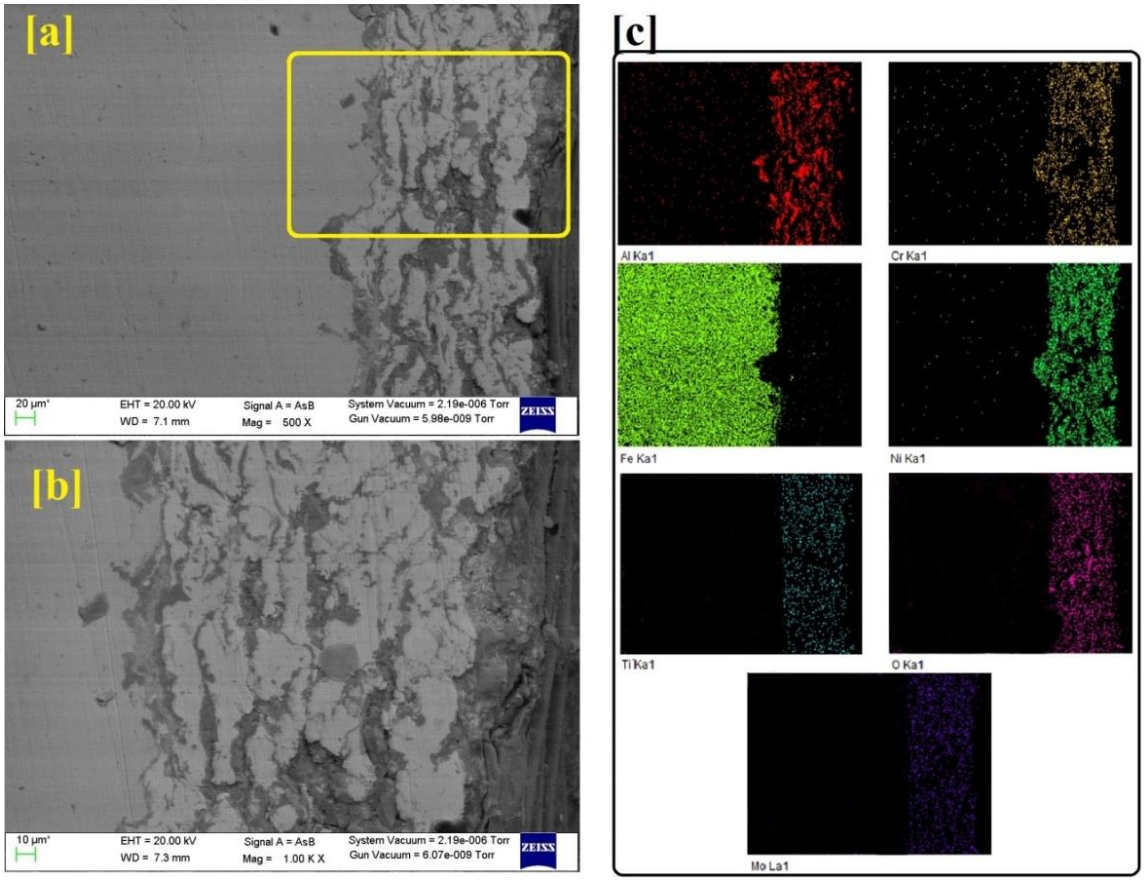

Fig.4.9. (a) Cross-sectional micrograph of IN625-ALN, (b) SEM micrograph at high magnification and, (c) x-ray maps corresponding to the SEM micrograph (Fig.4.9a).

On the other hand heat treated coatings showed a positive effect on to the characteristics of plasma sprayed coatings. It can be noticed that HT of as-sprayed coatings resulting in a homogeneous and dense microstructure. A total thickness of 250-300 µm was measured for both as-sprayed and heat-treated coatings. This demonstrated that HT has no effect on coating thickness. (Fernandez *et al.*, 2007) also found similar results.

However, after HT a slight uniform coating was noticed. There was a significant reduction in micro-cracks as well as a minor reduction in porosity. Elemental maps of Al, Ni, Cr, and Fe as shown in **Fig.4.8-4.10** and **Fig.4.13-4.15** corresponds to the cross-

sectional SEM images of as-sprayed and heat treated IN625-Al_2O_3 coating, respectively. The distribution of Al_2O_3 in the as-sprayed IN625-Al_2O_3 coatings may be shown in **Fig.4.8-4.10.** However, after post-coating HT (**Fig.4.13-4.15**), there is an even more uniform distribution of Al_2O_3, indicating that amorphous phases are normalised during HT. Similarly, the elemental maps of Fe in the cross-section of as-sprayed and heat treated coatings support the use of ASTM-SA210 GrA1 as a substrate.

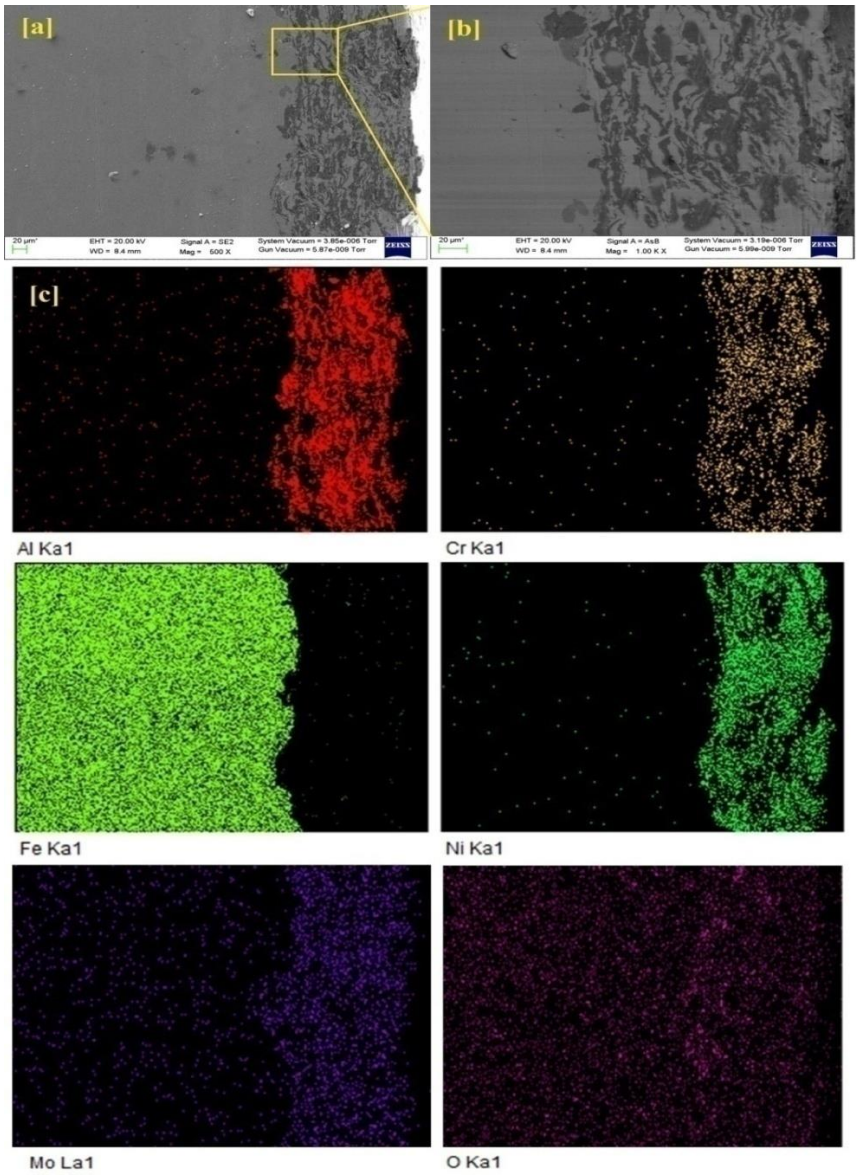

Fig.4.10.(a) Cross-sectional micrograph of IN625-ALB, (b) SEM micrograph at high magnification and, (c) x-ray maps corresponding to the SEM (Fig..4.10a).

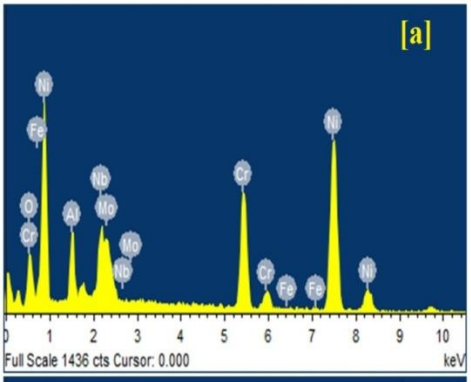

[d]

Elements	wt.%		
	IN625-ALC	IN625-ALN	IN625-ALB
Ni	52.38	50.14	50.93
Cr	22.88	21.94	16.72
Fe	00.22	0.25	00.22
Nb	04.38	05.85	02.66
Mo	05.47	05.82	01.00
Al	06.44	06.97	11.53
O	08.23	09.03	16.94

Fig.4.11 (a) EDS corresponding to the coating region across the cross-section for IN625-ALC, (b) IN625-ALN, (c) IN625-ALB and, (d) wt.% as per EDS taken for different coatings.

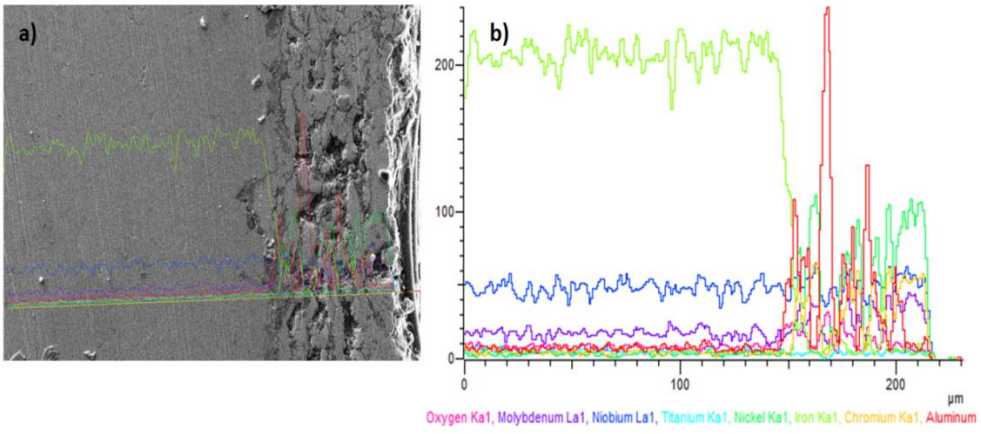

Fig.4.12 (a) Cross-sectional SEM image of IN625-ALN coating (b) Elemental distribution superimposed on the line scan area of Fig. 4.12a.

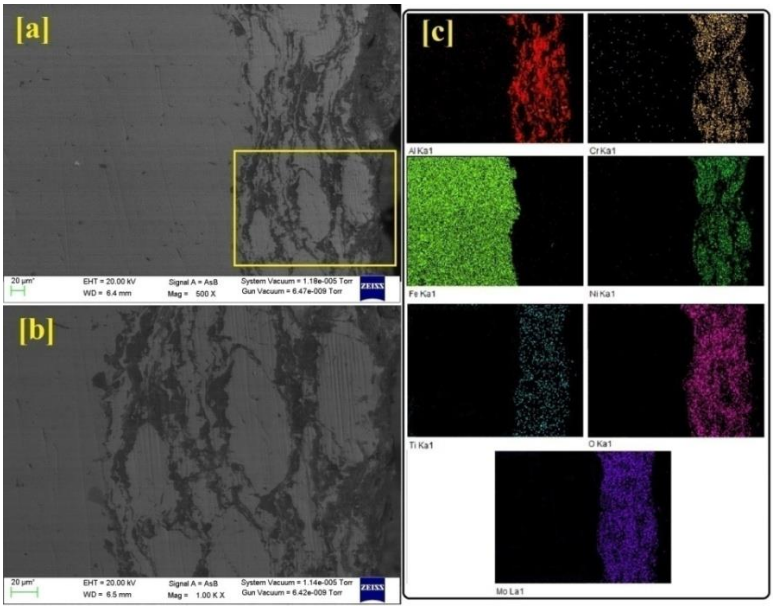

Fig.4.13 (a) Cross-sectional micrograph of IN625-CHT, (b) SEM micrograph at high magnification and, (c) x-ray maps corresponding to the SEM micrograph (Fig.4.13a).

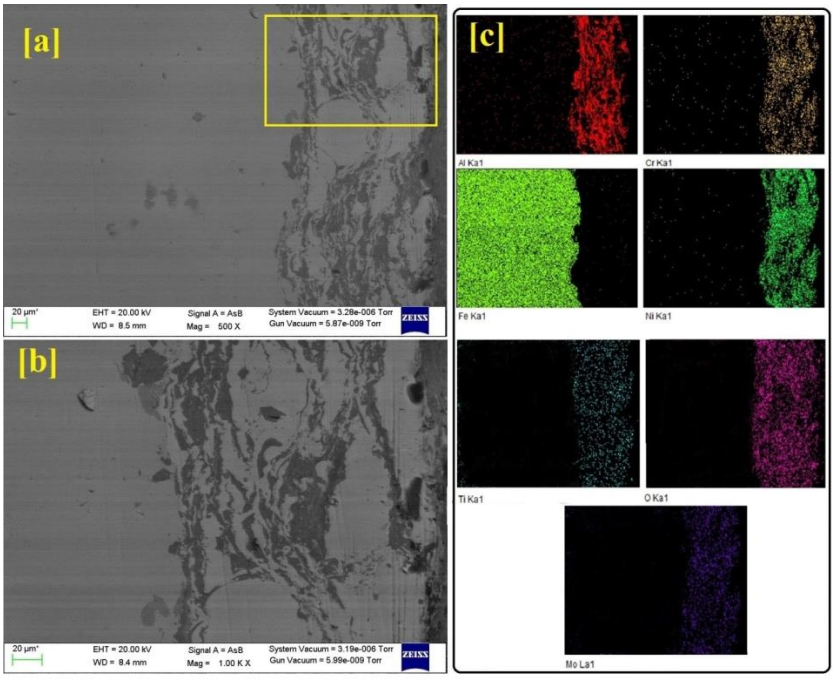

Fig.4.14 (a) Cross-sectional micrograph of IN625-NHT, (b) SEM micrograph at high magnification and, (c) x-ray maps corresponding to the SEM micrograph (Fig.4.14a).

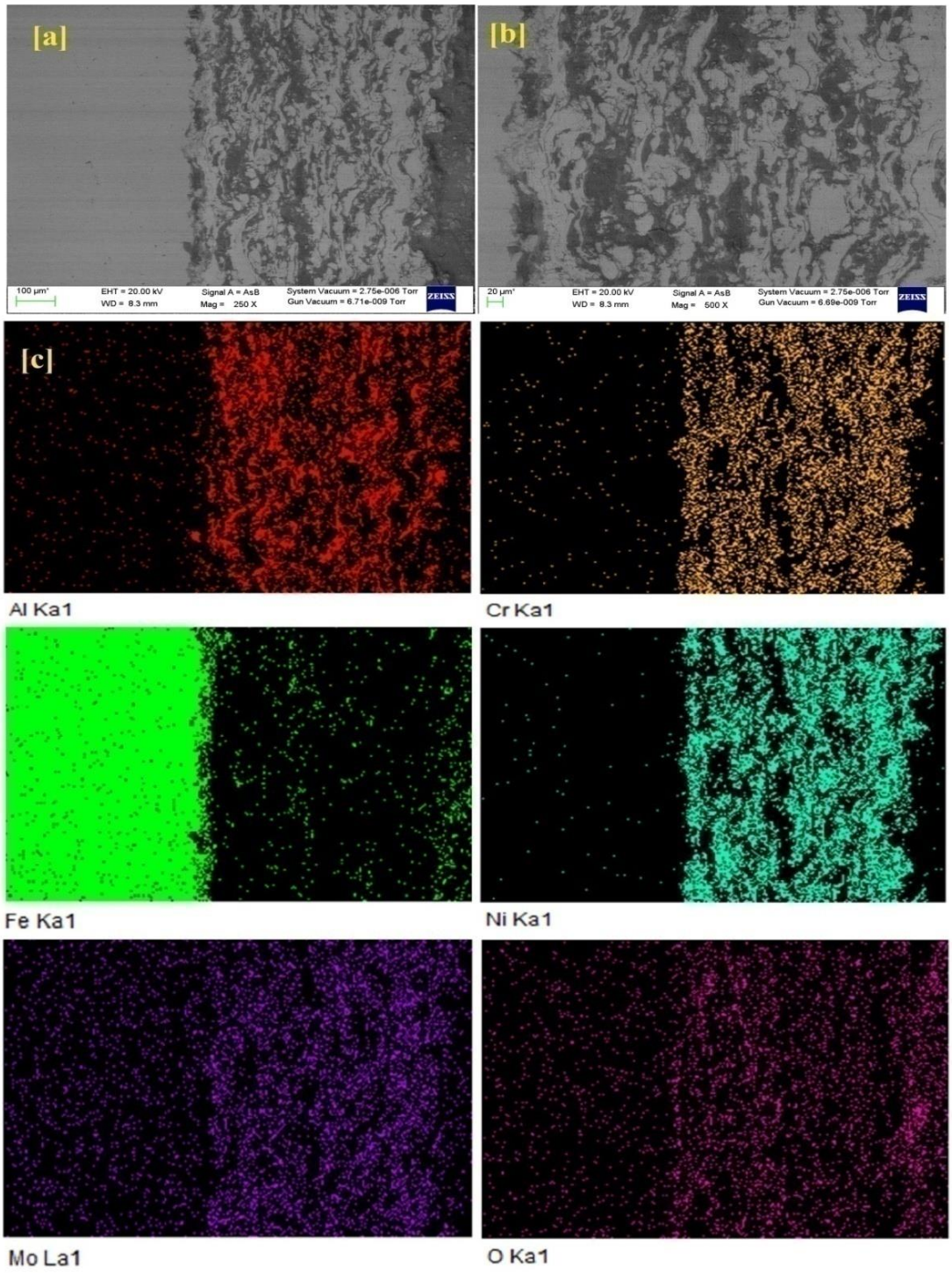

Fig.4.15 (a) Cross-sectional micrograph of IN625-BHT, (b) SEM micrograph at high magnification and, (c) x-ray maps corresponding to the SEM micrograph (Fig.4.15a).

4.6 POROSITY ANALYSIS

Porosity in the PS Al_2O_3 coatings is important for most engineering applications. Lower levels of porosity will lead in the enhancement of the mechanical properties (hardness) of the coatings which leads to improved wear resistance performance (Guilemany *et al.,* 2006; Dooley and Wiertel, 2009; Galedari *et al.,* 2019). Un-melted particles during spraying process are considered to be as the common source for coating porosity. Un-melted particles require higher impact velocity for better plastic deformation and also for better closer of the voids. If the velocity will be less than the solid particles will remain trapped inside the coating and due to this proper contact between the splats will not take place and voids occur. It is clear from vast technical literature that presence of pores significantly reduces the corrosion resistance (Guilemany andStaia2002; Camp *et al.,* 2009; Monticelli *et al.,* 2004; Bolelli et al., 2008b; Wang *et al.,* 2014; Milanti *et al.,* 2015; Zhang *et al.,* 2016). Porosity can be categorized differently by authors. (Thirumalai kumar asamy*et al.,* 2014) categorized pores according to the formation mechanism and size variation as type A (0 to 10µm) and type B (10 to 25µm). Type A is the result of interaction among gaseous medium and particles whereas type B is developed by splashing on impact with material deposited. Other researchers classified pores as open pore, closed pores and micro cracks. They reported that these types of pore and micro cracks occur due to enclosed gases and shrinkage of splats as a result of fast solidification (Ctibor *et al.*,2006; Konyashin and Chukalovskaya, 1997). Furthermore, others in addition to this categorization pores are classified as globular pore, flat pore and vertical pore. Globular pores are convex in shape whereas inter-lamellar flat pores are like thin voids perpendicular to the direction of spraying (Juzkova*et al.,* 2004).

Furthermore, porosities give rise to oxide content resulting in mass gain of coatings. Mass gain not only depends upon the porosity but also on to the pore structure morphology. Large porosity levels (open porosity) forms voids and results in forming of interconnected networks of pores which communicate with coating surface. This structure allows the oxygen to enter deep into coating and reach cavities to form oxides enhancing the mass gain of coatings (Sadeghimeresht, 2018).

The porosity commonly known as pores or voids in coatings was also evaluated via analyzing the top surface and the cross-section of composite coatings with help of Image analysis software. It was observed that pores present along the cross-section of composite coatings were completely dark in color. On the top surface of coatings value of porosity was found to be greater than along cross-sectional porosity. The IN625-ALC coating showed a porosity of 2.5%. The IN625-ALN displayed 1.9% porosity and IN625-ALB showed a porosity of 1.5%. For heat treated coating it is reported to be in the range 1% to 2%. This was related to the rapid diffusion process, which reduces cracks and fill pore/voids in the heat treated coatings (Gil *et al.,* 2002). Many authors in literature also reported that defects reduced and microstructure become homogeneous after HT of plasma sprayed coatings.

Other effective tools can be used to calculate the porosity level of coatings by considering the effective pores responsible for porosity (Nadaraia *et al.,* 2021). One reason is that during the plasma spray process, the coating is built layer via layer mechanism through the deposition of the used feedstock material. During coating formation, pores/cavities/voids in every single layer are filled by subsequent layers.

4.7 EVALUATION OF MICRO-HARDNESS

The micro-indentation technique was used to evaluate the micro-hardness of ASTM SA210 GrA1 substrate and composite coatings. The process of measuring the micro-hardness has already been explained in Section 3.3.4. The micro-hardness values of the coating combinations are represented in **Fig.4.16.** The composite coatings exhibited an increase in micro-hardness as compared to the substrate. The average micro-hardness value for substrate was about 220 $HV_{0.3}$. The addition of Al_2O_3 is responsible for the hardness increase in the composite coatings. The addition of 30wt% micrometric Al_2O_3 increases the hardness value of IN625-ALC coating. This improvement in hardness is attributed to differences among the values of the coefficient of thermal expansion of Al_2O_3 and IN625, respectively. This difference gives rise to geometric dislocations (GD) which creates strain hardening of the matrix (Vasudev *et al.,* 2022). During plastic

deformation, dislocations arise to interact with GD. As a result, movements of dislocation were restricted and improve the hardness. Another reason for improved hardness may be related to the load transfer effect. The micrometric-sized particles were further strained elastically resulting in the transfer of load from the matrix to the particle owing to enlargement in dislocations and initiations of slip-on secondary planes. It has contributed to the higher strength of the composite structure. In the case of IN625-ALN coating, hardness and strength have been improved due to the interaction of nano-sized particles with dislocations.

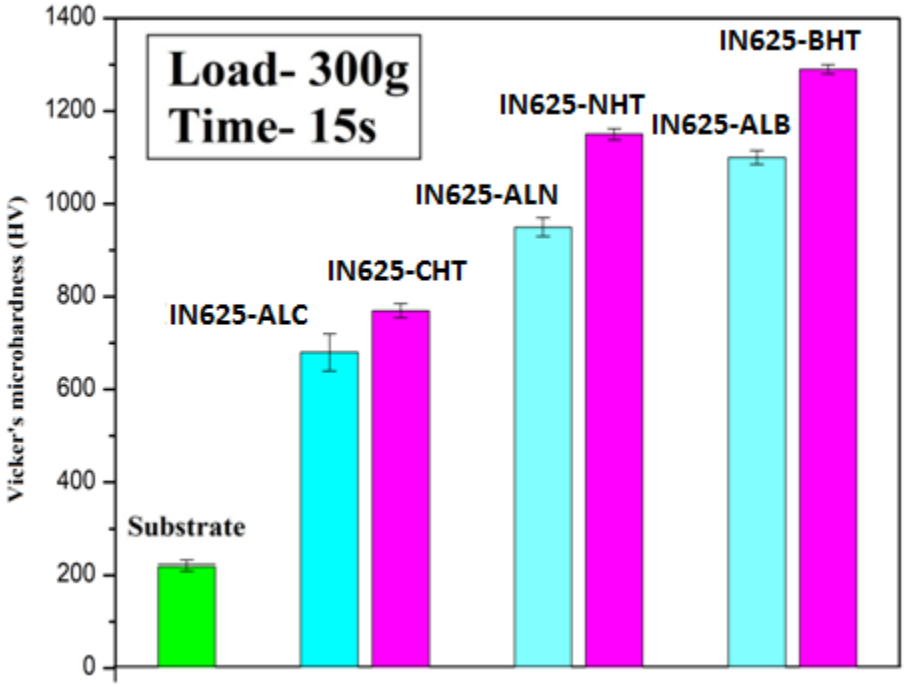

Fig.4.16 Micro-hardness of the developed coatings.

According to Orowan's strengthening mechanism, nano-sized particles effectively pin the movement of dislocations and nano-sized particles also reduce the inter-particle spacing. The hardness of IN625-ALB (1130±25 $Hv_{0.3}$) coating was higher in comparison to IN625-ALC (680±27 $Hv_{0.3}$) and IN625-ALN (960±30 $Hv_{0.3}$) coatings despite containing a lesser nano-particle proportion. This is attributed to the low volume fraction and small grain size of the nano-particles. Moreover, micrometric particles also resist particle cutting due to their bigger size. As explained earlier micrometric particles can

impede the movement of dislocations resulting in improved strength. Further, the incorporation of nano-sized particles also contributes toward high strength owing to Orowan strengthening mechanism. This may be understood in the way that dislocation motions bypassing the micrometric particles would be affected adversely. It has resulted in high strength as nano-sized particles also interact with GD present around the micrometric particles producing extra deformation complexity. The study conducted by (Deng *et al.,* 2012) also revealed the higher dislocation densities in the inter-particle zone among nano and micrometric particles. The combined effect as a result of interaction among nano and micrometric particles provides extra strength to IN625-ALB composite coating structures. This otherwise remained absent in either micrometric or nano-reinforced coatings. Studies available in the literature (Deng *et al.,* 2012; Deng *et al.,* 2012b; Skandan *et al.,* 2001) have exhibited that the bimodal structures possess good mechanical properties in comparison to the micrometric and nano-sized structures.

The comparative analysis of the micro-hardness values of Ni-Al_2O_3 system is presented in **Table 4.4.** The improvement in the micro-hardness values can be observed for the IN625-ALB coating for as-sprayed ones.

Table 4.4 Comparison of micro-hardness value of IN625-ALB composite coating with relevant Al_2O_3 reinforcement found in literature.

Coating	Micro-hardness (Hv)	Reference
Inconel718+30%(micrometric-Al_2O_3)	801 ± 40	(Vasudev *et al.*, 2022)
Inconel625+30%(micrometric-Al_2O_3)	585 ± 56	(Dosta *et al.,* 2020)
Ni+40%(micrometric-Al_2O_3)	714	(Grewal *et al.,* 2013)
NiCrSiB+40%(micrometric-Al_2O_3)	673	(Praveen *et al.,* 2015)
NiCr+50%(micrometric-Al_2O_3)	350	(Koivuluoto&Vuoristo,2009)
NiCrSiB+(nano-Al_2O_3)	748	(Praveen *et al.,* 2019)

Ni+40%(micrometric-Al_2O_3)	225	(Hu *et al.*, 2011)
Ni+(micrometric-Al_2O_3)	173	(Li *et al.*, 2008)
IN625-ALB	1130±25	This work

After HT the micro-hardness increases further. This latter value of hardness shows an increase of approx. 15% for IN625-BHT when compared with the micro-hardness value of IN625-ALB coating. The micro-hardness values of IN625-CHT and IN625-NHT also recorded an improvement in hardness of 15-20% when compared with IN625-ALC and IN625-ALN coatings, representing the outcome of the homogenous distribution of hard Al_2O_3 phase and a reduction in both the un-melted particles count and porosity content induced by HT.

4.8 Discussion

Detailed microstructural and mechanical investigations was carried out in current chapter to understand the structure–property correlations. The PS method was successfully used to deposit IN625-Al_2O_3 coating onto the ASTM SA210GrA1 substrate material. Pure IN625 and Al_2O_3 powders with average particle size in range of 40–50 µm were employed for the fabrication of the IN625-Al_2O_3 composite coating. Microstructure of the coating consists of splats, fully melted/un-melted particles, voids and pores which are common structural features of the PS coatings. EDS mapping reveals the presence of Ni, Cr, and Al in as-sprayed coatings. The coating thickness of the deposited coatings both as-sprayed and heat treated was measured along the cross-sections of specimens and was observed to be in the range of 250-300 µm, which is close to the desired value for combatting high temperature oxidation and similar findings observed by (Sidhu *et al.*,2005; Sidhu *et al.,* 2006c); (Grewal et al., 2013) and (Espallargas *et al.*,2008); (Roy *et al,.*2006) for Ni based coatings. However, after post-coating HT there is an even more uniform distribution of Al_2O_3 phase in composite coatings. For high-temperature applications, element diffusion between the substrate and coating can affect coating performance (Nicholls, 2000; Sundararajan *et al,.* 2005). There was no diffusion in the

coating, and (Sidhu *et al.,* 2006d; Sidhu *et al.,* 2006c); and (Kamal *et al.,*2008); have all reported on the influence of diffusion on coating performance.

A porosity value in range of 1–2.5% has been achieved for heat treated and as-sprayed coatings. After HT of the composite coatings porosity decreases owing to refinement in the microstructures of deposited coatings. Thermally sprayed coatings may be subjected to both erosion and oxidation attacks in various high-temperature hostile environments. Hence, at high temperatures, softer coatings may be more susceptible to erosion–oxidation attacks. The most frequently mentioned mechanical property of a thermal spray coating is micro-hardness. The micro-hardness analysis showed the maximum hardness of 1130 $HV_{0.3}$ for bi-modal coating, which is 5 times higher than the bare substrate owing to interaction among nano and micrometric particles that provides extra strength. After HT the micro-hardness increases further. This latter value of hardness shows an increase of approx. 25% for IN625-BHT when compared with the micro-hardness value of IN625-ALB coating representing the outcome of the homogenous distribution of hard Al_2O_3 phase and a reduction in both the un-melted particles count and porosity content induced by HT.

Chapter 5

CYCLIC OXIDATION STUDIES OF COATINGS

The oxidation behaviour of uncoated and Plasma sprayed ASTM-SA210 GrA1 coated samples exposed to oxidation at 900°C in air for 50 cycles is described in this chapter. Characterization of corrosion products was accomplished using FE-SEM/EDS and XRD methods. The results for uncoated ASTM-SA210 GrA1 and deposited coatings are presented in this chapter under different sub headings. The weight change values of each coating are shown alongside the bare ASTM-SA210 GrA1 for comparison. The value of the parabolic rate constant (K_p) for all samples was evaluated after 50 cycles of exposure in a silica tube furnace.

5.1 RESULTS

5.1.1 UN-COATED SUBSTRATE AND AS-SPRAYED OXIDIZED COATINGS

5.1.1.1 VISUAL EXAMINATION

The macrographs of uncoated ASTM-SA210 GrA1substrate and all deposited coatings following exposure to an oxidised environment at 900°C for 50 cycles are shown in **Fig.5.1 and 5.2.** The bare substrate, material spalled and peels off with a popping sound, resulting in thin chips, leading to a substantial mass gain after 50 cycles (**Fig.5.1a**). Color variations of un-coated substrate starts immediately with grey-bluish after first cycle and further after the completion of fifth cycle, the substrate color converted to grayish-black. Within eight cycles color of the substrate becomes completely black with a white layer of oxidized scale also visible on surface. The coated specimens, by and large, confirm the parabolic oxidation rate law, specifically the coated steel samples, for which divergences are very mere. The maximum wt. gain was recorded for IN625-ALC composite coating. This is attributes with the development of cracks

along the coating thickness after 15th cycle and with number of cycles increases further the crack width increases and a network of cracks formed all along the coating thickness (**Fig.5.1b**). In IN625-ALN coatings minute cracks were noticed after completion of 30th cycle (**Fig.5.1c**). Cracks may form owing to thermal shock during air cooling of samples. Minor spallation was seen on the IN625-ALN coatings surface, which turned to whitish at the edges. For IN625-ALB composite coating few minute cracks as shown in **Fig.5.1d** developed after 50 cycles and the coating adhered properly with the underlying substrate. This signifies that the IN625-ALB coated steel sample can serve as a diffusion barrier to harmful oxidizing species.

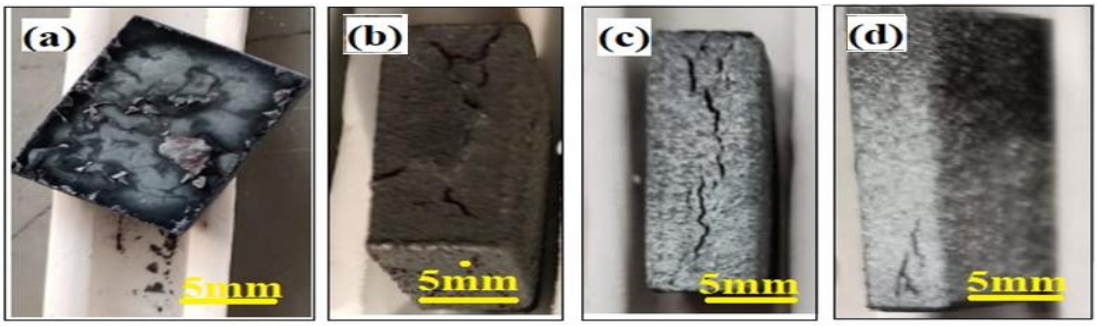

Fig.5.1**.** Macrographs of as-sprayed oxidized samples after 50 cycles: a) Substrate, b) IN625-ALC, c) IN625-ALN, and d) IN625-ALB.

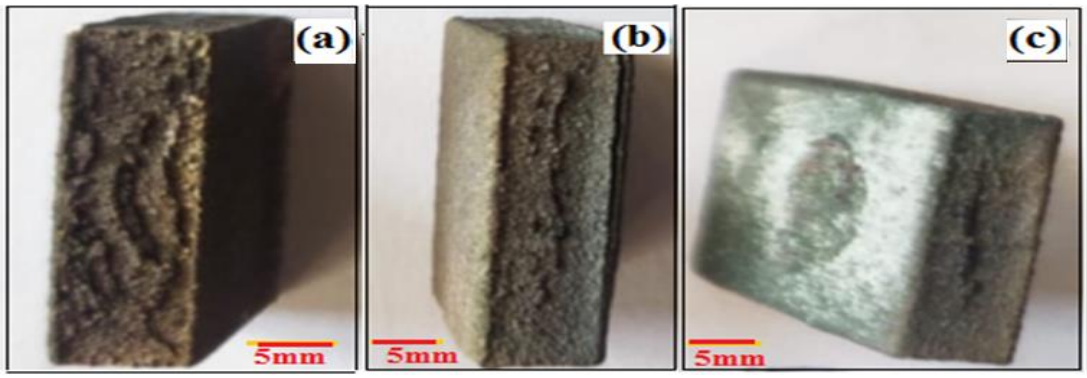

Fig.5.2**.** Macrographs of as-sprayed HT oxidized samples after 50 cycles: a) IN625-CHT, b) IN625-NHT and c) IN625-BHT.

On the other hand the macrographs of oxidized heat treated samples after 50 cycles are shown in **Fig.5.2.** The IN625-BHT composite coating has minimum weight gain out of all the samples. After the completion of 50 cycles minor swelling of coating was observed (inset **Fig.5.2c**) in comparison to the IN625-CHT, and IN625-NHT composite coatings. The swelling of coating was maximum in case of IN625-CHT coating as shown in **Fig.5.2a.** Moreover after the completion of 19^{th} cycle dark black spots can be noticed in case of IN625-CHT coating.

5.1.1.2 WEIGHT GAIN DATA

Weight change data of the composite coatings in (mg/cm^2) versus 50 cycles are depicted in **Fig.5.3a & b.** The ASTM-SA210 GrA1 boiler steel has maximum weight gain (101.9 mg/cm^2). Moreover, after the deposition of composite coatings it can be noticed that the weight gain reduces. IN625-ALC, IN625-ALN,IN625-ALB, IN625-CHT, IN625-NHT, and IN625-BHT has weight gain of 10.3 mg/cm^2, 9.03 mg/cm^2, 6.86 mg/cm^2, 6.03 mg/cm^2, 5.03 mg/cm^2, and 3.5 mg/cm^2 respectively. Thus, in weight gain terms, the Plasma sprayed IN625-BHT oxidized coating was best among all composite coatings and it reduces the weight gain of ASTM-SA210 GrA1 boiler steel by 96.5%. IN625-CHT and IN625-NHT reduces weight gain of bare ASTM-SA210 GrA1 boiler steel by 91.5%, and 94% respectively. Similarly, among as-sprayed oxidized coatings (IN625-ALC, IN625-ALN, and IN625-ALB), the bimodal IN625-ALB was the best performer and it reduces weight gain by 93% in comparison to 90%, and 91% for IN625-ALC, and IN625-ALN coating respectively, which is remarkable contribution with respect to control the high temperature oxidation of ASTM-SA210 GrA1 boiler steel used in boilers. The bare substrate, and the coated specimens, by and large, confirms the parabolic oxidation rate law, specifically the coated steel samples, for which divergences are very mere.

The value of the parabolic rate constant (K_p) for all samples was evaluated using a standard linear least-square algorithm in the equation form $(x)^2 = K_p\, t$, where, 'x' shows the weight gain/surface area (mg/cm^2) and 't' show the number of oxidation cycles

representing exposure time. The parabolic rate constants values for the samples are summarized in **Table 5.1.** These values of K_p indicate clearly that the Plasma sprayed coating successfully decreases the oxidation rate of boiler steel.

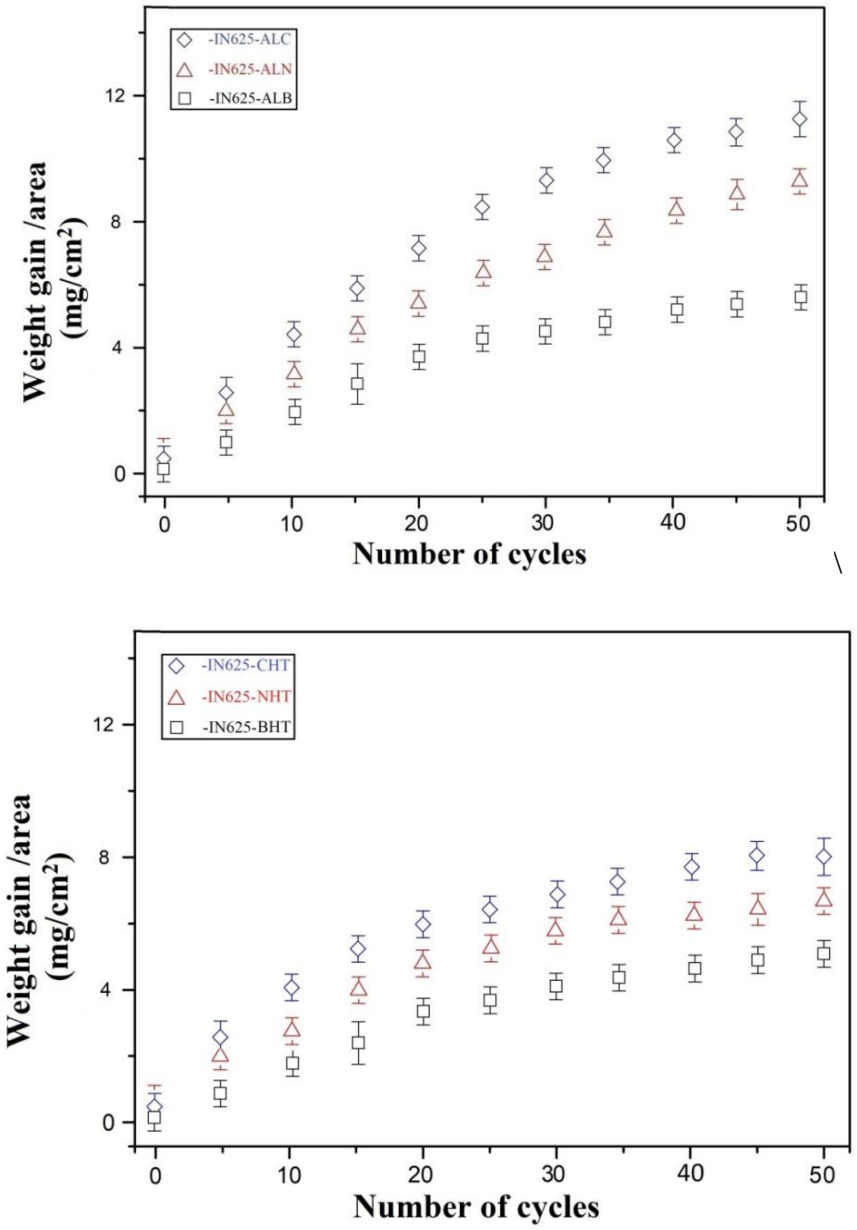

Fig.5.3.(**a)**Weight gain plots for Plasma sprayed coated samples exposed to cyclic oxidation studies in an air environment for 50 cycles at temperature 900 °C.(**b)**Weight

gain plots for Plasma sprayed heat treated samples exposed to cyclic oxidation studies in an air environment for 50 cycles at temperature 900 °C

Table 5.1 The parabolic rate constants values for the samples.

Specimens	**K_P ($10^{-4}mg^2cm^{-4}s^{-1}$)**
SA210 GrA1	619.35
IN625-ALC	6.36
IN625-ALN	4.89
IN625-ALB	2.82
IN625-CHT	2.16
IN625-NHT	1.5
IN625-BHT	0.7

5.1.1.3 X-RAY DIFFRACTION ANALYSIS OF BARE ASTM SA210 GRA1 AND COMPOSITE COATINGS FROM SURFACE

XRD analysis for the PS coatings on ASTM-SA210 GrA1oxidized boiler steel is shown in **Fig.5.4a.** From the XRD analysis of oxidized samples, it is found that the oxide scale present on the surface of bare ASTM-SA210 GrA1 boiler steel consists of Fe_2O_3 (hematite) as the leading phase. Hematite (Fe_2O_3) formation as shown by the XRD pattern in the oxidized scale of ASTM-SA210 GrA1 boiler steel is related to the reaction of Fe with O_2 since Fe is the prime constituent of the ASTM-SA210 GrA1 boiler steel. The development of hematite has also been discussed in previous studies during the failure investigations of boiler tubes. The IN625-ALC, IN625-ALN, and IN625-ALB coated oxidized samples (**Fig.5.4b,c&d**) shows the formation of phases like Ni-Cr, NiO, Cr_2O_3, Al_2O_3, TiO_2, and spinels $NiCr_2O_4$ and $CrNbO_4$ in the oxidized scale. When comparing IN625-ALB coating to the other two coatings, the intensity of alumina peaks was higher (**Fig.5.4d**). This suggests that at high temperatures, the stable state of reinforced alumina (α-Al_2O_3) in the IN625 matrix is maintained within IN625-ALB coating. The Al_2O_3 in the three coatings is corundum α-phase and this may be due to

following reasons: *a)* the lower spraying velocity achieved during plasma spray allowed for higher corundum content in the deposited coatings. This finding can be explained by the fact that the feedstock powder is fused in the hot flame of plasma during the deposition, resulting in the formation of γ-alumina. But γ-Al_2O_3 can convert back to corundum α-phase as the granules in the deposited coatings cool more slowly owing to lesser spraying velocities, *b)* Moreover due to shorter residence times at higher temperatures, part of the initial corundum α-phase does not convert to γ-alumina, and is retained in the final deposited coatings, thereby maintaining the primary powder nanostructure, and *c)* in the SEM micrographs (**Fig.4.4d&f**), Al_2O_3 particles can also be seen in the un-melted form in the deposited coating. A portion of the low-weight agglomerated Al_2O_3 feedstock cannot reach the spray flame's centre. In this situation, a portion of the feedstock could not melt properly, resulting in the formation of α-Al_2O_3 phase within the deposited coatings. The excess NiO which forms during oxidation as shown in XRD patterns reacts with Cr_2O_3 to form $NiCr_2O_4$ spinel. The following are some of the observed reactions:

$4Fe + 3O_2 \longrightarrow 2Fe_2O_3$

$4Fe_2O_3 + Fe \longrightarrow 3Fe_3O_4$

$Ni + ½\ O_2 \longrightarrow NiO$

$2Cr + 3/2\ O_2 \longrightarrow Cr_2O_3$

$NiO + Cr_2O_3 \longrightarrow NiCr_2O_4$

$½\ Cr_2O_3 + ½\ Nb_2O_5 \longrightarrow CrNbO_4$

$Al + 3/2\ O_2 \longrightarrow ½\ Al_2O_3$

On comparing the XRD patterns of IN625-ALB, and IN625-BHT oxidized coatings, in **Fig.5.4 and 5.5** it can be seen clearly that the intensity of peak as observed in XRD patterns corresponding to the Al_2O_3 phase was noticed to be higher in comparison to other composite coatings. It demonstrates that Al_2O_3 maintains its stability during

oxidation studies at high temperatures. At 900°C for 50 cycles in an air environment, the development of these Al_2O_3 phase in the oxide scale leads in decreased weight gain of the IN625-ALB, and IN625-BHT coatings (Singh, 2003).

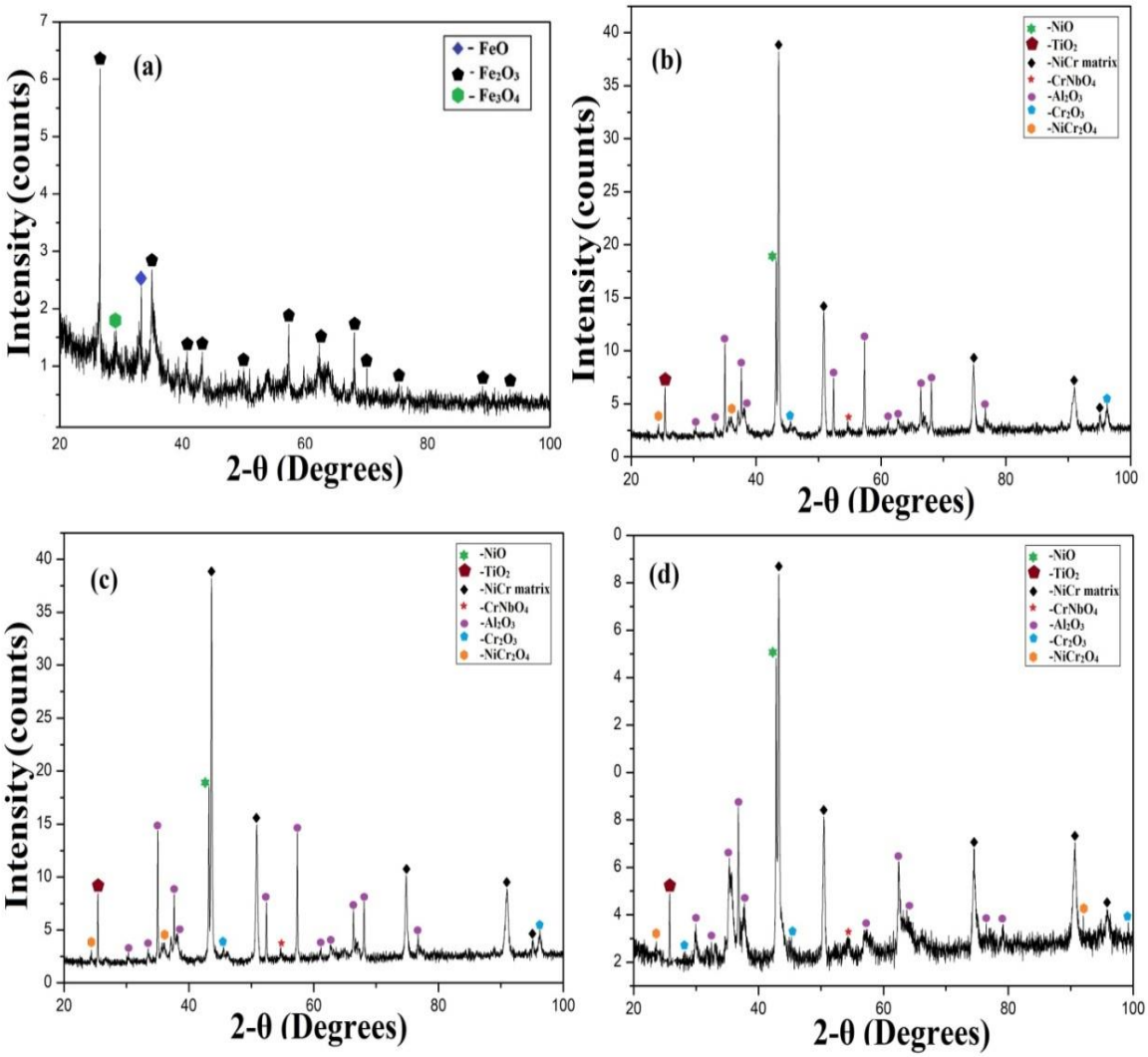

Fig.5.4. XRD analysis for the PS coatings on a) un-coated substrate, b) IN625-ALC, c) IN625-ALN, and d) IN625-ALB coatings after oxidation tests.

The thermal stability of Al_2O_3 is higher than that of other oxides such as chromium oxide, NiO, and others, and it also has a reactive influence on the growth of

other oxides (NiO, chromium oxide) during oxidation. The existence of alumina also aids in the improvement of the oxide scale's adhesion to the substrate (Vasudev *et al.*, 2020a and b). As a result, the alumina presence has aided in the improvement of IN625-ALB, and IN625-BHT composite coating oxidation resistance.

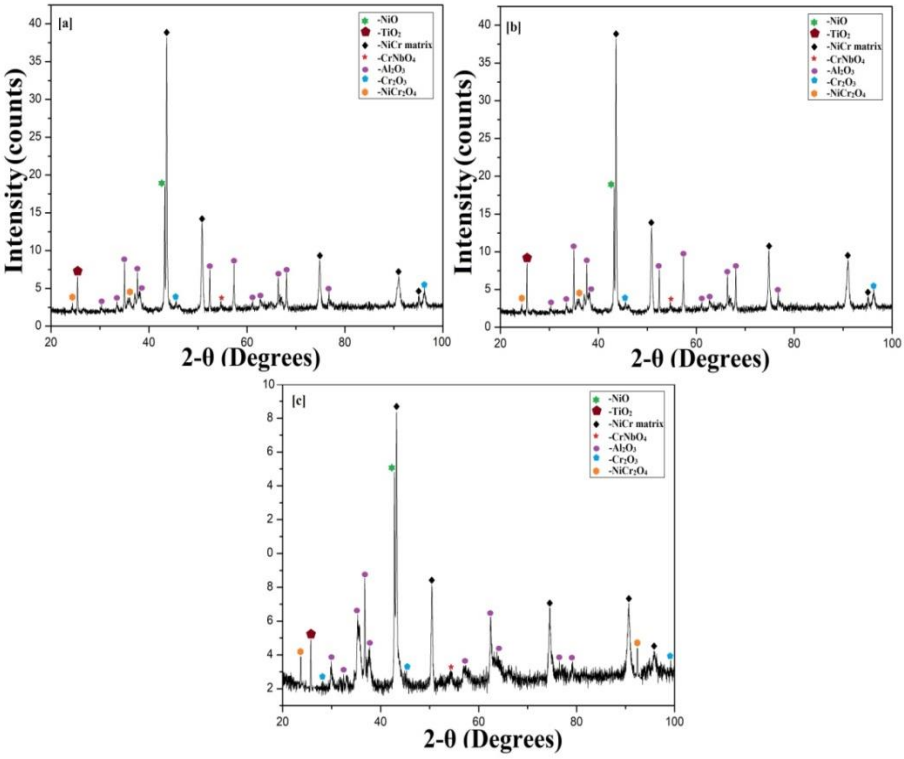

Fig.5.5**.** XRD analysis for the oxidized HT coatings.

5.1.1.4 SEM/EDS ANALYSIS

SEM/EDAX analysis of the bare ASTM-SA210 GrA1 boiler steel and the coated specimens exposed to cyclic air oxidation studies at 900ºC for 50 hrs is depicted in **Fig.5.6.** The SEM examination of the uncoated boiler steel (**Fig.5.6a**) reveals the appearance of a granulated scale (Kumar et al., 2014), whereas the EDAX analysis affirms that this granular scale comprises Fe and O throughout scale composition. This strongly confirms the possibility of the development of a weak Fe_2O_3 phase, and the same has also been exhibited by XRD analysis. A similar investigation of oxidized coated

samples, IN625-ALC, IN625-ALN, and IN625-ALB are depicted in **Fig.5.6b, c & d**, respectively, exhibits a scale having unique crystalline and pyramidal structure (Khoi *et al.*, 1975). The EDAX analysis of all oxidized coatings shows main elements as Ni and Cr along with a significant concentration of O also. Hence the composition of feedstock powder nevertheless remains the same after oxidation tests. The EDAX analysis of coatings IN625-ALN,and IN625-ALBreveals a significant amount of Aland Cr along with O in the oxidized coatings when exposed to oxidation studies in comparison to IN625-ALCcoating. This represents that nano Al_2O_3 and Cr_2O_3phase remains intact which indicates that at high temperatures they don't grow quickly resulting in little spallation of IN625-ALN,and IN625-ALBcoatings. Furthermore, nano Al_2O_3 remains stable at higher temperatures and produces a reactive effect on different oxides (Vasudev *et al.*, 2020a and b) which leads to the low oxidation rate of IN625-ALN,and IN625-ALB composite coatings. Nb was also seen in the EDAX analysis of all the coatings and a higher concentration of these elements specifically in IN625-ALB coating is considered to be beneficial for enhanced oxidation resistance (Azarmi *et al.*, 2008).

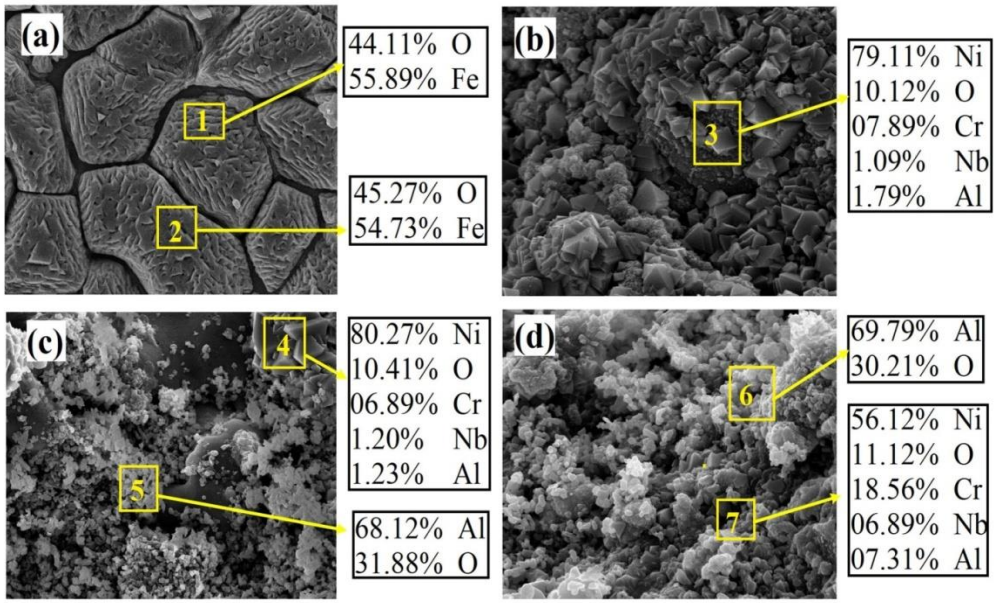

Fig.5.6**.** SEM micrographs and EDAX spectrum of oxidized: a) uncoated substrate, b) IN625-ALC, c) IN625-ALN, and d) IN625-ALB coatings after exposed to cyclic oxidation studies at 900 °C.

The SEM micrograph of the heat treated IN625-CHT, IN625-NHT and IN625BHT coating after oxidation has been shown in **Fig.5.7**, which depicts the dominance of Al, Ni, and Cr along with O in the scale as confirmed by EDS analysis (inset **Fig.5.7b, d & f**). The micrograph depicts an oxide scale made up of spherical particles with an uneven size distribution that appear to be rapidly expanding on the specimen's surface by filling in the dark gaps. The greater oxidation resistance of heat treated coatings could be attributed to the coatings' densification. Surface morphology and flaws have a direct impact on the corrosion behaviour of deposited coatings.

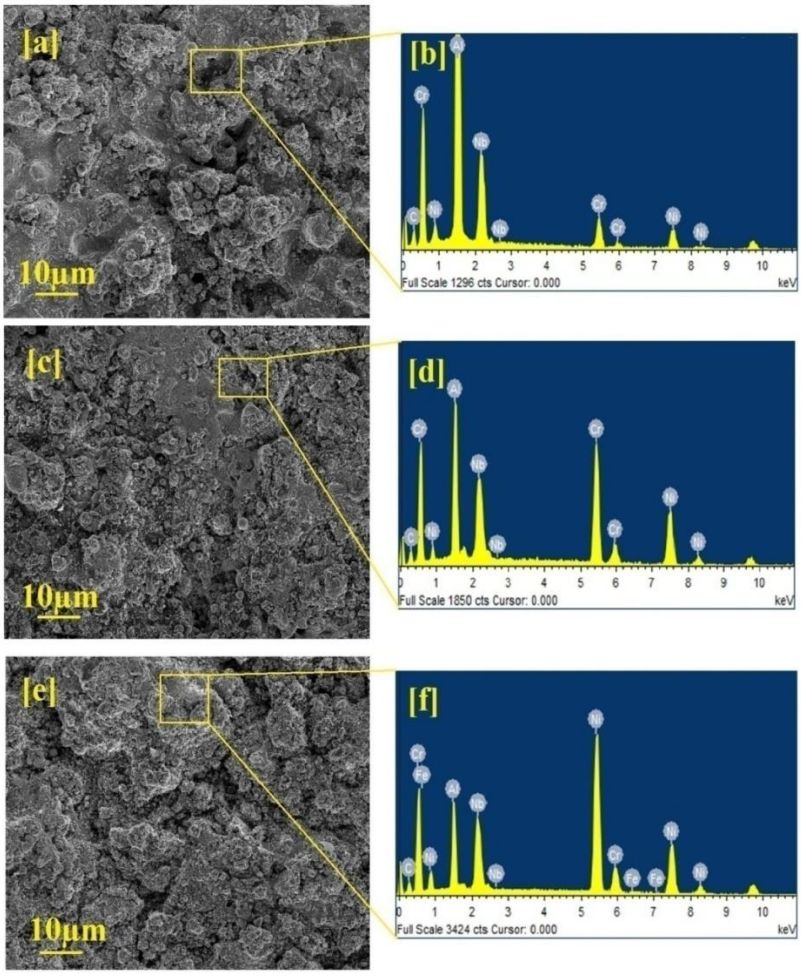

Fig.5.7**.** SEM micrographs and EDAX spectrum of oxidized: a) IN625-CHT, c) IN625-NHT, and e) IN625-BHT coatings after exposed to cyclic oxidation studies at 900 °C.

5.1.1.5 CROSS-SECTIONAL ANALYSIS AND X-RAY MAPPING

Cross-sectional analysis of all the samples (coated and bare) exposed to cyclic oxidation studies at 900 ºC for 50 hrs are shown in **Fig.5.8-5.11.** The oxide scale develops on the bare ASTM-SA210 GrA1 boiler steel indicates Fe oxides formation in outermost layers of the developed scale, which is complemented well by surface XRD reports. X-ray mappings of oxide scale of uncoated steel sample oxidized in cyclic air studies at 900ºC for 50 hrs are depicted in **Fig.5.8b.** It can be noticed clearly from the X-ray maps and line scan in **Fig.5.8b &c**, the overall oxide scale forms consist mainly of elements Fe and O, indicating the Fe_2O_3-rich scale. This is not desirable as it results in the loss of mechanical strength and reduces the oxidation resistance of steel. The air oxidation mechanism of iron-based alloy steels was explained in literature by researchers (Krzyzanowski *et al*., 2010). In their findings, the authors recommend that the oxidation rate of iron is regulated by the stabilities of different oxide phases having the uppermost layer of iron oxide. According to the equilibrium phase diagram, phases that were present at temperatures greater than 570ºC include FeO, Fe_3O_4, and Fe_2O_3. The formation of oxide phases FeO and Fe_3O_4 is governed by onward O_2 diffusion, while for Fe_2O_3 it is regulated by inward O_2 diffusion. The concept of diffusion is well supported by the reality that oxidation follows the parabolic rate law.

X-ray mappings of IN625-ALC, IN625-ALN, and IN625-ALB air oxidized coatings on steel substrate is depicted in **Fig.5.9-5.11.** XRD patterns of all the air oxidized coatings exhibit phases like Ni-Cr, NiO, Cr_2O_3, Al_2O_3, TiO_2, and spinels $NiCr_2O_4$ and $CrNbO_4$ in the oxidized scale. These phases were also affirmed by X-ray maps and SEM-EDAX analysis. Formation of NiO, Cr_2O_3, and $NiCr_2O_4$ phases in plasma-sprayed Ni-20Cr coatings was also shown by (Singh, 2003; Singh et al., 2007b) in their studies. The findings are also consistent with those of (Calvrin *et al* ., 2000) and (Longa-Nava *et al.,* 1996). Development of phases Cr_2O_3, Al_2O_3, TiO_2, and spinels $NiCr_2O_4$, $CrNbO_4$ were also affirmed by (Vasudev *et al.,* 2020a and b) on HVOF sprayed air oxidized Inconel718-Al_2O_3 coatings. The spinel $CrNbO_4$ forms during initial

oxidation stages via diffusion of Nb from grain boundaries (Doleker *et al.*, 2019). Due to $CrNbO_4$ formation (Qu *et al.*, 2007) found improved adhesion among oxidized scale and substrate. As a result, an alloy producing $CrNbO_4$ should expect to have a relatively good oxidation resistance. Cr has a stronger oxygen affinity than Ni, resulting in a more stable oxide. NiO has a lower stoichiometry than Cr_2O_3(Stott and Wood, 1988).

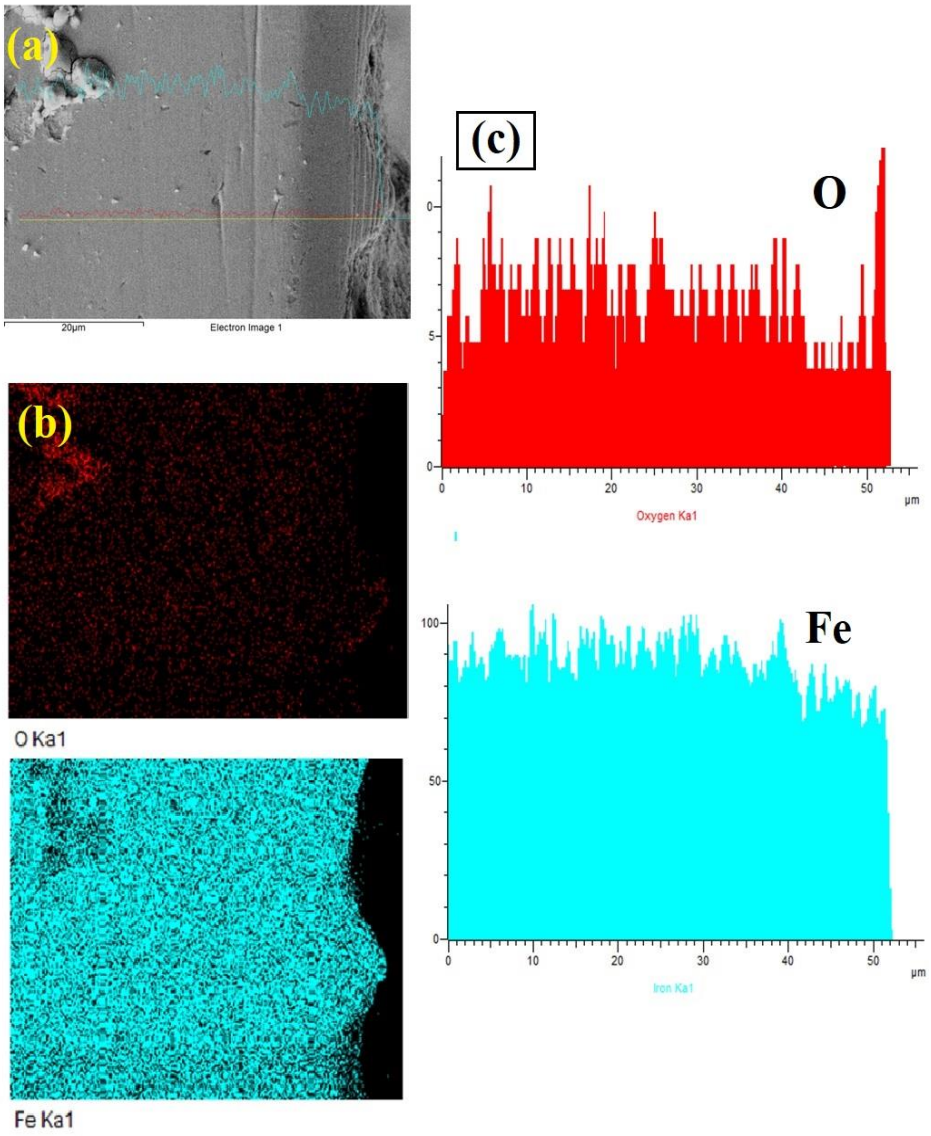

Fig.5.8**.** (a) SEM Cross-section images of oxidized un-coated oxidized boiler steel, (b) X-ray map and (c) line scan for distribution of elements corresponding to Figure.5.9**.**a

The nuclei of all stable oxide phases, NiO, and Cr_2O_3, develop on the surface during the early stages of oxidation of the Ni-Cr system, according to reports. NiO, the fastest developing phase, overgrows Cr_2O_3, forming a NiO layer on the surface. Because NiO is less stable than Cr_2O_3, it provides oxygen and has a sufficiently high dissociation pressure to react with Cr to form Cr_2O_3, resulting in the complete healing layer (Saunders and Nicholls, 1989).

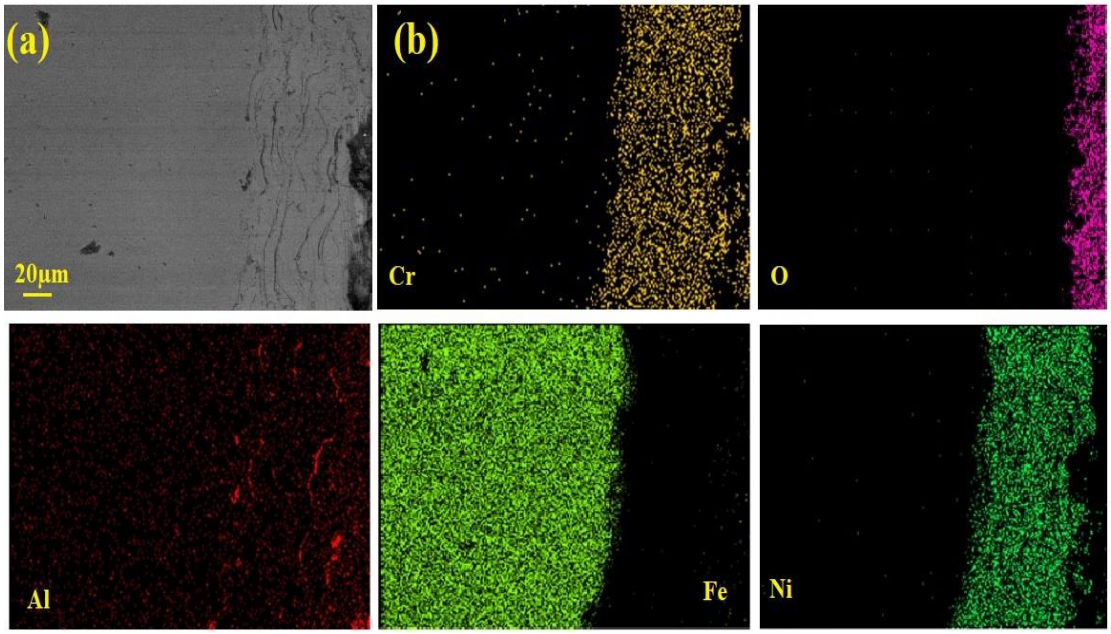

Fig.5.10**.** (a) SEM Cross-section images of the oxidized IN625-ALC coating, and (b) X-ray map

The interface of scale-substrate is found to be free from defects/cracks in **Fig.5.9a, 5.10a& 5.11a.** The micrograph of all the coatings reveals a dense scale, comprising mainly of elements Ni, Al, and Cr as shown in X-ray maps. O is noticed to be concentrated along with these elements and it helps to form different oxides and spinels in the outermost layer which can safeguard the underlying steel substrate and coating from severe oxidation attacks at high temperatures. These oxides and spinels were also confirmed in the XRD studies. Fe is mainly confined to the bare steel, which indicates

that all the coatings were successful enough to act as a diffusion barrier to the elements of the bare steel.

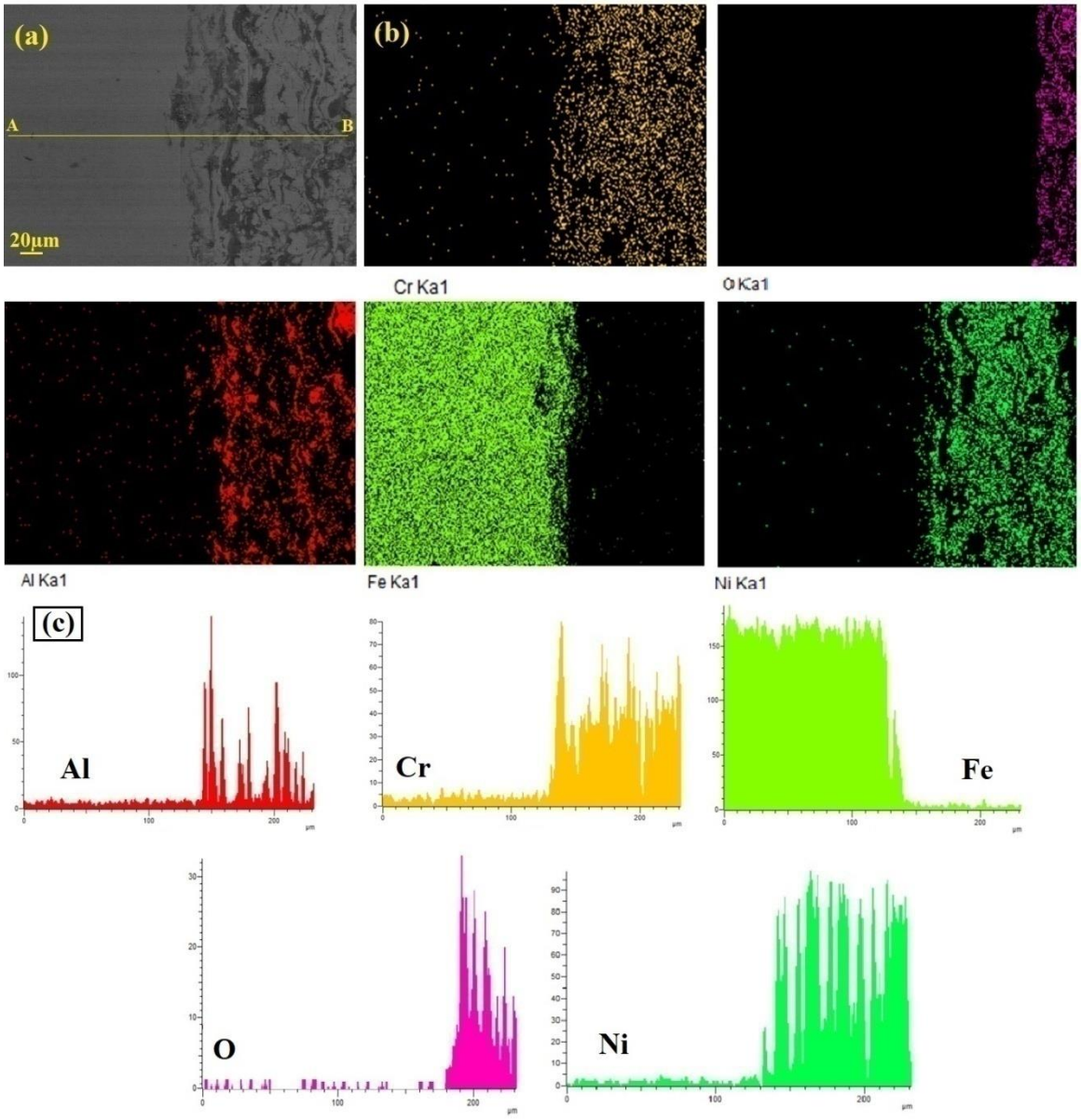

Fig.5.11. (a) SEM Cross-section images of oxidized IN625-ALN coating, (b) X-ray map, and (c) line scan for distribution of elements corresponding to Figure.5.10a.

The oxide scale develops on the IN625-ALC & IN625-ALN coating (**Fig.5.9 & 5.10**) indicates Al and Cr oxides formation in outermost layers of the developed scale, but

the oxides form on IN625-ALN coating after oxidation were dense and their distribution is uniform in comparison with IN625-ALC coating which is complemented well by surface X-ray maps (**Fig.5.10b**). The line scanning of the oxide scale of IN625-ALN sample oxidized in cyclic air studies at 900ºC for 50 hrs is depicted in **Fig.5.10c**. It can be noticed clearly that, the overall oxide scale forms consist mainly of elements Ni, Al, and Cr, indicating NiO, Al_2O_3, and Cr_2O_3-rich scale which is also well complemented in oxidized XRD patterns of IN625-ALN coating.

IN625-ALB coating is observed to be much dense in comparison to the other two coatings after the oxidation test as shown in **Fig.5.11**.

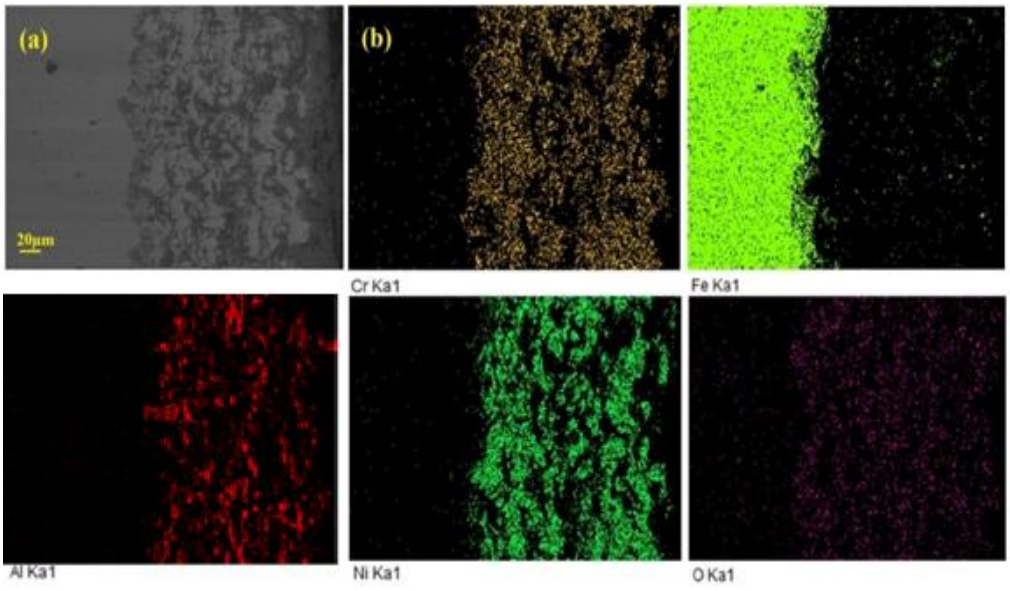

Fig.5.12**.** (a) SEM Cross-section images of the oxidized IN625-ALB coating, and (b) X-ray map.

The dark phase identified as Al_2O_3 is present in form of inter-lamella oxides. The development of coherent Al and Cr scales in IN625-ALB coating helps in increasing the oxidation performance of the coating. Furthermore, enrichment of Ti and Cr is also found in the oxidized coatings which results in the formation of Cr_2O_3 and TiO_2 and the same has been also confirmed in XRD analysis. **Fig.5.12** depicts the likely mechanism of oxidation for the coatings after 50 hrs of air exposure. Because of its high melting point,

the Cr_2O_3 phase is considered to be thermodynamically stable up to very high temperatures and forms a dense, continuous, and adherent layer that prevents oxygen from interacting with the underlying coating/substrate (Vasudev *et al.*, 2020a and b). Due to the larger Cr content in IN625-ALB coating, the Cr was capable of forming a continuous protective film, which might have resulted in higher oxidation resistance than IN625-ALC and IN625-ALN coatings. The existence of a spinel $NiCr_2O_4$ phase in the oxidized scale may have also aided in the development of greater oxidation resistance in the IN625-ALB coating, as spinel phases typically have lower cation and anion transport coefficients than their parent oxides (Chatterjee, 2001). Furthermore, Al_2O_3 remains stable at higher temperatures and produces a reactive effect on different oxides which leads to the low oxidation rate of IN625-ALB composite coatings (Vasudev *et al.*, 2020a and b). It was found that adding Al_2O_3 to coatings increased the cohesiveness of the metallic phase (Grewal *et al.*, 2013). As a result, dense IN625-ALB coatings prevent oxygen from penetrating the substrate at high temperatures.

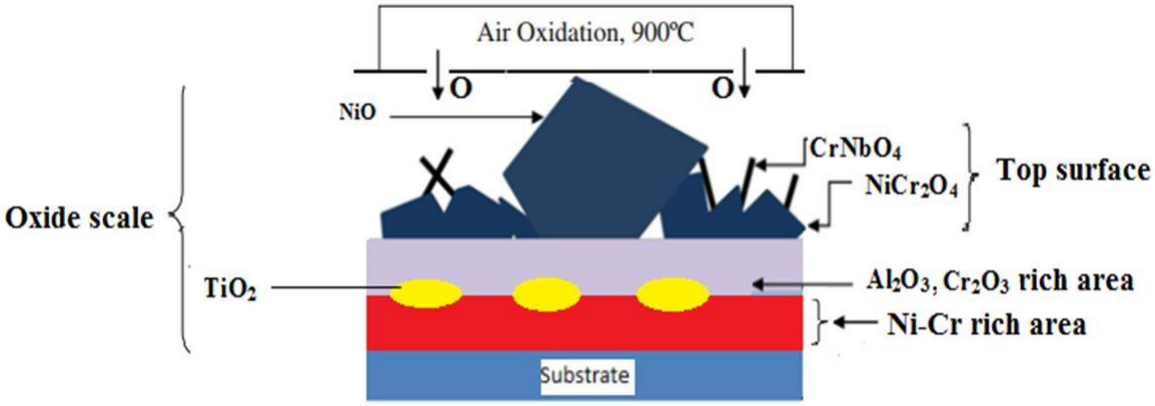

Fig.5.13**.** The probable mechanism of oxidation for the coatings after 50 hr of air exposure

5.1.1.6 SEM ANALYSIS FOR OXIDIZED HEAT TREATED COATINGS

X-ray mappings and cross-sectional SEM micrographs of IN625-CHT air oxidized coatings on steel substrate is depicted in **Fig.5.13.** The interface of scale-substrate is found to be free from defects/cracks. The micrograph of the IN625-CHT coating reveals

a dense scale, comprising mainly of elements Ni, Al, and Cr as shown in X-ray maps in **Fig.5.13b.** Fe is mainly confined to the bare steel, which indicates that the coatings were successful enough to act as a diffusion-barrier to the elements of the bare steel.

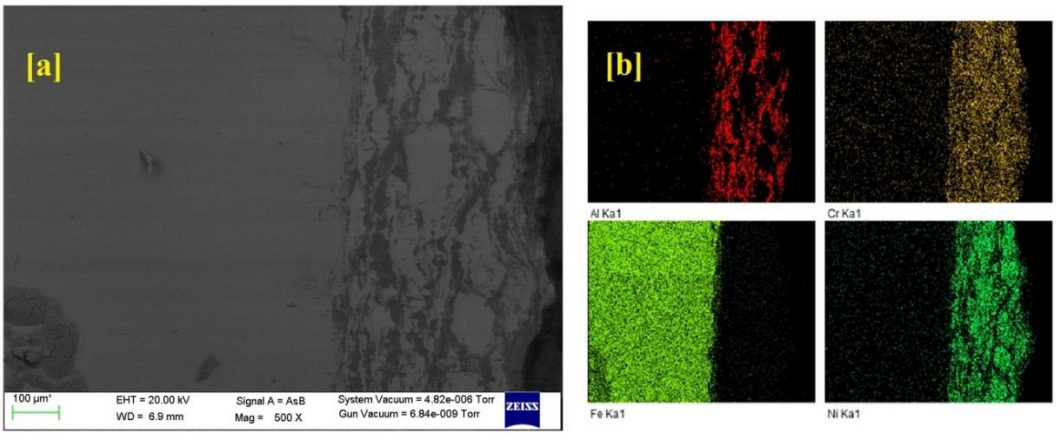

Fig.5.14**.** (a) SEM Cross-section images of the oxidized IN625-CHT coating and (b) X-ray map

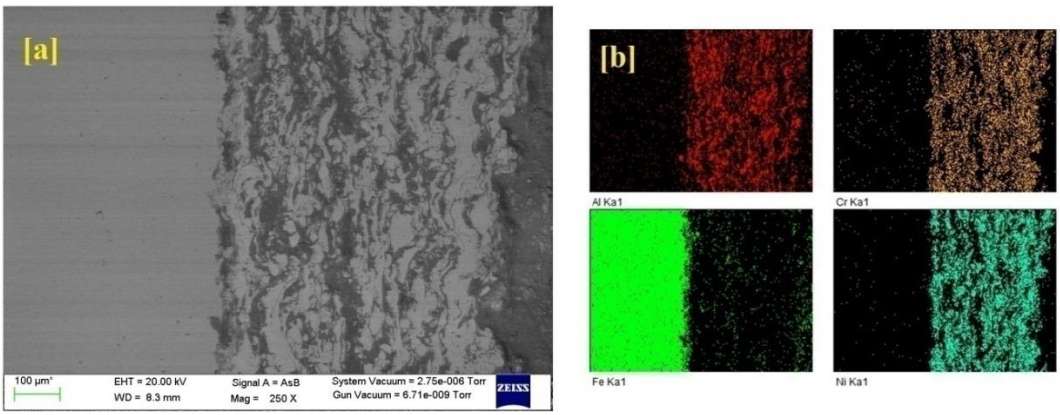

Fig.5.15**.** (a) SEM Cross-section images of the oxidized IN625-NHT coating, and (b) X-ray map

The SEM micrographs of IN625-ALN with X-ray maps at the cross-section of oxidized coatings, is presented in **Fig.5.14.**A decrease in the value of weight gain reported for IN625-NHT coating are associated to the formation of protective oxide phases like Cr_2O_3, and Al_2O_3 in the coating topmost layers. Moreover, major elements concentration

(Al, Cr, Ni) is also on higher side in the oxide layer of IN625-NHT coating as seen in the coating X-ray maps **Fig.5.14b**. These major elements create a coherent and non-porous layer, which is well adherent to the surface of IN625-NHT coating, which at high temperature serves as an elemental diffusion barrier.

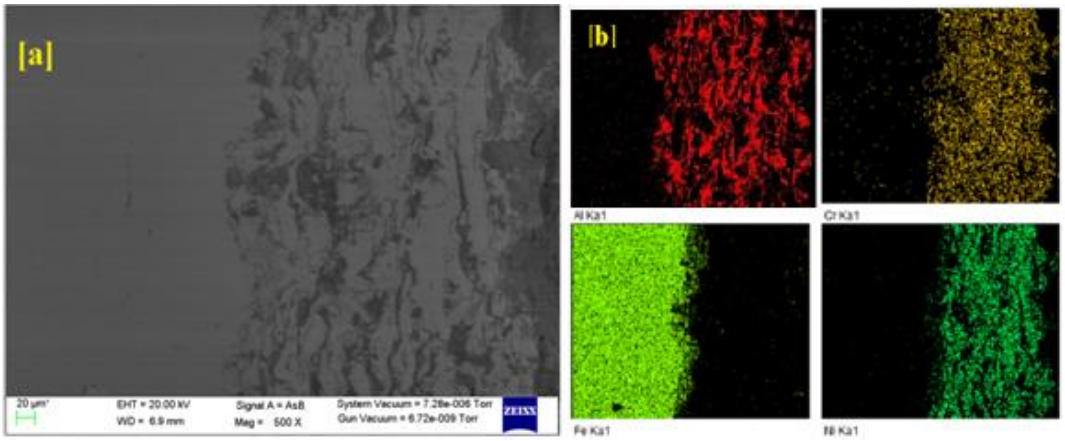

Fig.5.16**.** (a) SEM Cross-section images of the oxidized IN625-BHT coating and (b) X-ray map

The bimodal IN625-BHT coating is observed to be much dense in comparison to other tested coatings after oxidation test (**Fig.5.15**). The dark phase identified as Al_2O_3 is present in form of inter-lamella oxides and is well complemented by the higher intensity of Al_2O_3 peaks in the XRD pattern of IN625-BHT coatings. Development of coherent Al and Cr scales in bimodal coating helps in increasing the oxidation performance of the coating. Better oxidation resistance of heat treated coatings may be associated to the rapid development of oxides at the splat boundaries of the coating and within open pores owing to penetration of the oxidizing species via the boundaries of splat or open pores during HT of the coated samples in oxidizing condition .(Guilemany et al., 2002) reported the development of Cr_2O_3 by heat treating the Cr_3C_2–NiCr coating at temperature 1153 K for 60 min in an oxidizing atmosphere. The coating becomes dense after the oxides form at splat boundaries and locations of porosity; as a result, corroding species diffusion to the internal portions of the coatings is hindered, and oxide growth is constrained mostly to the specimen's surface (Mahesh *et al.*, 2008). This in turn enhances the coatings

resistance to combat corrosion. Nb and Mb were also seen in the coating and higher concentration of these elements is considered to be beneficial for corrosion resistance. Furthermore, enrichment of Ti and Cr is also found in the oxidized coatings which results in the formation of Cr_2O_3 and TiO_2 and same has been also confirmed in XRD analysis. The Cr_2O_3 phase is said to be thermodynamical stable phase up-to very high-temperatures due to its very high melting point and forms a dense, continuous and adherent layer that inhibits interaction of oxygen with the underlying coating/substrate.

5.2 SUMMARY

Initially three set of Inconel625-Al_2O_3composite coatings were developed by varying Al_2O_3 particle sizes in micrometric, nano, and bimodal forms. The Inconel625+30wt.% micrometricAl_2O_3, Inconel625+30 wt.% nano-Al_2O_3 and Inconel625+15 wt.% micrometric Al_2O_3+15%nano-Al_2O_3 combinations were considered. In weight gain terms, the Plasma sprayed IN625-BHT oxidized coating was best among all composite coatings and it reduces the weight gain of ASTM-SA210 GrA1 boiler steel by 96.7%. (Bala *et al.*, 2017) also noticed the performance of Ni based NiCrTiC and NiCrTiCRe coatings deposited by cold spray (CS) technique for high temperature oxidation conditions at 700°C. The authors have reported an almost 78 % reduction in the corrosion rate of substrate material with the aid of such Ni-based coating. High denseness combined with low oxide content is the most vital properties that guarantee high resistance to erosion and corrosion of the Ni coating. It was suggested by many authors in literature that addition of Al_2O_3 hard particles in the nimonic (NiCr) coating, will enhance corrosion, and erosion resistance of the composite coating and represent a promising candidate for the power generation sector applications.

In high temperature applications like boilers and gas turbines, the optimum combinations of mechanical properties are needed, and this could be attained only with development of composite coatings. The use of composite coatings in literature with Ni as a ductile matrix and alumina as a hard phase showed a better performance against

slurry erosion in comparison to the substrate up to 2.5 times (Grewal *et al.*, 2013). The surface has to withstand high-temperature oxidation and erosion at same time.

The oxidation study of all composite coatings on ASTM SA210 GrA1 substrate yield the better results against oxidation as compared to bare ASTM SA210 GrA1 substrate when exposed to cyclic oxidation at 900°C. The IN625-BHT showed minimum weight gain 3.36 mg/cm^2 amongst all deposited composite coatings. Therefore this coating gives maximum oxidation resistance at high temperatures as compared to other deposited coatings. The oxide phases Al_2O_3 Cr_2O_3, TiO_2, and spinels $NiCr_2O_4$, $CrNbO_4$ developed during the oxidation process were responsible for the better oxidation resistance of bimodal heat treated IN625-BHT coating. According to (Ul-Hamid, 2003) and (Sundararajan et al., 2004), these oxides are protective. (Ren et al.,2005) reported the production of $NiCr_2O_4$ spinel in oxide scales by solid phase reaction between NiO and Cr_2O_3, which aids in the development of oxidation resistance because the spinel phase has lower cation and anion diffusion coefficients than parent oxides (Kamal *et al.*, 2009). The better outcome of bimodal heat treated coatings was related to refined microstructures and development of protective oxides.

CHAPTER 6

HIGH TEMPERATURE EROSION STUDIES

This chapter discusses the high-temperature erosion behaviour of bare ASTM-SA210 GRA1 substrate, and Plasma-sprayed coatings. The elevated temperature erosion tests for bare substrate and coatings were conducted at 900 °C by using an erosion test rig (air jet) at two impingement angles 30° and 90°. By studying the eroded surfaces through scanning electron microscopy (SEM) micrographs, the mechanism of material removal was predicted. The coated and uncoated samples were tested for 10 min duration. Thereafter, mass loss was calculated with weight measurement of the eroded samples. The erosive wear rate (g/g) is calculated as the ratio of erosive wear mass loss to erodent particle mass.

6.1 RESULTS AND DISCUSSIONS

The erosion testing was carried out on a hot air-jet erosion test rig apparatus *(Model: TR-471-800, Manufacturer: Ducom instruments-India)* with ASTM standard G76-02 available with GNE, Ludhiana, India as discussed in Chapter-4. The next sections detail the results obtained after subjecting test specimens to various characterizations.

6.1.1 EROSION TESTING

6.1.1.1 IMAPCT ANGLES EFFECT ON EROSION

The solid particle erosion testing was carried out at a temperature of 900°C on the bare ASTM-SA210 GrA1 and plasma sprayed IN625-ALC, IN625-ALN and IN625-ALB coated samples at impingement angles of 30° and 90°, respectively. Optical photographs of samples at low magnification subjected to two test angles are presented in **Fig.6.1.** The composite structures suffered less damage in comparison to the bare ASTM-SA210 GrA1 substrate at both testing angles. The resistance to high-temperature erosion for both

coated and uncoated material can be examined by their impression size and shape (wear area). The erosion wear rates (g/g) for bare ASTM-SA210 GrA1 and coated specimens were evaluated and presented in **Fig.6.2a & b.**

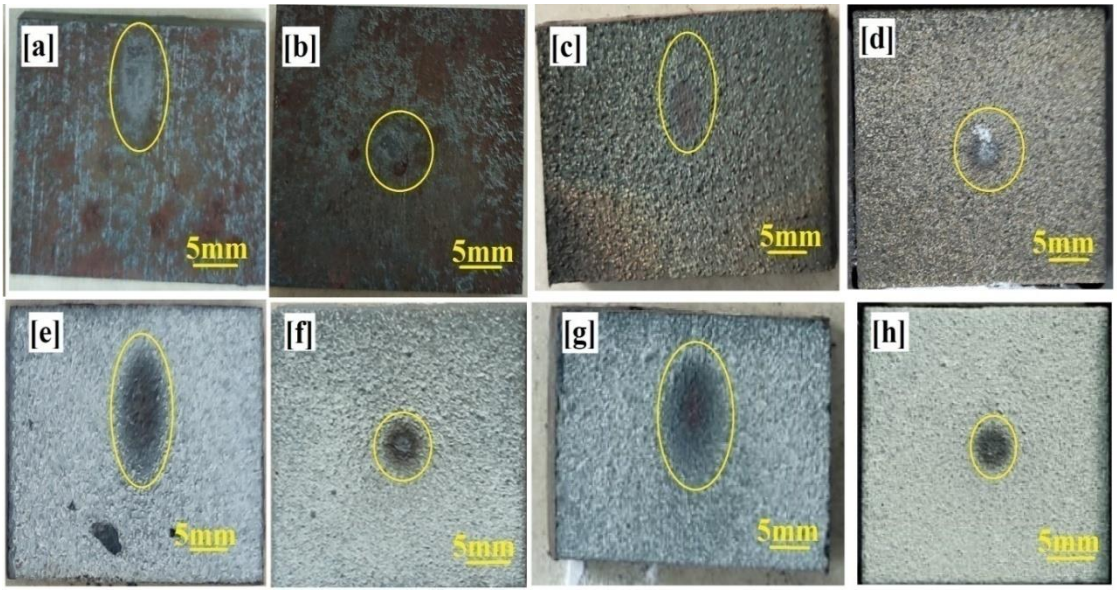

Fig.6.1. Optical macrograph of eroded samples: (a-b) Un-coated, (c-d) IN625-ALC at 30° and 90° impingement angles, (e-f) IN625-ALN at 30° and 90° impingement angles and, (g-h) IN625-ALB at 30° and 90° impingement angles.

For as-sprayed eroded coatings shown in Fig.6.2a, IN625-ALB composite coating has the maximum erosion resistance followed by IN625-ALN coating and IN625-ALC coatings at both testing angles. The erosive wear resistance of IN625-ALB composite coating was approximately 4.57 times and 3.9 times better in comparison with bare ASTM-SA210 GrA1 at 30º and 90º impingement angles, respectively. Simultaneously, nano-Al_2O_3 reinforced coating has shown a better distribution of nano-Al_2O_3 reinforcement in the IN-625 matrix and exhibited 2.6 times and 2.75 times better erosion resistance as compared to the substrate at 30º and 90º impingement angles respectively. That was followed by micrometric reinforced Al_2O_3 coating which exhibited ~2.2 times and ~1.68 time's better erosion resistance at 30º and 90º impingement angles, respectively. The erosive wear resistance of IN625-BHT composite coating was

approximately 6.8 times and 8.2 times better in comparison with bare ASTM-SA210 GrA1 at 30º and 90º impingement angles, respectively. Simultaneously, nano-Al_2O_3 reinforced coating has shown a better distribution of nano-Al_2O_3 reinforcement after HT in the IN-625 matrix and exhibited 3.4 times and 5.5 times better erosion resistance as compared to the substrate at 30º and 90º impingement angles respectively.

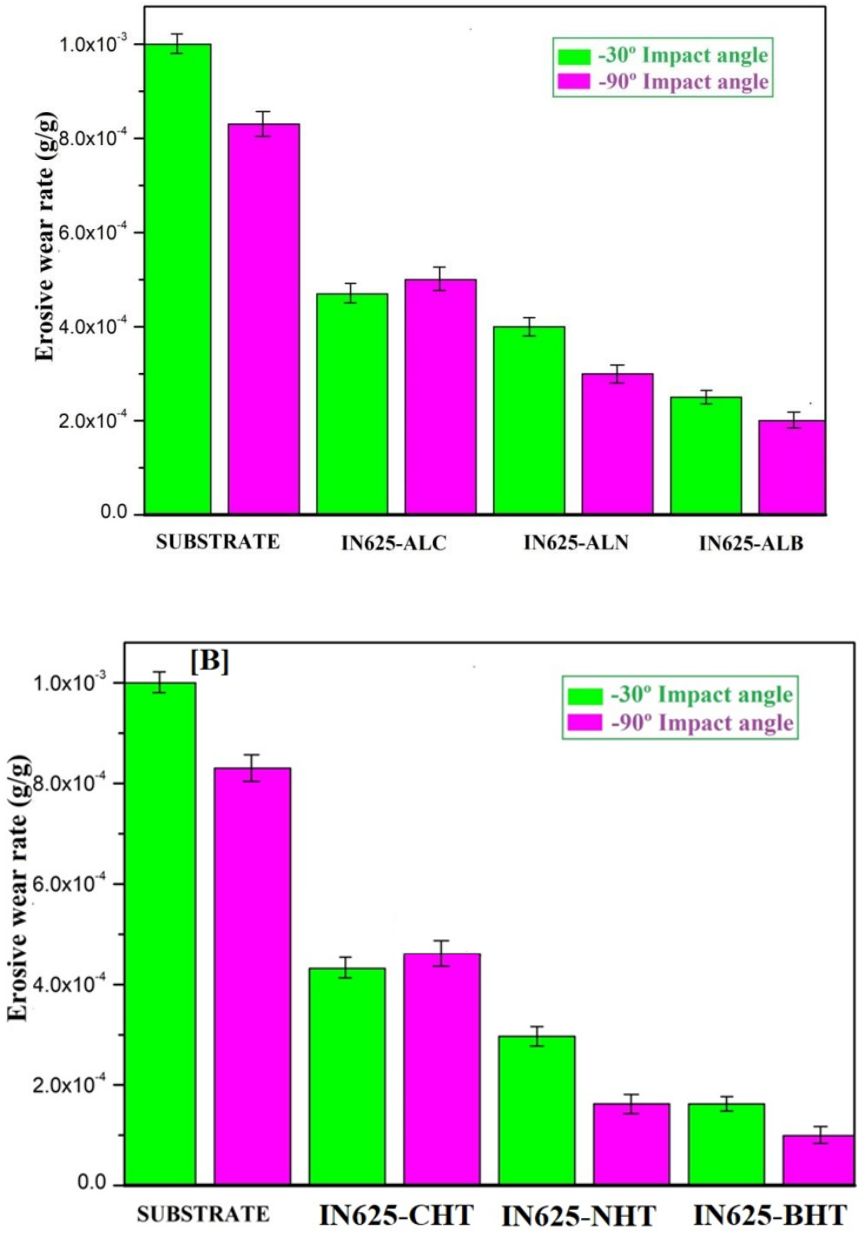

Fig.6.2(a) The erosion wear rates (g/g) for bare ASTM-SA210 GrA1 and coated specimens, (b)The erosion wear rates (g/g) for post treated coated specimens

That was followed by micrometric reinforced Al_2O_3 coating which exhibited ~2.3 times and ~1.72 time's better erosion resistance at 30º and 90º impingement angles after HT, respectively. Therefore, the outcomes show the usefulness of the IN625-BHTcomposite structure in combating high-temperature erosion in both testing conditions. The enhanced performance of the IN625-BHT composite can be related to high hardness and better resistance to plastic defromation. Higher hardness increases the ability of a material to resist plastic deformation. This resistance against plastic deformation further improves coatings fracture toughness by reducing the crack front propagation. The Al_2O_3 particle reinforcement in the micrometric and nano-sized coatings contributes toward dispersion strengthening. That has resulted in a further increase in hardness and erosive resistance for the reinforced coatings. The synergy of micrometric and nano-sized particles contributes toward enhanced hardness as dislocations induced through plastic deformations interact with GD and thereby enhanced the erosion resistance. Further, stable oxides like Cr_2O_3 and Al_2O_3 also contributed to enhanced erosion resistance of composite structures.

6.1.1.2 EROSION MECHANISM

The erosive wear mechanism of the worn-out surface of ASTM-SA210 GrA1 and plasma spray IN625-ALC, IN625-ALN, and IN625-ALB coated samples were analyzed using SEM micrographs. The erosion mechanism was controlled by synergistic effects of erosion and oxidation. At higher temperatures, higher impact velocities and feed rates of oxidation appear, and the effect of oxidation was also noticed on the surface of a bare substrate as exhibited in **Fig.6.2a.** The boiler steels showed a thin scale at this temperature range. Due to erosion, the scale on the substrate surface was cleaned in the eroded zone. Erodent impact further removes the scale present on substrate down to the interface of substrate-scale as exhibited in **Fig6.2a(**Kumar and Sapra, 2016). The **Fig.6.3.**shows SEM images of the bare substrate obtained after the erosion testing carried out at high temperatures. The material removal rate depends upon the various impingement angles during the erosion tests. At low angles, material removal occurs owing to the micro-cutting action of incoming erodent particles. The appearance of

ploughing marks in **Fig.6.3a**, exhibits resemblance with the existing studies on the wear characteristics of ductile materials (Laguna-Camacho *et al.*, 2013). The SEM images of the bare substrate (Fig.6.3a) indicated the displaced material. The degraded surface shows signs of deformation and indentations (scratches). Moreover, the plastic deformation with raised lips was also observed on the eroded surface. In **Fig.6.3b**, craters, ploughing, and scratches were seen at a 90° impact angle. Therefore, it may be inferred that the uncoated substrate has a ductile mode of erosion, in which material was removed mostly through plastic deformation (Laguna-Camacho *et al.*, 2013). At an angle of 30º, maximum material removal occurs and less material removal was noticed at the normal angle.

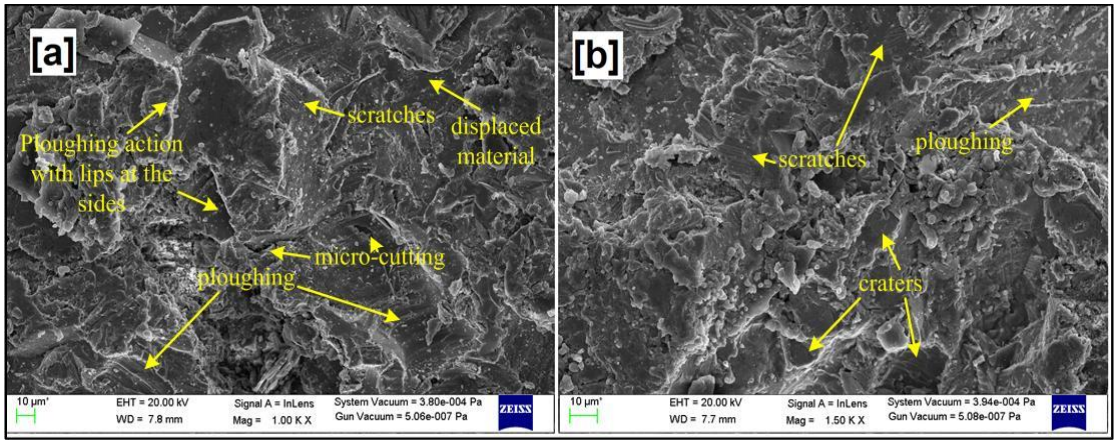

Fig.6.3 SEM micrographs of eroded un-coated samples: (a) at 30° impingement angle and (b) at 90° impingement angle.

The SEM surface morphologies of IN625-ALC, IN625-ALN, and IN625-ALB coated samples at 30° and 90° impact angles are shown in **Fig.6.4-6.6.** The splat removal, cracks, and fracture are the major erosion mechanism responsible for material removal in coated samples. At an angle of 30°, the existence of sites indicates that material removal takes place by the medium of splats removal as shown in **Fig.6.4a and 6.4b**, respectively. At oblique impact angle, tangential forces acting on splats owing to incoming erodent particles were high which results in detachment of splats (Praveen *et al.*, 2015; Vasudev *et al.*, 2022). IN625-ALC composite structure exhibited better erosive wear resistance at an angle of 30° in comparison to 90° impingement angle due to the shielding effect of

blocky Al_2O_3 particles. Identical results were also observed in the literature previously (Vasudev *et al.,* 2022). At glancing impingement, in the case of IN625-ALN (**Fig.6.5a & b**) and IN625-ALB (**Fig.6.6 a &b**) composite coatings, the reinforcement of nano-Al_2O_3 enhances the cohesion of powder particles in contrast to the IN625-ALC coatings. The SEM micrographs of eroded IN625-ALN coating (**Fig.6.5 b&c**) showed the existence of fractured Al_2O_3 splats, cracks, and detached splats.

The micrographs (**Fig.6.4 c-d**) of eroded surfaces indicate Al_2O_3 fractured splats, cracks, and removed splats as the main erosion mechanism at a 90º impingement angle (Grewal *et al.,* 2013 and 2014). At an impingement angle of 90º, the eroded IN625-ALN (**Fig.6.5 c-d**) and IN625-ALB (**Fig.6.6 c-d**) coating surfaces showed impressions of cutting produced by incoming eroded particles. However, in the case of IN625-ALC coating (**Fig.6.4c-d**), it experienced more material removal via cracking and spalling as compared to IN625-ALN and IN625-ALB coatings, respectively. This confirms identical findings by the studies of the erosive wear mechanism of Inconel718-Al_2O_3 coatings (Vasudev *et al.,* 2022). At 90° impingement angle, all the composite coatings exhibited brittle erosion mode and detached finally from the surface of the coating with further impingements. In addition, at normal impacts Al_2O_3 particles shielding effect also reduces and dislocation accumulation in the frail bonding boundaries of alumina particles accelerates their pull-out. However, the nano-Al_2O_3 powder particles were evenly disseminated throughout the microstructure of the coating. Thus, they provide enhanced erosion resistance of IN625-ALN and IN625-ALB composite coatings at normal impact angles by providing dispersion strengthening.

IN625-ALB coated samples depict better erosive wear resistance among all the coatings at both testing angles. Because erosive wear resistance of the composite structure is a function of the material hardness and resistance to plastic deformation which controls the erosion behavior of coating. The hardness value were more for the IN625-ALB composite coating followed by the other two coatings. Thus, an optimum mix of the hardness arising from the positive interaction among the micrometric and nano-Al_2O_3 particles helped in enhancing the erosion performance of IN625-ALB coated

samples. The erosive wear mechanism of coatings at oblique and normal impacts was summarized in **Fig.6.7.**

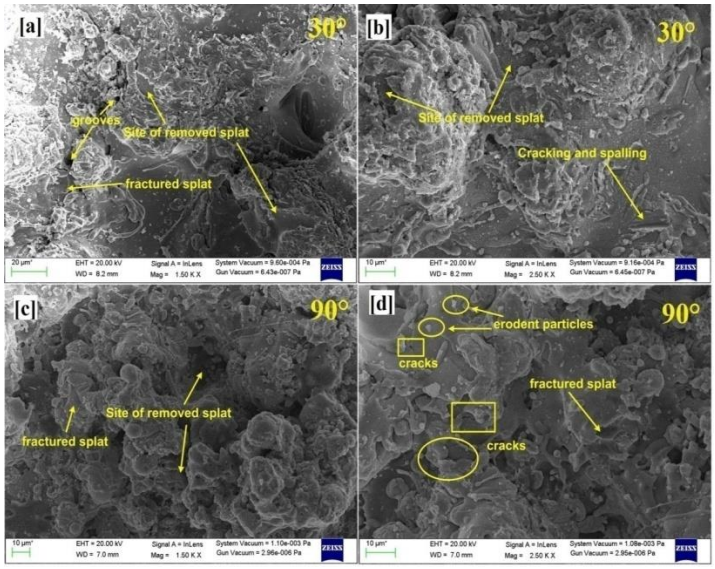

Fig.6.4. SEM images of: (a-b) eroded IN625-ALC coatings at 30° impingement angle and , (c-d) eroded IN625-ALC coatings C at 90° impingement angle.

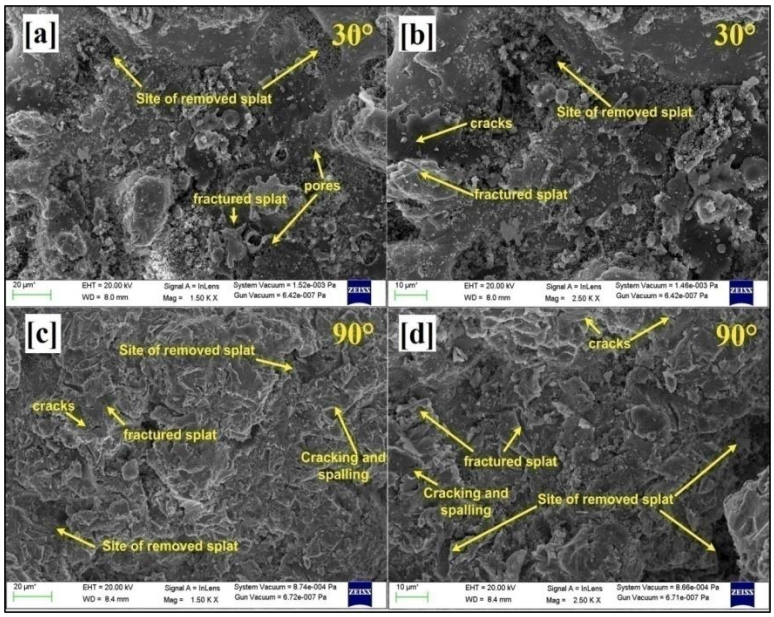

Fig.6.5. SEM images of: (a-b) eroded IN625-ALN coatings at 30° impingement angle and, (c-d) eroded IN625-ALN coatings C at 90° impingement angle

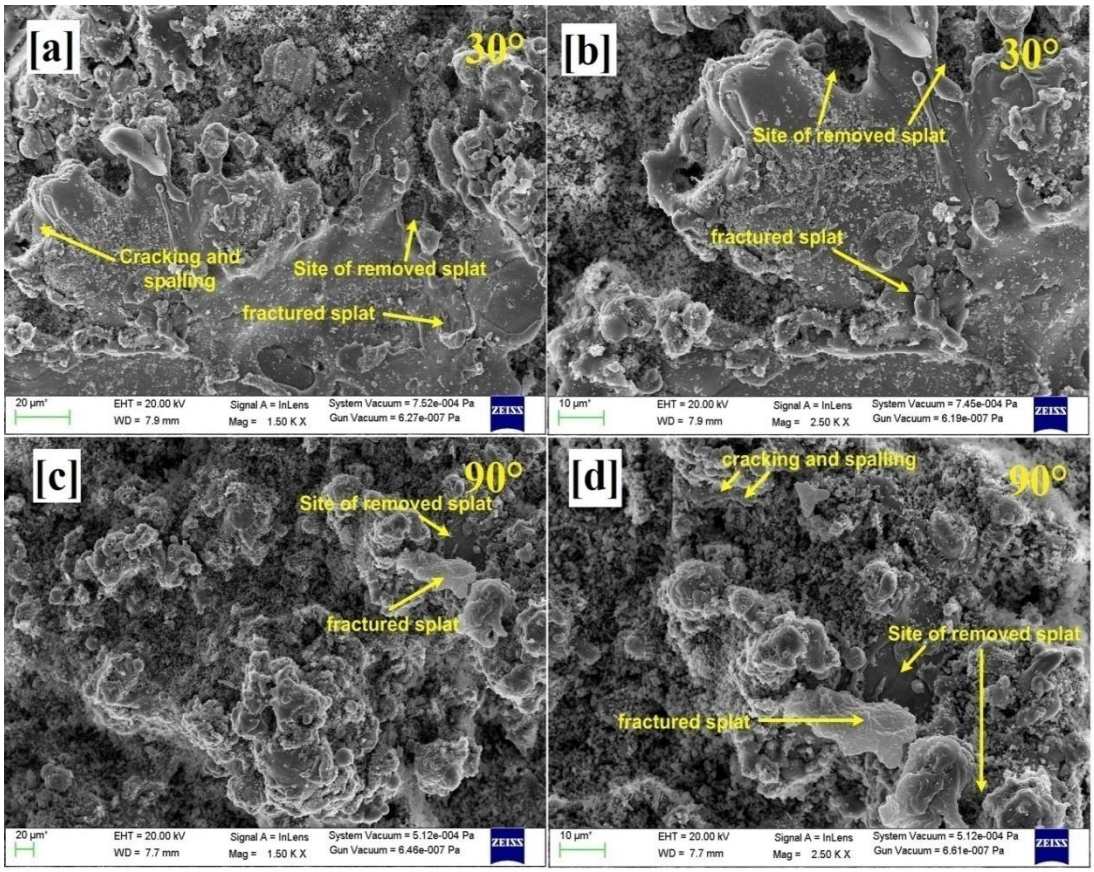

Fig.6.6. SEM images of: (a-b) eroded IN625-ALB coatings at 30° impingement angle and , (c-d) eroded IN625-ALB coatings at 90° impingement angle.

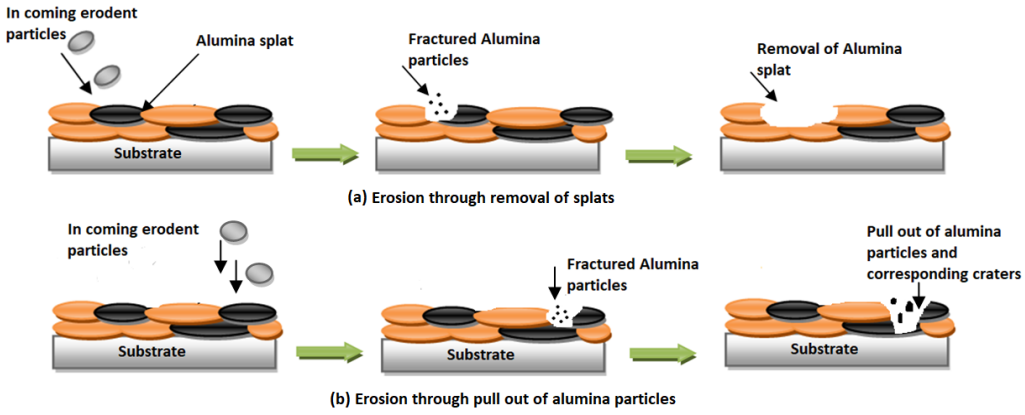

Fig.6.7. Mechanism of erosion at: (a) oblique impingement angle (30º), and (b) at normal impingement angle (90º).

6.2 ERODED AREA ANALYSIS OF HEAT TREATED SAMPLES

6.2.1 EFFECT OF HEAT TREATING

The eroded macrophotographs of the surfaces of heat treated samples are depicted in **Fig.6.8.** The impression shapes is elliptical for low impact angle (30º) and tends to become of a circular shape when angle of impact reaches 90º. On comparing the imprints shown in **Fig.6.8**, with the macrographs shown in**Fig.6.1**, it can be noticed that HT does not induce any remarkable variation in the shape of erosion marks. However, this type of post HT may remarkably enhance the hot erosion resistance of composite coatings.

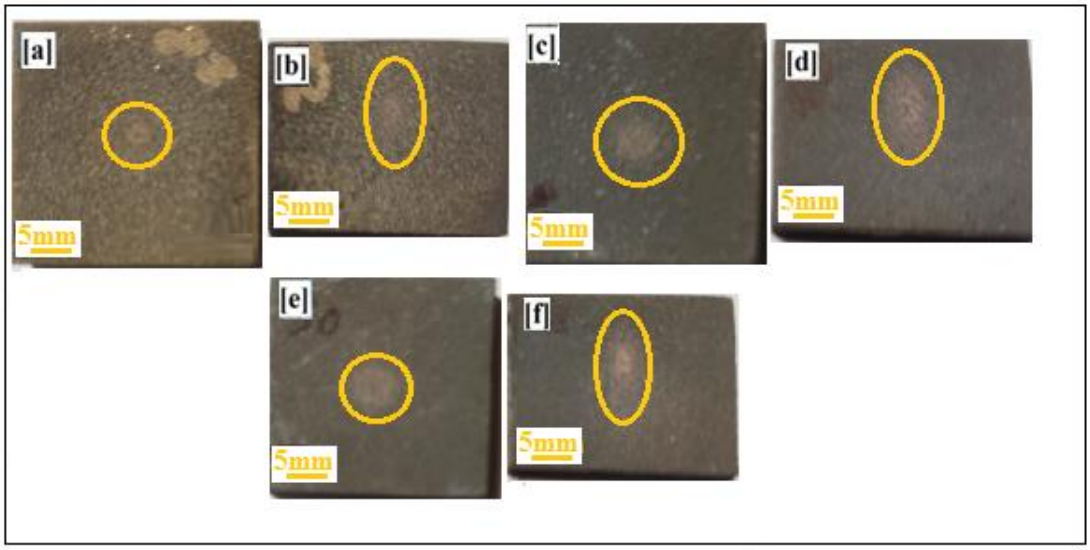

Fig.6.8. Optical macrograph of eroded samples: (a-b) IN625-CHT at 90° and 30° impingement angles, (c-d) IN625-NHT at 90° and 30° impingement angles and, (e-f) IN625-BHT at 90° and 30° impingement angles.

In most of other studies post HT were conducted at 800–1100ºC (Moskowitz, 1997; Gutleber*et al.,* 1997; Khor and Cheang, 1994; Matsubara *et al.,* 1998; Wielage and Fleischer, 1998).In those investigations, post-HT usually includes laser heating, or thermal flame heating. Such HT could result in fusing or sintering of the deposits thereby changing their phase and microstructure. HT was only carried out at temperatures as low

as 720°C in this study, and no notable microstructure changes were observed. Heat-treating increased the hardness and minimizes the porosity content of all three coatings, as discussed earlier. This, in turn, could explain why heat-treated coatings are more resistant to hot erosion in comparison to as-sprayed ones. However, the function of HT is not restricted to increase hardness or reduce porosity content. HT of sprayed coatings can help reduce residual stress and improve coating adhesion strength and ductility (Ahmaniemi *et al.,* 2000; Stokes and Looney, 2000). This can contribute towards improved erosion resistance (Wang, B.Q. and Verstak, 1999) as thermally sprayed coatings with higher levels of residual stresses were more sensitive to micro-cracking that might promote higher erosion rates (Hearley *et al.,* 1999).

6.2.2 EFFECT OF IMPACT ANGLE

Three reference coatings ie, IN625-CHT, IN625-NHT and IN625-BHT behaved like a typical brittle erosion manner. At 90° impingement angle, all the composite coatings exhibited brittle erosion mode and detached finally from the surface of the coating with further impingements (**Fig.6.9c-d, 6.10c-d and 6.11c-d**). For first composition (IN625-CHT or IN625-ALC) regardless of as-sprayed or heat treated maximum erosion occurs at 90º angle showing characteristics of brittle erosion material. Maximum erosion at 90º angle in case of IN625-CHT coating in comparison to IN625-NHT and IN625-BHT and it occurs due to fracture and pull out of conventional Al_2O_3 particles from the matrix. The examination of the surfaces of the IN625-CHT coating eroded at impact angles 90° shows that in this case the erosion mechanism seems to be entirely cracking and chipping (inset **Fig.6.9c-d**) brittle mode without ductile deformation. Obviously, a significant number of particles chipped off and a big volume of material removed resulted in a coarse and rough surface morphology, which explains their larger erosion waste at 90° than that eroded at 30° impact angles. At 30º impact angle (inset **Fig.6.9a-b**) small craters were developed and the striations were developed on the ductile nickel matrix either as a replica of the erodents or due to the repetitive impact of their sharp edges causing only slight erosion wastage. Splat removal, and cutting marks are the major erosion mechanism responsible for material removal in IN625-CHT coated

sample. At an angle of 30° existence of craters indicates that material removal takes place by medium of splats removal.

SEM surface morphology of IN625-NHT and IN625-BHTcoating samples at 90º impact angle is presented in **Fig.6.10c-d and 6.11c-d** ;appeared to be solely cracking and chipping brittle mechanism. At 30º impact angle presented in **Fig.6.10a-b and 6.11a-b**; the surfaces shows small craters and striations indicating a ductile deformation mode, but cracking and chipping brittle mechanism also contributed to the erosion mechanism.

6.3 EFFECT OF PARTICLE SIZE

IN625-NHT and IN625-BHT has higher erosion resistance at 90º impact angles in comparison to IN625-CHT coating. The existence of Al_2O_3 nanoparticles in IN625-NHT coating prevented the platelet formation that is commonly fostered in case of metallic materials (Bergmann and Vicenzi, 2011). This occurs because erodents contact with multiple nanostructured Al_2O_3 particles that are at least two orders of magnitude smaller in size than the striking alumina particles when they collide. Moreover, nanostructured Al_2O_3 particles also assist in crack arrest and prevent its propagation in the matrix. (Triantou *et al.*, 2015)studied the effect of Al_2O_3 addition on the sliding wear resistance of Cu coatings, concluded that the presence of small sized Al_2O_3, particle sizes, acts beneficiary and reduces mass loss of the coatings.

The better performance of IN625-BHT coating amongst all the heat treated coatings is related with the positive interactions among micron and nanostructured Al_2O_3 particles. Micron-sized Al_2O_3 particles assist in the deflection of the crack path whereas presence of nanostructured Al_2O_3 particles around its vicinity can successfully increases the fracture energy via crack blunting. Post heat-treating, according to (Wang, 2003), was helpful in improving coatings' high-temperature erosion resistance.

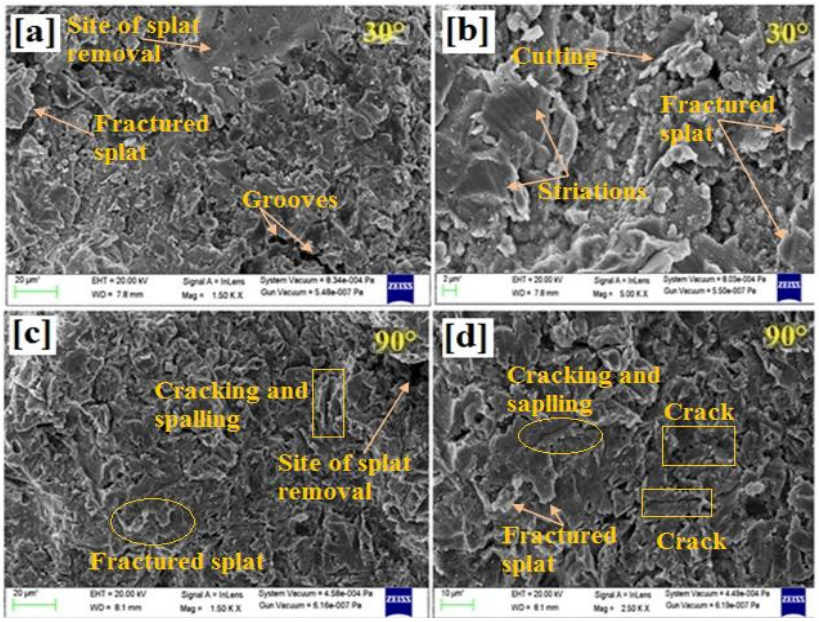

Fig.6.9 SEM images of: (a-b) eroded IN625-CHT coatings at 30° impingement angle and, (c-d) eroded IN625-CHT coatings at 90° impingement angle.

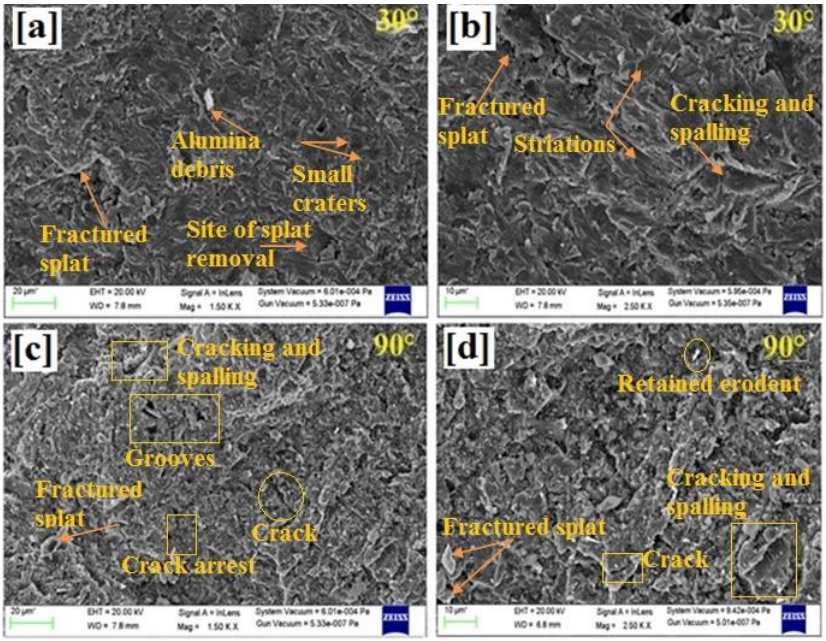

Fig.6.10 SEM images of: (a-b) eroded IN625-NHT coatings at 30° impingement angle and, (c-d) eroded IN625-CHT coatings at 90° impingement angle.

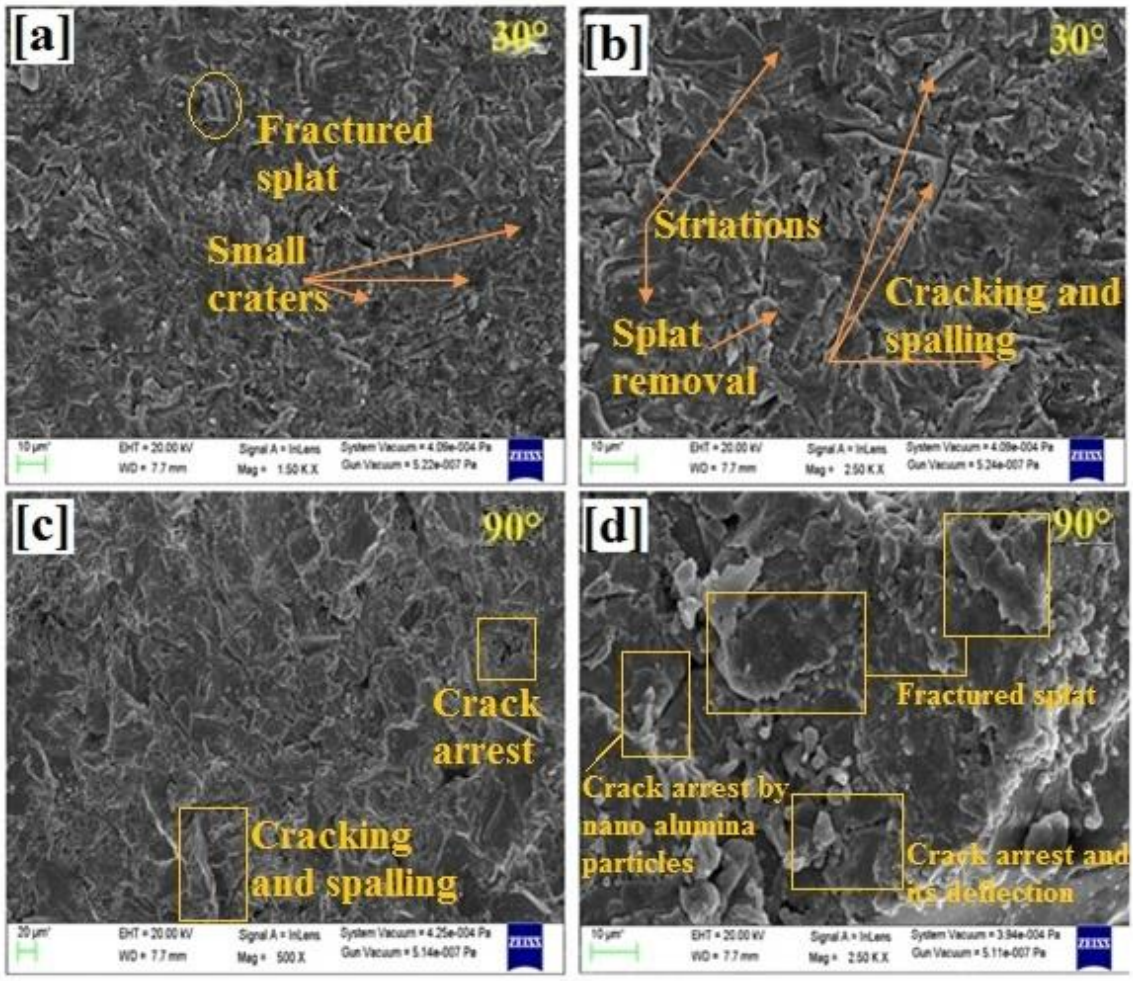

Fig.6.11 SEM images of: (a-b) eroded IN625-BHT coatings at 30° impingement angle and , (c-d) eroded IN625-BHT coatings at 90° impingement angle.

Chapter 7

COMPARATIVE DISCUSSION

The results of the current experiment have been presented in this chapter by comparing the performance of uncoated, PS coated (with and without HT) ASTM-SA210 GrA1 substrate. The effect of the addition of 30 wt% Al_2O_3 as reinforcement by varying the particle size in micrometric, nanometric, and bi-modal forms was discussed. There is a difference in the values of micro-hardness and porosity for IN625-ALC, IN625-ALN, IN625-ALB, IN625-CHT, IN625-NHT, and IN625-BHT composite coatings and it has been discussed in this section. The performance of uncoated and coated composite coatings in aggressive cyclic oxidation has been presented. In addition to that the hot erosion performance of uncoated and coated composite coatings has also been discussed for all the deposited coatings.

7.1 POROSITY AND MICRO-HARDNESS

The IN625-ALC coating showed a porosity of 2.5%. The IN625-ALN displayed 1.9% porosity and IN625-ALB showed a porosity of 1.5%. For heat treated coating it is reported to be in the range 1% to 2%.

The hardness of IN625-ALB (1130±25 $Hv_{0.3}$) coating was higher in comparison to IN625-ALC (680±27 $Hv_{0.3}$) and IN625-ALN (960±30 $Hv_{0.3}$). After HT the micro-hardness increases further. This latter value of hardness shows an increase of approx. 25% for IN625-BHT when compared with the micro-hardness value of IN625-ALB coating. The micro-hardness values of IN625-CHT and IN625-NHT also recorded an improvement in hardness of 15-20% when compared with IN625-ALC and IN625-ALN coatings, representing the outcome of the homogenous distribution of hard Al_2O_3 phase and a reduction in both the un-melted particles count and porosity content induced by

HT. **Table 7.1** shows the comparative values of porosity and micro-hardness for developed coatings.

Table 7.1 Comparative average values of the porosity and micro-hardness for all composite coatings.

Coating	**Porosity %**	**Micro-hardness $H_{V0.3}$**
IN625-ALC	2.5	680±27
IN625-ALN	1.9	960±30
IN625-ALB	1.5	1130±25
IN625-CHT	2	716±27
IN625-NHT	1.4	1152±30
IN625-BHT	1	1299±25

7.2 OXIDATION STUDIES OF ASTM-SA210 GRA1 SUBSTRATE AND PS DEPOSITED COMPOSITE COATINGS

Weight change data of the composite coatings in (mg/cm^2) versus 50 numbers of cycles are depicted in **Table 7.2**. The ASTM-SA210 GrA1 under examination has shown least oxidation resistance against severe cyclic conditions at 900°C, and the IN625-Al_2O_3 coatings have successfully reduced total weight gain for all the tested combinations of feedstock powders when compared to bare substrate, as indicated in the **Table 7.1**. The weight gain for uncoated ASTM-SA210 GRA1 grows as the exposure period increases, eventually reaching its greatest weight among all the specimens exposed to the cyclic oxidation tests. The SEM examination of the uncoated boiler steel (**Fig.5.6a**) reveals the appearance of a thick, fragile and granulated scale, whereas the EDAX analysis affirms

that this granular scale comprises Fe and O throughout scale composition. This strongly confirms the possibility of the development of a weak Fe_2O_3 phase, and the same has also been exhibited by XRD analysis.

Table 7.2 Cumulative weight gain of the bare substrate and all composite coatings during cyclic oxidation exposures at 900°C.

Specimens	**Weight gain (mg/cm^2)**
Bare ASTM-SA210 GRA1	101.6
IN625-ALC	10.3
IN625-ALN	9.03
IN625-ALB	6.86
IN625-CHT	6.03
IN625-NHT	5.03
IN625-BHT	3.5

Thus, in weight gain terms, the PS IN625-BHT oxidized coating was best among all the composite coatings. The microstructure of IN625-BHT appears to be dense and homogenous after HT resulting in reduction of pores and cracks. The simultaneous interactions of micron and nano-sized Al_2O_3 in IN625-BHT coating increases its hardness and also the presence of nano-sized Al_2O_3 in bimodal composition increases the oxidation resistance due to its inertness and high melting point. The development of coherent protective phases like, Al_2O_3 Cr_2O_3, TiO_2 and spinels $NiCr_2O_4$ and $CrNbO_4$ along with Ni-Cr matrix in IN625-BHT coating as confirmed by XRD patterns increases its oxidation resistance. Better oxidation resistance of IN625-BHT coating may be associated to the rapid development of oxides of Cr and Al at the splat boundaries of the coating and within open pores owing to penetration of the oxidizing species via boundaries of splat or open pores during HT of the coated samples in oxidizing

conditions. The coating becomes dense after the oxides form at splat boundaries and locations of porosity; as a result, corroding species diffusion to the internal portions of the coatings is hindered, and oxide growth is constrained mostly to the specimen's surface and as a result steady state rate of oxidation is achieved (Sidhu *et al.*, 2006d). The parabolic rate constants values for the samples are summarized in **Table 5.1.**already in Chapter-5. The bare ASTM-SA210 GRA1 substrate had the highest parabolic rate constant, and the most protective coating was IN625-BHT with the lowest k_p.

7.3 HIGH TEMPERATURE EROSION STUDIES

The uncoated substrate has a ductile mode of erosion, in which material was removed mostly through plastic deformation. The minimum erosion occurs at 30º angle indicating ductile mode of erosion.

All composite coatings with or without HT exhibited the brittle erosion mode irrespective of the impact angle. The splat removal, cracks, and fracture are the major erosion mechanism responsible for material removal in coated IN625-ALC, IN625-ALN, and IN625-ALB samples.SEM surface morphology of IN625-CHT, IN625-NHT and IN625-BHT coating samples appeared to be solely cracking, splat removal and chipping brittle mechanism. The comparative erosive wear rate in g/g is depicted in **Fig.6.2 a & b**. The better performance of IN625-BHT coating amongst all the coatings is related with the positive interactions among micron and nanostructured Al_2O_3 particles. Micron-sized Al_2O_3 particles assist in the deflection of the crack path whereas presence of nanostructured Al_2O_3 particles around its vicinity can successfully increases the fracture energy via crack blunting.

The developed cracks were arrested and deflected in the bimodal structure of the IN625-BHT coating and therefore providing maximum erosion resistance. The erosive wear resistance of IN625-BHT composite coating improves approximately 6.8 times and 8.2 times in comparison with bare ASTM-SA210 GrA1 at 30º and 90º impact angles respectively. The erosive wear rate in g/g for ASTM-SA210 GrA1 substrate and different coatings were summarized in **Table 7.3**

Table 7.3 The erosive wear rate in g/g for ASTM-SA210 GrA1 substrate and different coatings

Specimens	**Erosive wear rate [g/g] at 30°**	**Erosive wear rate [g/g] at 90°**
Bare ASTM-SA210 GrA1	1.0×10^{-3}	8.2×10^{-4}
IN625-ALC	4.7×10^{-4}	4.9×10^{-4}
IN625-ALN	4.0×10^{-4}	3.0×10^{-4}
IN625-ALB	2.5×10^{-4}	2.1×10^{-4}
IN625-CHT	4.4×10^{-4}	4.8×10^{-4}
IN625-NHT	3.0×10^{-4}	1.5×10^{-4}
IN625-BHT	1.5×10^{-4}	1.0×10^{-4}

Chapter 8

CONCLUSIONS AND FUTURE SCOPE

8.1 CONCLUSIONS

The following conclusions have been drawn based on the experimental results collected and their interpretation in this work:

1. Three combinations of IN625-AL_2O_3 coatings were successfully developed by using the plasma spraying technique.
2. The cross-section of the developed coatings showed a typical coating thickness of 250-300 µm and coatings showed well bonding at the interface without any sign of diffusion of elements.
3. The porosity of the developed surfaces was found to be in a range of 1.5 to 2.5% for as-sprayed IN625-AL_2O_3 coatings. For heat treated IN625-AL_2O_3 coatings it is reported to be in the range 1% to 2%. This was related to the rapid diffusion process, which reduces cracks and fill pore/voids in the heat treated coatings. The dark phase corresponds to the presence of Al_2O_3 in all the coatings.
4. The micro-hardness analysis showed the maximum hardness of 1130 $HV_{0.3}$ for bi-modal coating, which is 5 times higher than the bare substrate owing to interaction among nano and micrometric particles that provides extra strength. After HT the micro-hardness increases further. This latter value of hardness shows an increase of approx. 15% for IN625-BHT coating when compared with the micro-hardness value of IN625-ALB coating.
5. The oxide scale develops on the bare ASTM-SA210 GrA1 boiler steel indicates Fe oxides formation in outermost layers of the developed scale, which is complemented well by surface XRD reports. It can be noticed clearly from the X-ray maps and line scan the overall oxide scale forms consist mainly of elements

Fe and O, indicating the Fe_2O_3-rich scale. This is not desirable as it results in the loss of mechanical strength and reduces the oxidation resistance of steel.

6. In weight gain terms, the PS IN625-BHT oxidized coating was best among all the composite coatings when exposed to cyclic oxidation studies at 900ºC. The development of coherent protective phases like, Al_2O_3 Cr_2O_3, TiO_2 and spinels $NiCr_2O_4$ and $CrNbO_4$ along with Ni-Cr matrix in IN625-BHT coating as confirmed by XRD patterns increases its oxidation resistance.
7. The parabolic rate constants for deposited PS coatings were reduced significantly and minimal value of K_P was recorded in case of IN625-BHT coating in order of 0.7 and therefore responsible for superior oxidation resistance amongst all PS deposited coatings. For uncoated ASTM-SA210 GRA1, the value of K_P was found to be 619.35.
8. The existence of grooves and lips at 30º and 90 º impingement angles on surfaces indicate the erosion mechanism consists of ploughing and micro-cutting action for the substrate. All composite coatings exhibited brittle erosion mode. The detached splats, fracture, and cracks were the responsible mechanism of erosion in coatings at 30º and 90º impingement angles. The erosive wear resistance of IN625-ALB composite coating improves approximately 6.8 times and 8.2 times in comparison with bare ASTM SA210 GrA1 at 30º and 90º impact angles respectively.
9. The better performance of IN625-BHT coating amongst all the coatings is related with the positive interactions among micron and nanostructured Al_2O_3 particles. Micron-sized Al_2O_3 particles assist in the deflection of the crack path whereas presence of nanostructured Al_2O_3 particles around its vicinity can successfully increases the fracture energy via crack blunting.

8.2 FUTURE SCOPE

1. Nano-IN625 could be used instead of micron sized IN625 and other ceramics powders like TiO_2 may be used.
2. The hot corrosion testing in presence of the salts can be done on the coatings in order to know the effect of hot corrosion on the performance of the coatings.
3. The abrasive wear and electrochemical testing of the coatings may also be performed for specific high temperature applications like blades of turbine.
4. Testing can be performed in actual boiler conditions.

Chapter 9

BIBLIOGRAPHY

1. Ahmaniemi, S., Rajamäki, E., Vuoristo, P. and Mäntylä, T., 2000, May. Effect of aluminum phosphate sealing treatment on properties of thick thermal barrier coatings. In *ITSC 2000* (pp. 1081-1086). ASM International.
2. Ansari, M.S., Chawla, V., Bansal, A. and Aggarwal, V., 2022. Comparative Study of High-Temperature Oxidation Behavior of Bare and Plasma Sprayed Al2O3-40% TiO2 Coated T-91, A-1 Boiler Steel and Superfer800H Superalloy in Air. *Journal of Materials Engineering and Performance*, *31*(1), pp.753-768.
3. Aung, N.N. and Liu, X., 2014. Effect of temperature on coal ash hot corrosion resistance of Inconel 740 superalloy. *Corrosion Science*, *82*, pp.227-238.
4. Awasthi, S., Pandey, S.K., Arunan, E. and Srivastava, C., 2021. A review on hydroxyapatite coatings for the biomedical applications: Experimental and theoretical perspectives. *Journal of Materials Chemistry B*, *9*(2), pp.228-249.
5. Azarmi, F., Saaedi, J., Coyle, T.W. and Mostaghimi, J., 2008. Microstructure characterization of alloy 625 deposited on nickel foam using air plasma spraying. *Advanced Engineering Materials*, *10*(5), pp.459-465.
6. Bala, N., Singh, H. and Prakash, S., 2010. High temperature corrosion behavior of cold spray Ni-20Cr coating on boiler steel in molten salt environment at 900 C. *Journal of Thermal Spray Technology*, *19*(1), pp.110-118.
7. Bala, N., Singh, H. and Prakash, S., 2011. Characterization and high-temperature oxidation behavior of cold-sprayed Ni-20Cr and Ni-50Cr coatings on boiler steels. *Metallurgical and Materials Transactions A*, *42*(11), pp.3399-3416.
8. Bala, N., Singh, H. and Prakash, S., 2017. Performance of cold sprayed Ni based coatings in actual boiler environment. *Surface and Coatings Technology*, *318*, pp.50-61.

9. Bansal, A. and Zafar, S., 2017. Influence of heat treatment on microstructure and mechanical properties of Inconel-625 clad deposited on mild steel.
10. Bansal, A., Zafar, S. and Sharma, A.K., 2017. Influence of heat treatment on microstructure of Inconel 718 microwave clads. *Surface Engineering*, *33*(3), pp.167-174.
11. Bergant, Z. and Grum, J., 2009. Quality improvement of flame sprayed, heat treated, and remelted NiCrBSi coatings. *Journal of thermal spray technology*, *18*(3), pp.380-391.
12. Bergant, Z., Trdan, U. and Grum, J., 2014. Effect of high-temperature furnace treatment on the microstructure and corrosion behavior of NiCrBSi flame-sprayed coatings. *Corrosion Science*, *88*, pp.372-386.
13. Bergmann, C.P. and Vicenzi, J., 2011. Protection against erosive wear using thermal sprayed cermet: a review. *Protection against Erosive Wear Using Thermal Sprayed Cermet*, pp.1-77.
14. Birks, N., Meier, G.H. and Pettit, F.S., 2006. *Introduction to the high temperature oxidation of metals*. Cambridge university press.
15. Bolelli, G., Lusvarghi, L. and Barletta, M., 2008a. Heat treatment effects on the corrosion resistance of some HVOF-sprayed metal alloy coatings. *Surface and Coatings Technology*, *202*(19), pp.4839-4847.
16. Bolelli, G., Lusvarghi, L. and Giovanardi, R., 2008b. A comparison between the corrosion resistances of some HVOF-sprayed metal alloy coatings. *Surface and Coatings Technology*, *202*(19), pp.4793-4809.
17. Boulos, M.I., Fauchais, P.L. and Heberlein, J.V., 2021. *Thermal spray fundamentals: from powder to part*. Springer International Publishing.
18. Calvarin, G., Molins, R. and Huntz, A.M., 2000. Oxidation mechanism of Ni—20Cr foils and its relation to the oxide-scale microstructure. *Oxidation of Metals*, *53*(1), pp.25-48.

19. Campo, M., Carboneras, M., López, M.D., Torres, B., Rodrigo, P., Otero, E. and Rams, J., 2009. Corrosion resistance of thermally sprayed Al and Al/SiC coatings on Mg. *Surface and Coatings Technology*, *203*(20-21), pp.3224-3230.
20. Chatha, S.S., Sidhu, H.S. and Sidhu, B.S., 2013. High-temperature behavior of a NiCr-coated T91 boiler steel in the platen superheater of coal-fired boiler. *Journal of thermal spray technology*, *22*(5), pp.838-847.
21. Chatha, S.S., Sidhu, H.S. and Sidhu, B.S., 2016. Performance of 75Cr3C2-25NiCr coating produced by HVOF process in a coal-fired thermal power plant. In *Advanced Materials Research* (Vol. 1137, pp. 88-100). Trans Tech Publications Ltd.
22. Chatterjee, U.K., Bose, S.K. and Roy, S.K., 2001. *Environmental degradation of metals: corrosion technology series/14*. CRC Press.
23. Ctibor, P., Lechnerová, R. and Beneš, V., 2006. Quantitative analysis of pores of two types in a plasma-sprayed coating. *Materials Characterization*, *56*(4-5), pp.297-304.
24. Daram, P. and Banjongprasert, C., 2020. The influence of post treatments on the microstructure and corrosion behavior of thermally sprayed NiCrMoAl alloy coating. *Surface and Coatings Technology*, *384*, p.125166.
25. Davis, J.R. ed., 2004. *Handbook of thermal spray technology*. ASM international.
26. Deb, D., Iyer, S.R. and Radhakrishnan, V.M., 1996. A comparative study of oxidation and hot corrosion of a cast nickel base superalloy in different corrosive environments. *Materials Letters*, *29*(1-3), pp.19-23.
27. Delaunay, F., Berthier, C., Lenglet, M. and Lameille, J.M., 2000. SEM-EDS and XPS studies of the high temperature oxidation behaviour of Inconel 718. *Microchimica Acta*, *132*(2), pp.337-343.
28. Deng, K., Shi, J., Wang, C., Wang, X., Wu, Y., Nie, K. and Wu, K., 2012a. Microstructure and strengthening mechanism of bimodal size particle reinforced magnesium matrix composite. *Composites Part A: Applied Science and Manufacturing*, *43*(8), pp.1280-1284.

29. Deng, K.K., Wang, X.J., Wang, C.J., Shi, J.Y., Hu, X.S. and Wu, K., 2012b. Effects of bimodal size SiC particles on the microstructure evolution and fracture mechanism of AZ91 matrix at room temperature. *Materials Science and Engineering: A*, *553*, pp.74-79.
30. Deuerling, C., Maguhn, J., Nordsieck, H., Benker, B., Zimmermann, R. and Warnecke, R., 2009. Investigation of the mechanisms of heat exchanger corrosion in a municipal waste incineration plant by analysis of the raw gas and variation of operating parameters. *Heat transfer engineering*, *30*(10-11), pp.822-831.
31. Doleker, K.M., Odabas, O., Ozgurluk, Y., Askerov, H. and Karaoglanli, A.C., 2019. Effect of high temperature oxidation on Inconel 718 and Inconel 718/YSZ/Gd2Zr2O7. *Materials Research Express*, *6*(8), p.086456.
32. Dooley, R. and Wiertel, E., 2009, January. A survey of erosion and corrosion resistant materials being used on boiler tubes in waste to energy boilers. In *North American Waste-to-Energy Conference* (Vol. 48807, pp. 37-41).
33. Dooley, R. and Wiertel, E., 2009, January. A survey of erosion and corrosion resistant materials being used on boiler tubes in waste to energy boilers. In *North American Waste-to-Energy Conference* (Vol. 48807, pp. 37-41).
34. Dorcheh, A.S., Durham, R.N. and Galetz, M.C., 2016. Corrosion behavior of stainless and low-chromium steels and IN625 in molten nitrate salts at 600 C. *Solar Energy Materials and Solar Cells*, *144*, pp.109-116.
35. Dosta, S., Cinca, N., Silvello, A. and Cano, I.G., 2020. Alumina Reinforcement of Inconel 625 Coatings by Cold Gas Spraying. *Metals*, *10*(9), p.1263.
36. Dzhurinskiy, D., Babu, A., Pathak, P., Elkin, A., Dautov, S. and Shornikov, P., 2021. Microstructure and wear properties of atmospheric plasma-sprayed Cr3C2-NiCr composite coatings. *Surface and Coatings Technology*, *428*, p.127904.
37. Edris, H., McCartney, D.G. and Sturgeon, A.J., 1997. Microstructural characterization of high velocity oxy-fuel sprayed coatings of Inconel 625. *Journal of materials science*, *32*(4), pp.863-872.

38. Espallargas, N., Berget, J., Guilemany, J.M., Benedetti, A.V. and Suegama, P.H., 2008. Cr3C2–NiCr and WC–Ni thermal spray coatings as alternatives to hard chromium for erosion–corrosion resistance. *Surface and Coatings Technology*, *202*(8), pp.1405-1417.
39. Fantozzi, D., Matikainen, V., Uusitalo, M., Koivuluoto, H. and Vuoristo, P., 2017. Chlorine-induced high temperature corrosion of Inconel 625 sprayed coatings deposited with different thermal spray techniques. *Surface and Coatings Technology*, *318*, pp.233-243.
40. Fernández, J., Gaona, M. and Guilemany, J.M., 2007. Effect of heat treatments on HVOF hydroxyapatite coatings. *Journal of thermal spray technology*, *16*(2), pp.220-228.
41. Gagliano, M., Hack, H. and Stanko, G., 2009. Update on the fireside corrosion resistance of proposed advanced ultra supercritical super heater and re heater materials:
laboratory and field test results, *The 34th Clear Conference on Coal Utilization and Fuel Systems*, Clearwater, FL, USA, 2009, 31.05-04.06.2009.
42. Galedari, S.A., Mahdavi, A., Azarmi, F., Huang, Y. and McDonald, A., 2019. A comprehensive review of corrosion resistance of thermally-sprayed and thermally-diffused protective coatings on steel structures. *Journal of Thermal Spray Technology*, *28*(4), pp.645-677.
43. Gao, Y., Xu, X., Yan, Z. and Xin, G., 2002. High hardness alumina coatings prepared by low power plasma spraying. *Surface and Coatings Technology*, *154*(2-3), pp.189-193.
44. Gil, L. and Staia, M.H., 2002. Influence of HVOF parameters on the corrosion resistance of NiWCrBSi coatings. *Thin Solid Films*, *420*, pp.446-454.
45. Gil, L., Prato, M.A. and Staia, M.H., 2002. Effect of post-heat treatment on the corrosion resistance of NiWCrBSi HVOF coatings in chloride solution. *Journal of thermal spray technology*, *11*(1), pp.95-99.

46. Grewal, H.S., Agrawal, A., Singh, H. and Shollock, B.A., 2014. Slurry erosion performance of Ni-Al2O3 based thermal-sprayed coatings: effect of angle of impingement. *Journal of thermal spray technology*, *23*(3), pp.389-401.
47. Grewal, H.S., Singh, H. and Agrawal, A., 2013. Microstructural and mechanical characterization of thermal sprayed nickel–alumina composite coatings. *Surface and coatings Technology*, *216*, pp.78-92.
48. Gross, K.A., Gross, V. and Berndt, C.C., 1998. Thermal analysis of amorphous phases in hydroxyapatite coatings. *Journal of the American Ceramic Society*, *81*(1), pp.106-112.
49. Guilemany, J.M., Dosta, S. and Miguel, J.R., 2006. The enhancement of the properties of WC-Co HVOF coatings through the use of nanostructured and microstructured feedstock powders. *Surface and Coatings Technology*, *201*(3-4), pp.1180-1190.
50. Guilemany, J.M., Miguel, J.M., Vizcaıno, S., Lorenzana, C., Delgado, J. and Sanchez, J., 2002. Role of heat treatments in the improvement of the sliding wear properties of Cr3C2–NiCr coatings. *Surface and Coatings Technology*, *157*(2-3), pp.207-213.
51. Gutleber, J., Sampath, S. and Usmani, S., 1997, September. Processing and thermal cycling effects on the erosion behavior of thermal barrier coatings. In *ITSC 1997* (pp. 285-289). ASM International.
52. He, J.L., Chen, K.C., Chen, C.C., Leyland, A. and Matthews, A., 2001. Cyclic oxidation resistance of Ni–Al alloy coatings deposited on steel by a cathodic arc plasma process. *Surface and Coatings Technology*, *135*(2-3), pp.158-165.
53. Hearley, J.A., Little, J.A. and Sturgeon, A.J., 1999. The erosion behaviour of NiAl intermetallic coatings produced by high velocity oxy-fuel thermal spraying. *Wear*, *233*, pp.328-333.
54. Heath, G.R., Heimgartner, P., Irons, G., Miller, R.D. and Gustafsson, S., 1997. An assessment of thermal spray coating technologies for high temperature corrosion

protection. In *Materials science forum* (Vol. 251, pp. 809-816). Trans Tech Publications Ltd.

55. Hidalgo, V.H., Varela, J.B., Menéndez, A.C. and Martınez, S.P., 2001. High temperature erosion wear of flame and plasma-sprayed nickel–chromium coatings under simulated coal-fired boiler atmospheres. *Wear*, *247*(2), pp.214-222.
56. Hoop, P.J. and Allen, C., 1999. The high temperature erosion of commercial thermally sprayed metallic and cermet coatings by solid particles**.** Wear, 233–235, p.334.
57. Hu, H.X., Jiang, S.L., Tao, Y.S., Xiong, T.Y. and Zheng, Y.G., 2011. Cavitation erosion and jet impingement erosion mechanism of cold sprayed Ni–Al2O3 coating. *Nuclear Engineering and Design*, *241*(12), pp.4929-4937.
58. Husain, A. and Habib, K., 2005. Investigation of tubing failure of super-heater boiler from Kuwait Desalination Electrical Power Plant. *Desalination*, *183*(1-3), pp.203-208.
59. Hussain, T., Dudziak, T., Simms, N.J. and Nicholls, J.R., 2013b. Fireside corrosion behavior of HVOF and plasma-sprayed coatings in advanced coal/biomass co-fired power plants. *Journal of thermal spray technology*, *22*(5), pp.797-807.
60. Hussain, T., Syed, A.U. and Simms, N.J., 2013a. Trends in fireside corrosion damage to superheaters in air and oxy-firing of coal/biomass. *Fuel*, *113*, pp.787-797.
61. Ji, G.C., Wang, H.T., Chen, X., Bai, X.B., Dong, Z.X. and Yang, F.G., 2013. Characterization of cold-sprayed multimodal WC-12Co coating. *Surface and Coatings Technology*, *235*, pp.536-543.
62. Jiménez, S. and Ballester, J., 2005. Influence of operating conditions and the role of sulfur in the formation of aerosols from biomass combustion. *Combustion and Flame*, *140*(4), pp.346-358.
63. Jůzková, R., Ctibor, P. and Beneš, V., 2004. Analysis of porous structure in plasma-sprayed coating. *Image Analysis & Stereology*, *23*(1), pp.45-52.

64. Kamal, S., Jayaganthan, R. and Prakash, S., 2009. Evaluation of cyclic hot corrosion behaviour of detonation gun sprayed Cr3C2–25% NiCr coatings on nickel-and iron-based superalloys. *Surface and coatings technology*, *203*(8), pp.1004-1013.
65. Kamal, S., Jayaganthan, R. and Prakash, S., 2010a. Hot corrosion behaviour of D-gun sprayed NiCoCrAlYTa coated superalloys at 900° C in molten salt environment. *Surface engineering*, *26*(6), pp.453-462.
66. Kamal, S., Jayaganthan, R. and Prakash, S., 2010b. High temperature cyclic oxidation and hot corrosion behaviours of superalloys at 900 C. *Bulletin of Materials Science*, *33*(3), pp.299-306.
67. Kamal, S., Jayaganthan, R., Prakash, S. and Kumar, S., 2008. Hot corrosion behavior of detonation gun sprayed Cr3C2–NiCr coatings on Ni and Fe-based superalloys in Na2SO4–60% V2O5 environment at 900° C. *Journal of alloys and compounds*, *463*(1-2), pp.358-372.
68. Kaur, M., Singh, H. and Prakash, S., 2009. High-temperature corrosion studies of HVOF-sprayed Cr3C2-NiCr coating on SAE-347H boiler steel. *Journal of thermal spray technology*, *18*(4), pp.619-632.
69. Kaur, M., Singh, H. and Prakash, S., 2012. High-temperature behavior of a high-velocity oxy-fuel sprayed Cr3C2-NiCr coating. *Metallurgical and Materials Transactions A*, *43*(8), pp.2979-2993.
70. Kaushal, G., Bala, N., Kaur, N., Singh, H. and Prakash, S., 2014. Comparative high-temperature corrosion behavior of Ni-20Cr coatings on T22 boiler steel produced by HVOF, D-Gun, and cold spraying. *Metallurgical and Materials Transactions A*, *45*(1), pp.395-410.
71. Kaushal, G., Kaur, N., Singh, H. and Prakash, S., 2012. Oxidation behaviour of D-Gun spray Ni-20Cr coated ASTM A213 347H steel at 900 C. *Int. J. Surf. Eng. Mater.Technol*, *2*(1), pp.33-38.
72. Kaushal, G., Saheet, H.S. and Prakash, S., 2010. Cyclic Oxidation Behavior of Detonation Gun Sprayed Ni-20 Cr Coating on a Boiler Steel at 900. *Minerals,*

Metals and Materials Society/AIME, 420 Commonwealth Dr., P. O. Box 430 Warrendale PA15086 USA.[np]. 14-18 Feb

73. Kaushal, G., Singh, H. and Prakash, S., 2011. Comparative high temperature analysis of HVOF-sprayed and detonation gun sprayed Ni–20Cr coating in laboratory and actual boiler environments. *Oxidation of metals*, *76*(3), pp.169-191.
74. Khoi, N.N., Smeltzer, W.W. and Embury, J.D., 1975. Growth and structure of nickel oxide on nickel crystal faces. *Journal of the Electrochemical Society*, *122*(11), p.1495.
75. Khor, K.A. and Cheang, P., 1994. Laser post treatment of thermally sprayed hydroxyapatite coatings, in: C.C. Berndt, S. Sampath (Eds.), Thermal Spray Industrial Applications, *Proceedings of NTSC'94,* ASM International, Materials Park, OH, USA, (pp. 153–157).
76. Koivuluoto, H. and Vuoristo, P., 2009. Effect of ceramic particles on properties of cold-sprayed Ni-20Cr+ Al2O3 coatings. *Journal of Thermal Spray Technology*, *18*(4), pp.555-562.
77. Konyashin, I.Y. and Chukalovskaya, T.V., 1997. A technique for measurement of porosity in protective coatings. *Surface and Coatings Technology*, *88*(1-3), pp.5-11.
78. Krzyzanowski, M., Beynon, J.H. and Farrugia, D.C., 2010. *Oxide scale behavior in high temperature metal processing*. John Wiley & Sons.
79. Kumar, A. and Sapra, P.K., 2016. Tribological characterisation of SA210 Gr A1 boiler steels for different temperature applications. *International Journal of Surface Science and Engineering*, *10*(4), pp.375-388.
80. Kumar, M., Singh, H. and Singh, N., 2013. Study of Ni-20Cr coatings for high temperature applications-a review. *Archives of Metallurgy and Materials*, *58*.
81. Kumar, M., Singh, H. and Singh, N., 2014. Production of nanocrystalline Ni-20Cr coatings for high-temperature applications. *Journal of thermal spray technology*, *23*(4), pp.692-707.

82. Kumar, M., Singh, H., Singh, N. and Joshi, R.S., 2015. Erosion–corrosion behavior of cold-spray nanostructured Ni–20Cr coatings in actual boiler environment. *Wear*, *332*, pp.1035-1043.
83. Kumar, N., Prashar, G. and Dhawan, R.K., 2012. To check the feasibility of Cr2O3 coating on boiler steel tubes simulated coal fired boiler conditions to prevent the erosion.
84. Kumar, R., Bhandari, S. and Goyal, A., 2017. Slurry erosion performance of high-velocity flame-sprayed Ni-20Al2O3 and Ni-10Al2O3-10TiO2 coatings under accelerated conditions. *Journal of Thermal Spray Technology*, *26*(6), pp.1279-1291.
85. Laguna-Camacho, J. R., Marquina-Chávez, A., Mendez-Mendez, J. V., Vite-Torres, M., and Gallardo-Hernandez, E. A., 2013. Solid particle erosion of AISI 304, 316 and 420 stainless steels. *Wear*, *301*(1-2), pp.398-405.
86. Li, B., Li, C., Gao, Y., Guo, H., Zheng, Q., Kang, Y. and Zhao, S., 2019. Influence of Heat Treatment on Corrosion–Wear Behavior of Ni-Based Coating in Artificial Seawater. *Journal of Materials Engineering and Performance*, *28*(12), pp.7828-7834.
87. Li, W., Huang, C., Yu, M., Liu, D., Feng, Y. and Liao, H., 2014. Investigation of high temperature oxidation behavior and tribological performance on cold sprayed nickel–alumina composite coating. *Surface and Coatings Technology*, *239*, pp.95-101.
88. Li, W.Y., Zhang, C., Liao, H., Li, J. and Coddet, C., 2008. Characterizations of cold-sprayed nickel–alumina composite coating with relatively large nickel-coated alumina powder. *Surface and Coatings Technology*, *202*(19), pp.4855-4860.
89. Liu, L., Xu, H., Xiao, J., Wei, X., Zhang, G. and Zhang, C., 2017. Effect of heat treatment on structure and property evolutions of atmospheric plasma sprayed NiCrBSi coatings. *Surface and Coatings Technology*, *325*, pp.548-554.

90. Liu, Y., Liu, W., Ma, Y., Meng, S., Liu, C., Long, L. and Tang, S., 2017. A comparative study on wear and corrosion behaviour of HVOF-and HVAF-sprayed WC–10Co–4Cr coatings. *Surface Engineering*, *33*(1), pp.63-71.
91. Lobley, G.R. and Al-Otaibi, W.L., 2008. Diagnosing boiler tube failures related to overheating. In *Advanced Materials Research* (Vol. 41, pp. 175-181). Trans Tech Publications Ltd.
92. Longa-Nava, Y., Zhang, Y.S., Takemoto, M. and Rapp, R.A., 1996. Hot corrosion of nickel-chromium and nickel-chromium-aluminum thermal-spray coatings by sodium sulfate-sodium metavanadate salt. *Corrosion*, *52*(09).
93. Lu, J., Huang, J., Yang, Z., Zhou, Y., Dang, Y., Zhao, X. and Yuan, Y., 2018. Effect of cobalt content on the oxidation and corrosion behavior of ni–fe-based superalloy for ultra-supercritical boiler applications. *Oxidation of Metals*, *89*(1), pp.197-209.
94. Mahesh, R.A., Jayaganthan, R. and Prakash, S., 2008. A study on hot corrosion behaviour of Ni–5Al coatings on Ni-and Fe-based superalloys in an aggressive environment at 900° C. *Journal of alloys and compounds*, *460*(1-2), pp.220-231.
95. Malik, A.U., Ismail, A., Mohammad, M., Fahd, A.M. and Mohammad, A.H., 2005. Corrosion of boiler tubes some case studies. 4th SWCC Acquired Experience Symposium held at Jeddah in 2005, pp. 739–763
96. Manikandan, D.W.M., 2018. High-temperature corrosion behaviour of HVOF sprayed Cr3C2-25NiCr coated on alloy X22CrMoV12-1 at 600° C. *J Therm Spray Eng*, *1*(1), p.7.
97. Matsubara, Y., Tomiguchi, A., Haraguchi, H., Hayashi, H. and Ito, H., 1998, May. Post Treatment of Plasma Sprayed WC-Co-Ni Coatings by High Frequency Induction Heating. In *ITSC 1998* (pp. 1415-1418). ASM International.
98. Matthews, S., James, B. and Hyland, M., 2009. High temperature erosion of Cr3C2-NiCr thermal spray coatings—The role of phase microstructure. *Surface and Coatings Technology*, *203*(9), pp.1144-1153.

99. Meier, G.H., 1989. A review of advances in high-temperature corrosion. *Materials Science and Engineering: A*, *120*, pp.1-11.

100. Milanti, A., Matikainen, V., Koivuluoto, H., Bolelli, G., Lusvarghi, L. and Vuoristo, P., 2015. Effect of spraying parameters on the microstructural and corrosion properties of HVAF-sprayed Fe–Cr–Ni–B–C coatings. *Surface and Coatings Technology*, *277*, pp.81-90.

101. Mishra, S.B. and Prakash, S., 2015. Erosion–corrosion behaviour of Ni–20Cr plasma coating in actual boiler environment. *Surface Engineering*, *31*(1), pp.29-38.

102. Mishra, S.B., Chandra, K. and Prakash, S., 2013. Erosion–corrosion performance of NiCrAlY coating produced by plasma spray process in a coal-fired thermal power plant. *Surface and Coatings Technology*, *216*, pp.23-34.

103. Mishra, S.B., Chandra, K. and Prakash, S., 2017. Studies on erosion-corrosion behaviour of plasma sprayed Ni3Al coating in a coal-fired thermal power plant environment at 540° C. *Anti-Corrosion Methods and Materials*, *64(5)*, pp.540-549.

104. Misra, A.K., 1986. Mechanism of Na2 SO 4-Induced Corrosion of Molybdenum Containing Nickel-Base Superalloys at High Temperatures: I. Corrosion in Atmospheres Containing Only. *Journal of the Electrochemical Society*, *133*(5), p.1029.

105. Mohamed, M.H. and Wilson, V.H., 2015. Analysis of boiler super heater tubes from high flue gas temperature. *Int. J. Innov. Res. Adv. Eng.(IJIRAE)*, *2*, pp.1-4.

106. Monticelli, C., Frignani, A. and Zucchi, F., 2004. Investigation on the corrosion process of carbon steel coated by HVOF WC/Co cermets in neutral solution. *corrosion science*, *46*(5), pp.1225-1237.

107. Morks, M.F., 2008. Fabrication and characterization of plasma-sprayed HA/SiO2 coatings for biomedical application. *Journal of the mechanical behavior of biomedical materials*, *1*(1), pp.105-111.

108. Moskowitz, L., 1997, September. The effects of post heating an HVOF sprayed fusible coating. In *ITSC 1997* (pp. 519-525). ASM International.

109. Nadaraia, K.V., Suchkov, S.N., Imshinetskiy, I.M., Mashtalyar, D.V., Sinebrykhov, S.L. and Gnedenkov, S.V., 2021. Some new aspects of the study of dependence of properties of PEO coatings on the parameters of current in potentiodynamic mode. *Surface and Coatings Technology*, *426*, p.127744.

110. Nicholls, J.R., 2000. Designing oxidation-resistant coatings. *JoM*, *52*(1), pp.28-35.

111. Ohkubo, N., Miyakusu, K., Uematsu, Y. and Kimura, H., 1994. Effect of alloying elements on the mechanical properties of the stable austenitic stainless steel. *ISIJ international*, *34*(9), pp.764-772.

112. Oksa, M., Auerkari, P., Salonen, J. and Varis, T., 2014. Nickel-based HVOF coatings promoting high temperature corrosion resistance of biomass-fired power plant boilers. *Fuel processing technology*, *125*, pp.236-245.

113. Pawlowski, L., 2008. *The science and engineering of thermal spray coatings*. John Wiley & Sons.

114. Pereira, J.C., Zambrano, J.C., Tobar, M.J., Yañez, A. and Amigó, V., 2015. High temperature oxidation behavior of laser cladding MCrAlY coatings on austenitic stainless steel. *Surface and Coatings Technology*, *270*, pp.243-248.

115. Pereira, J.M. and Lerch, B.A., 2001. Effects of heat treatment on the ballistic impact properties of Inconel 718 for jet engine fan containment applications. *International Journal of Impact Engineering*, *25*(8), pp.715-733.

116. Peters, K.R., Whittle, D.P. and Stringer, J., 1976. Oxidation and hot corrosion of nickel-based alloys containing molybdenum. *Corrosion Science*, *16*(11), pp.791-804.

117. Prakash, S., Singh, S., Sidhu, B.S. and A. Madeshia, A., 2001. Tube failures in coal fired boilers. *in Proc. National Seminar on Advances in Material and Processing*, *9–10*, pp. 245–253.

118. Praveen, A.S. and Arjunan, A., 2019. Effect of nano-Al2O3 addition on the microstructure and erosion wear of HVOF sprayed NiCrSiB coatings. *Materials Research Express*, *7*(1), p.015006.

119. Praveen, A.S., Sarangan, J., Suresh, S. and Subramanian, J.S., 2015. Erosion wear behaviour of plasma sprayed NiCrSiB/Al2O3 composite coating. *International Journal of Refractory Metals and Hard Materials*, *52*, pp.209-218.

120. Premkumar, K., and Balasubramanian, K.R., 2018. Investigation of Erosion Behaviour on Nanocrystalline Composite Thermal Spray Coating under Hot Air Jet Condition. *Jour of Adv Research in Dynamical & Control Systems, Vol. 10, 04*-Special Issue.

121. Price, M.O., Jackson, J.E. and Quets, J.M., Union Carbide Coatings Service Technology Corp, 1992. *Process for producing chromium carbide-nickel base age hardenable alloy coatings and coated articles so produced*. U.S. Patent 5,137,422.

122. Qu, S.Y., Han, Y.F., Song, J.X. and Kang, Y.W., 2007. Effects of Cr and Al on high temperature oxidation resistance of Nb-Si system intermetallics. In *Materials science forum* (Vol. 546, pp. 1485-1488). Trans Tech Publications Ltd.

123. Rana, R.S., Purohit, R. and Das, S., 2012. Reviews on the influences of alloying elements on the microstructure and mechanical properties of aluminum alloys and aluminum alloy composites. *International Journal of Scientific and research publications*, *2*(6), pp.1-7.

124. Rapp, R.A., 1984. High temperature oxidation of metals forming cation-diffusing scales. *Metall. Trans., B;(United States)*, *15*.

125. Reddy, N.C., Koppad, P.G., Reddappa, H.N., Ramesh, M.R., Babu, E.R. and Varol, T.E.M.E.L., 2019. Hot corrosion behaviour of HVOF sprayed Ni3Ti and Ni3Ti+(Cr3C2+ 20NiCr) coatings in presence of Na2SO4-40% V2O5 at 650° C. *Surface Topography: Metrology and Properties*, *7*(2), p.025019.

126. Reid, W.T., 1971. External corrosion and deposits: boilers and gas turbines.

127. Ren, X., Wang, F. and Wang, X., 2005. High-temperature oxidation and hot corrosion behaviors of the NiCr–CrAl coating on a nickel-based superalloy. *Surface and coatings Technology*, *198*(1-3), pp.425-431.

128. Roy, M., 2006. Elevated temperature erosive wear of metallic materials. *Journal of Physics D: Applied Physics*, *39*(6), p.R101.

129. Roy, M., Bandyopadhyay, A. and Bose, S., 2011. Induction plasma sprayed nano hydroxyapatite coatings on titanium for orthopaedic and dental implants. *Surface and Coatings Technology*, *205*(8-9), pp.2785-2792.

130. Sadeghi, E., Markocsan, N. and Joshi, S., 2019. Advances in corrosion-resistant thermal spray coatings for renewable energy power plants. part I: effect of composition and microstructure. *Journal of Thermal Spray Technology*, *28*(8), pp.1749-1788.

131. Sadeghimeresht, E., 2018. *Ni-based coatings for high temperature corrosion protection* (Doctoral dissertation, University West).

132. Sadeghimeresht, E., Markocsan, N. and Nylén, P., 2016. A comparative study of corrosion resistance for HVAF-sprayed Fe-and Co-based coatings. *Coatings*, *6*(2), p.16.

133. Saunders, S.R.J. and Nicholls, J.R., 1989. Coatings and surface treatments for high temperature oxidation resistance. *Materials science and technology*, *5*(8), pp.780-798.

134. Shukla, V.N., Jayaganthan, R. and Tewari, V.K., 2012. Hot corrosion studies of HVOF-sprayed Cr3C2-NiCr coating on 310S stainless steel in an actual environment of a coal fired boiler. In *Advanced Materials Research* (Vol. 585, pp. 483-487). Trans Tech Publications Ltd.

135. Sidhu, B.S. and Prakash, S., 2005a. Degradation behavior of Ni3Al plasma-sprayed boiler tube steels in an energy generation system. *Journal of materials engineering and performance*, *14*(3), pp.356-362.

136. Sidhu, B.S. and Prakash, S., 2005b. High-temperature oxidation behavior of NiCrA1Y bond coats and stellite-6 plasma-sprayed coatings. *Oxidation of metals*, *63*(3), pp.241-259.

137. Sidhu, B.S. and Prakash, S., 2006. Evaluation of the behavior of shrouded plasma spray coatings in the platen superheater of coal-fired boilers. *metallurgical and Materials Transactions A*, *37*(6), pp.1927-1936.

138. Sidhu, H.S., Sidhu, B.S. and Prakash, S., 2006b. Evaluation of the hot corrosion behavior of LPG assisted HVOF NiCr wire sprayed boiler tube steels in molten salt environments. *ISIJ international*, *46*(7), pp.1067-1074.

139. Sidhu, T.S., Agrawal, R.D. and Prakash, S., 2005. Hot corrosion of some superalloys and role of high-velocity oxy-fuel spray coatings—a review. *Surface and coatings technology*, *198*(1-3), pp.441-446.

140. Sidhu, T.S., Prakash, S. and Agrawal, R.D., 2006a. Hot corrosion behaviour of HVOF-sprayed NiCrBSi coatings on Ni-and Fe-based superalloys in Na2SO4–60% V2O5 environment at 900° C. *Acta materialia*, *54*(3), pp.773-784.

141. Sidhu, T.S., Prakash, S. and Agrawal, R.D., 2006c. Characterizations and hot corrosion resistance of Cr3C2-NiCr coating on Ni-base superalloys in an aggressive environment. *Journal of thermal spray technology*, *15*(4), pp.811-816.

142. Sidhu, T.S., Prakash, S. and Agrawal, R.D., 2006d. Performance of high-velocity oxyfuel-sprayed coatings on an fe-based superalloy in Na2SO4-60% V2O5 environment at 900° C Part I: Characterization of the coatings. *Journal of materials engineering and performance*, *15*(1), pp.122-129.

143. Singh, B. Ph.D. Thesis, Indian Institute of Technology Roorkee, Roorkee, India, 2003

144. Singh, G., Bala, N. and Chawla, V., 2017. High temperature oxidation behaviour of HVOF thermally sprayed NiCrAlY Coating on T-91 boiler tube steel. *Materials Today: Proceedings*, *4*(4), pp.5259-5265.

145. Singh, G., Bala, N. and Chawla, V., 2020. Microstructural analysis and hot corrosion behavior of HVOF-sprayed Ni-22Cr-10Al-1Y and Ni-22Cr-10Al-1Y-SiC (N) coatings on ASTM-SA213-T22 steel. *International Journal of Minerals, Metallurgy and Materials*, *27*(3), pp.401-416.

146. Singh, H., Puri, D., Prakash, S. and Ghosh, T.K., 2007a. Hot corrosion of a plasma sprayed Ni3Al coating on a Ni-base superalloy. *Materials and Corrosion*, *58*(11), pp.857-866.

147. Singh, H., Puri, D., Prakash, S. and Hira, D.S., 2007c. Investigations on role of plasma sprayed NiCrAlY and Ni–20Cr coatings to combat hot corrosion. *Materials science and technology*, *23*(6), pp.736-744.

148. Singh, H., Puri, D., Prakash, S. and Maiti, R., 2007. Characterization of oxide scales to evaluate high temperature oxidation behavior of Ni–20Cr coated superalloys. *Materials Science and Engineering: A*, *464*(1-2), pp.110-116.

149. Singh, H., Puri, D., Prakash, S. and Maiti, R., 2007b. Characterization of oxide scales to evaluate high temperature oxidation behavior of Ni–20Cr coated superalloys. *Materials Science and Engineering: A*, *464*(1-2), pp.110-116.

150. Singh, H., Sidhu, T.S. and Kalsi, S.B.S., 2015. Behaviour of cold sprayed superalloy in incinerator at 900° C. *Surface Engineering*, *31*(11), pp.846-852.

151. Singh, S., Goyal, K..and Goyal, R., 2016. Performance of Cr3C2-25(Ni-20Cr) and Ni-20Cr coatings on T91 boiler tube steel in simulated boiler environment at 900°C. *Chemical and materials engineering, 4 (4,)* pp.57–64.

152. Skandan, G., Yao, R., Kear, B.H., Qiao, Y., Liu, L. and Fischer, T.E., 2001. Multimodal powders: a new class of feedstock material for thermal spraying of hard coatings. *Scripta materialia*, *44*(8-9), pp.1699-1702.

153. Stein-Brzozowska, G., Flórez, D.M., Maier, J. and Scheffknecht, G., 2013. Nickel-base superalloys for ultra-supercritical coal-fired power plants: Fireside corrosion. Laboratory studies and power plant exposures. *Fuel*, *108*, pp.521-533.

154. Stokes, J. and Looney, L., 2000, May. Properties of WC-Co components produced using the HVOF thermal spray process. In *ITSC 2000* (pp. 263-271). ASM International.

155. Stott, F.H. and Wood, G.C., 1988. Internal oxidation. *Materials Science and Technology*, *4*(12), pp.1072-1078

156. Stringer, J., 1987. High-temperature corrosion of superalloys. *Materials Science and Technology*, *3*(7), pp.482-493.

157. Stringer, J., 1995. Practical experience with wastage at elevated temperatures in coal combustion systems. *Wear*, *186*, pp.11-27.

158. Suckling, M. and Allen, C., 1997. Critical variables in high temperature erosive wear. *Wear*, *203*, pp.528-536.

159. Sun, H., Yi, G., Wan, S., Kong, C., Zhu, S., Bai, L. and Yang, J., 2021. Effect of Cr2O3 addition on mechanical and tribological properties of atmospheric plasma-sprayed NiAl-Bi2O3 composite coatings. *Surface and Coatings Technology*, *427*, p.127818.

160. Sundararajan, G., Sen, D. and Sivakumar, G., 2005. The tribological behaviour of detonation sprayed coatings: the importance of coating process parameters. *Wear*, *258*(1-4), pp.377-391.

161. Sundararajan, G., Sudharshan Phani, P., Jyothirmayi, A. and Gundakaram, R.C., 2009. The influence of heat treatment on the microstructural, mechanical and corrosion behaviour of cold sprayed SS 316L coatings. *Journal of materials science*, *44*(9), pp.2320-2326.

162. Sundararajan, T., Kuroda, S. and Abe, F., 2004. Steam oxidation studies on 50Ni-50Cr HVOF coatings on 9Cr-1Mo steel: change in structure and morphology across the coating/substrate interface. *Materials Transactions*, *45*(4), pp.1299-1305.

163. Swaminathan, S., Hong, S.M., Kumar, M., Jung, W.S., Kim, D.I., Singh, H. and Choi, I.S., 2019. Microstructural evolution and high temperature oxidation characteristics of cold sprayed Ni-20Cr nanostructured alloy coating. *Surface and Coatings Technology*, *362*, pp.333-344.

164. Tan, X., 2012. Supercritical and ultrasupercritical coal-fired power generation. *Business and Public Administration Studies*, *7*(1), pp.53-53.

165. Thirumalaikumarasamy, D., Shanmugam, K. and Balasubramanian, V., 2014. Establishing empirical relationships to predict porosity level and corrosion rate of atmospheric plasma-sprayed alumina coatings on AZ31B magnesium alloy. *Journal of Magnesium and Alloys*, *2*(2), pp.140-153.

166. Triantou, K.I., Pantelis, D.I., Guipont, V. and Jeandin, M., 2015. Microstructure and tribological behavior of copper and composite copper+ alumina cold sprayed coatings for various alumina contents. *Wear*, *336*, pp.96-107.

167. Tucker, R.C., 2013. ASM handbook, volume 5A: thermal spray technology. *ASM International*, *57*.

168. Ul-Hamid, A., 2003. Diverse scaling behavior of the Ni–20Cr alloy. *Materials chemistry and physics*, *80*(1), pp.135-142.

169. Uusitalo, M.A., Vuoristo, P.M.J. and Mäntylä, T.A., 2004. High temperature corrosion of coatings and boiler steels below chlorine-containing salt deposits. *Corrosion science*, *46*(6), pp.1311-1331.

170. Vasudev, H., Prashar, G., Thakur, L. and Bansal, A., 2021b. Microstructural characterization and electrochemical corrosion behaviour of HVOF sprayed Alloy718-nanoAl2O3 composite coatings. *Surface Topography: Metrology and Properties*, *9*(3), p.035003.

171. Vasudev, H., Singh, P., Thakur, L. and Bansal, A., 2020c. Mechanical and microstructural characterization of microwave post processed Alloy-718 coating. *Materials Research Express*, *6*(12), p.1265f5.

172. Vasudev, H., Thakur, L., Bansal, A., Singh, H. and Zafar, S., 2019. High temperature oxidation and erosion behaviour of HVOF sprayed bi-layer Alloy-718/NiCrAlY coating. *Surface and Coatings Technology*, *362*, pp.366-380.

173. Vasudev, H., Thakur, L., Singh, H. and Bansal, A., 2018. Mechanical and microstructural behaviour of wear resistant coatings on cast iron lathe machine beds and slides. *Kovove Materialy, Metallic Materials*, *56*(1), pp.55-63.

174. Vasudev, H., Thakur, L., Singh, H. and Bansal, A., 2020a. An investigation on oxidation behaviour of high velocity oxy-fuel sprayed Inconel718-Al2O3 composite coatings. *Surface and Coatings Technology*, *393*, p.125770.

175. Vasudev, H., Thakur, L., Singh, H. and Bansal, A., 2020b. A study on processing and hot corrosion behaviour of HVOF sprayed Inconel718-nano Al2O3 coatings. *Materials Today Communications*, *25*, p.101626.

176. Vasudev, H., Thakur, L., Singh, H. and Bansal, A., 2021a. Erosion behaviour of HVOF sprayed Alloy718-nano Al2O3 composite coatings on grey cast iron at

elevated temperature conditions. *Surface Topography: Metrology and Properties*, *9*(3), p.035022.

177. Vasudev, H., Thakur, L., Singh, H. and Bansal, A., 2022. Effect of addition of Al2O3 on the high-temperature solid particle erosion behaviour of HVOF sprayed Inconel-718 coatings. *Materials Today Communications*, *30*, p.103017.

178. Verma, R. and Kaushal, G., 2021. Comparative high temperature oxidation studies of HVOF IN 625 coating on T22 boiler steel at 900° C and 700° C. *Materials Today: Proceedings*, *41*, pp.812-820.

179. Wang, B. and Lee, S.W., 2000. Erosion–corrosion behaviour of HVOF NiAl–Al2O3 intermetallic-ceramic coating. *Wear*, *239*(1), pp.83-90.

180. Wang, B., 1996. Erosion-corrosion of thermal sprayed coatings in FBC boilers. *Wear*, *199*(1), pp.24-32.

181. Wang, B.Q. and Verstak, A., 1999. Elevated temperature erosion of HVOF Cr3C2/TiC–NiCrMo cermet coating. *Wear*, *233*, pp.342-351.

182. Wang, B.Q., 2003. Hot erosion behavior of two new iron-based coatings sprayed by HVCC process. *Wear*, *255*(1-6), pp.102-109.

183. Wang, X., Fang, M., Zhang, L.C., Ding, H., Liu, Y.G., Huang, Z., Huang, S. and Yang, J., 2013. Solid particle erosion of alumina ceramics at elevated temperature. *Materials Chemistry and Physics*, *139*(2-3), pp.765-769.

184. Wang, Y., Normand, B., Mary, N., Yu, M. and Liao, H., 2014. Microstructure and corrosion behavior of cold sprayed SiCp/Al 5056 composite coatings. *Surface and Coatings Technology*, *251*, pp.264-275.

185. Wen, Z.H., Bai, Y., Yang, J.F., Huang, J. and Zhang, L., 2015. Effect of vacuum remelting on microstructure and wear resistance of NiCrMoY coatings deposited by supersonic atmospheric plasma spraying. *Surface and Coatings Technology*, *281*, pp.62-67.

186. Wielage, B. and Fleischer, K., 1998, May. Electron beam posttreatment of coatings plasma sprayed onto magnesium alloys. In *Proc. Int. Thermal Spray Conf* (Vol. 2, pp. 1449-1453).

187. Yang, G.J., Li, C.J., Zhang, S.J. and Li, C.X., 2008. High-temperature erosion of HVOF sprayed Cr3C2-NiCr coating and mild steel for boiler tubes. *Journal of Thermal Spray Technology*, *17*(5), pp.782-787.

188. Yang, J.Z., Fang, M.H., Huang, Z.H., Hu, X.Z., Liu, Y.G., Sun, H.R., Huang, J.T. and Li, X.C., 2012. Solid particle impact erosion of alumina-based refractories at elevated temperatures. *Journal of the European Ceramic Society*, *32*(2), pp.283-289.

189. Yin, Z., Tao, S., Zhou, X. and Ding, C., 2007. Tribological properties of plasma sprayed Al/Al2O3 composite coatings. *Wear*, *263*(7-12), pp.1430-1437.

190. Yu, X.Q., Fan, M. and Sun, Y.S., 2002. The erosion–corrosion behavior of some Fe3Al-based alloys at high temperatures. *Wear*, *253*(5-6), pp.604-609.

191. Zahrani, E.M. and Alfantazi, A.M., 2014. High temperature corrosion and electrochemical behavior of INCONEL 625 weld overlay in PbSO4–Pb3O4–PbCl2–CdO–ZnO molten salt medium. *Corrosion science*, *85*, pp.60-76.

192. Zhang, H., Dong, X. and Chen, S., 2017. Solid particle erosion-wear behaviour of Cr3C2–NiCr coating on Ni-based superalloy. *Advances in Mechanical Engineering*, *9*(3), p.1687814017694580.

193. Zhang, S.D., Wu, J., Qi, W.B. and Wang, J.Q., 2016. Effect of porosity defects on the long-term corrosion behaviour of Fe-based amorphous alloy coated mild steel. *Corrosion Science*, *110*, pp.57-70.

194. Zhao, S., Xie, X., Smith, G.D. and Patel, S.J., 2005. The corrosion of INCONEL alloy 740 in simulated environments for pulverized coal-fired boiler. *Materials chemistry and physics*, *90*(2-3), pp.275-281.

195. Zhou, J. and Bahadur, S., 1995. Erosion characteristics of alumina ceramics at high temperatures. *Wear*, *181*, pp.178-188.

APPENDIX

Model: D8 Advance
Make: Bruker AXS Instruments, Germany
Radiation: Cu-Kα
Scan rate: 0.5 to 1° min−1
Scan range: 20° to 100°

Figure A-1: View of the X-Ray Diffraction Equipment Used for Phase Analysis.

Model:LT 23B
Make: Dewinter, India
Magnification :50 x, 100 x, 200 x, 500 x
Display: Large field
Interface: With USB Digital camera and Image Analysis Software (Dewinter Material Plus, Version 4.2)

Figure A-2: View of Optical Microscope.

Model: FEI Quanta 200
Make: FEG-SEM, Czech Republic
Operating voltage: 2-25 kV
Magnification : 25 x to 100000 x
Gun: Field Emission Gun (FEG)

Figure A-3: Typical View of the Field Emission Scanning Electron Microscope (FE-SEM) Used for Microstructural Investigation

Model: Economet VH–1 MD
Make: Chennai Metco, India
Indenters: Vickers
Test Load: 10 – 1000 gf
Operating Time: 15sec
Min Measuring Unit: 0.05 μm
Hardness Measuring Range: 5~2500 HV
Test Microscope Magnification: 400X (Measuring), 100X (Observation).

Data Output: LCD screen display, Inside Printer, RS-232.

Max. Sample Height: ~100 mm

Figure A-4: Typical View of the Vicker's Micro-hardness tester

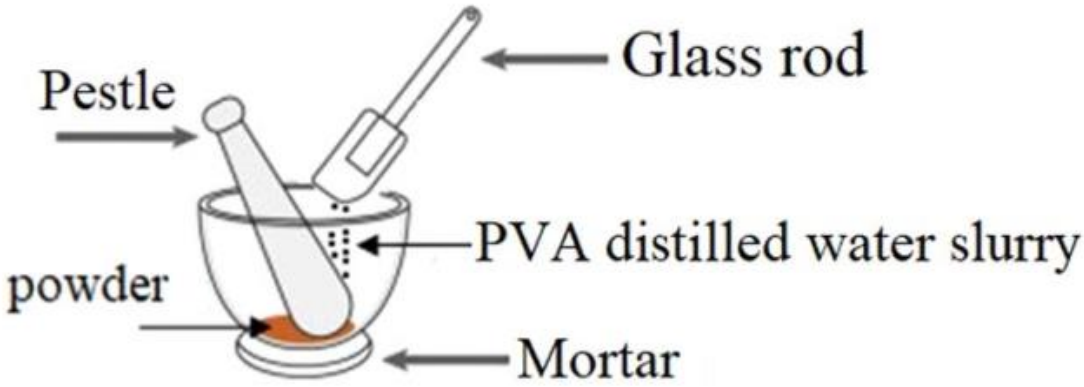

Figure A-5: Schematic illustration of manual granulation process using pestle and mortar.

Model: Mettalurgical sample saw MS-10
Make: Ducom Pvt. Ltd, Bangalore, India
Capacity: 240 RPM
Blade Thickness: 200 µm

Figure A-6 :View of the Diamond Cutter Used for Sample Cutting.

List of Publications

1. **G. Prashar** and H. Vasudev, Structure-property correlation and high-temperature erosion performance of Inconel625-Al_2O_3 plasma sprayed bimodal composite coatings, *Surface and Coatings Technology*, (439)2022 (**Elsevier, SCI, IF: 4.15**). https://doi.org/10.1016/j.surfcoat.2022.128450
2. **G. Prashar** and H. Vasudev, Structure-property correlation of Plasma-sprayed Inconel625-Al_2O_3 bimodal composite coatings for high temperature oxidation protection, *Journal of Thermal spray Technology;* 2022,https://doi.org/10.1007/s11666-022-01466-1 (**Springer,SCI, IF: 2.83).**
3. **G. Prashar** and H. Vasudev, "Surface topology analysis of plasma sprayed Inconel625-Al_2O_3 composite coating," Materials Today: Proceedings, Vol. 50(5), 2022, Pages 607-611. **(Elsevier, Scopus Indexed).** https://doi.org/10.1016/j.matpr.2021.03.090
4. **G. Prashar,** H. Vasudev and L. Thakur**, "**High-temperature oxidation and erosion resistance of Ni-based thermally-sprayed coatings used in power generation machinery: A Review**,** 2230003, 2022. **(World Scientific, SCI, IF: 1.1).** https://doi.org/10.1142/S0218625X22300039
5. **G. Prashar,** H. Vasudev and L. Thakur, **"**Influence of heat treatment on surface properties of HVOF deposited WC and Ni-based powder coatings: a review**,** Vol.9(4), 043002, 2021, **(Surface Topography: Metrology and Properties, SCI, IF: 2.0).** https://doi.org/10.1088/2051-672X/ac3a52
6. **G. Prashar** and H. Vasudev, "Hot corrosion behavior of superalloys," Materials Today: Proceedings, Vol. 26, 2020, Pages 1131-1135. **(Elsevier, Scopus Indexed).**https://doi.org/10.1016/j.matpr.2020.02.226

List of Conferences/Workshops

1. 10th International conferences on Materials Processing and characterization (ICMPC-2020) at GLA University, Mathura.
2. 2nd International conferences on Functional Materials, Manufacturing and Performances (ICFMMP-2021) at LPU, Phagwara.
3. Attended Seven day workshop from 16-2-2022 to 22-02-2022 organized on "*Surface Engineering & Coatings: Fundamentals, Practice & Applications*", by IKGPTU, Kapurthala.
4. Attended two day national workshop from 9-11-2019 to10-11-2019 organized on "*X-Ray Diffraction: Theory and Practices&*", by LPU, Phagwara.